INTERNAL FINGERPRINT EXTRACTION

A thesis submitted in fulfilment of the
requirements for the degree of

MASTER OF SCIENCE

of

RHODES UNIVERSITY

by

LUKE NICHOLAS DARLOW

February 2016

Abstract

Fingerprints are a non-invasive biometric that possess significant advantages. However, they are subject to surface erosion and damage; distortion upon scanning; and are vulnerable to fingerprint spoofing. The internal fingerprint exists as the undulations of the papillary junction – an intermediary layer of skin – and provides a solution to these disadvantages. Optical coherence tomography is used to capture the internal fingerprint.

A depth profile of the papillary junction throughout the OCT scans is first constructed using fuzzy c-means clustering and a fine-tuning procedure. This information is then used to define localised regions over which to average pixels for the resultant internal fingerprint.

When compared to a ground-truth internal fingerprint zone, the internal fingerprint zone detected automatically is within the measured bounds of human error. With a mean-squared-error of 21.3 and structural similarity of 96.4%, the internal fingerprint zone was successfully found and described. The extracted fingerprints exceed their surface counterparts with respect to orientation certainty and NFIQ scores (both of which are respected fingerprint quality assessment criteria).

Internal to surface fingerprint correspondence and internal fingerprint cross correspondence were also measured. A larger scanned region is shown to be advantageous as internal fingerprints extracted from these scans have good surface correspondence (75% had at least one true match with a surface counterpart). It is also evidenced that internal fingerprints can constitute a fingerprint database. 96% of the internal fingerprints extracted had at least one corresponding match with another internal fingerprint. When compared to surface fingerprints cropped to match the internal fingerprints' representative area and locality, the internal fingerprints outperformed these cropped surface counterparts.

The internal fingerprint is an attractive biometric solution. This research develops a novel approach to extracting the internal fingerprint and is an asset to the further development of technologies surrounding fingerprint extraction from OCT scans. No earlier work has extracted or tested the internal fingerprint to the degree that this research has.

Acknowledgements

The authors would like to thank the CSIR national Laser Center for providing the OCT scans used in this research. The authors would also like to thank the team at CSIR's Modelling and Digital Science for assisting and providing tools for obtaining surface fingerprints.

The authors thank Mrs J. Cyrus for assistance in proof-reading this thesis.

Contents

List of Figures

List of Tables

Abbreviations

CCD	**C**harge **C**oupled **D**evice
en-face	***f***ace on; parellel to fingerprint
H	**H**ausdorff distance
MRI	**M**agnetic **R**esonance **I**maging
NFIQ	**N**IST **F**ingerprint **I**mage **Q**uality
NIST	**N**ational **I**nstitute of **S**tandards and **T**echnology
MSE	**M**ean **S**quared **E**rror
NL	**N**on **L**ocal
OCL	**O**rientation **C**ertainty **L**evel
OCT	**O**ptical **C**oherence **T**omography
OBNLM	**O**ptimised **B**lockwise **N**on **L**ocal **M**eans
PPI	**P**ixels **P**er **I**nch
RMS-C	**R**oot **M**ean **S**quared **C**ontrast
ROI	**R**egion **O**f **I**nterest
SSIM	**S**tructural **SIM**milarity

Symbols

c	number of clusters for fuzzy c-means
G	ground-truth papillary junction upper-edge co-ordinates
GC	ground-truth papillary junction centre co-ordinates
k	number of clusters for other clustering algorithms
m	cluster membership threshold multiplication factor
n	number of local maxima extracted per A-line
P	papillary junction upper-edge co-ordinates
PC	papillary junction center co-ordinates
T	cluster membership threshold
$window\_size$	size of the window used to calculate statistics for extraction

Chapter 1

Introduction

This research intends to show the existence and potential viable use of the internal fingerprint. The internal fingerprint is a biometric inheriting the same structural features and high-performance of the surface fingerprint, while having fewer disadvantages. Correspondence between the surface and internal fingerprint will be shown. The process of obtaining the internal fingerprint from optical coherence tomography (OCT) fingertip scans will be detailed and extensively tested. This involves signal processing and image enhancement and utilises fuzzy c-means clustering as a means of fingerprint zone-detection.

Various image and signal processing techniques are combined in a novel manner to yield an important contribution to the field of fingerprint acquisition – an internal fingerprint that is of high-quality; is difficult to fake; and is resistant to damage and erosion.

The following section introduces optical coherence tomography.

1.1 Optical Coherence Tomography

OCT is a technology used for obtaining high-resolution three-dimensional images of light scattering media such as biological tissue. Specific to the context of this research, it is considered high-resolution as it is able to provide fingerprint detail that is much higher than conventional fingerprint scans (over $1300dpi$ versus $500dpi$). OCT operates by sending a light beam into the imaged media and measuring the echo delay between

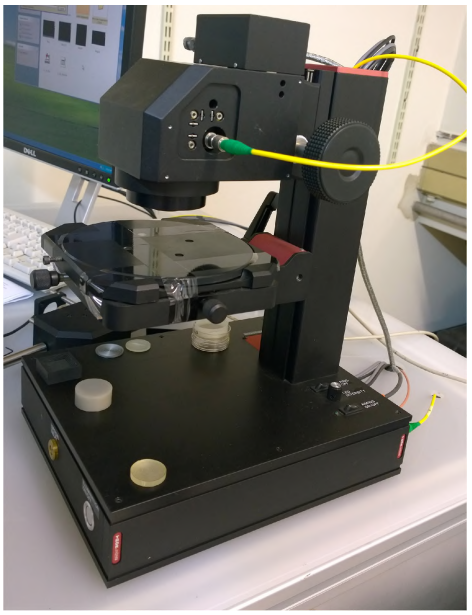

FIGURE 1.1: **The OCT system used** (Thorlabs OCS1300SS). The laser source itself is not visible here. An external system is required for processing the data output from the scanner.

the returned signal and a reference signal. OCT is able to provide a cross-sectional representation of the imaged media by scanning the light beam in a transverse direction. A series of cross-sectional dimensionally-related slices provides the three-dimensional representation. The OCT system used in this research is a swept source OCT system from Thorlabs (OCS1300SS). The scanner is shown in Figure 1.1.

Each cross-sectional image consists of a series of A-lines. Each A-line corresponds to a column in a single OCT image. These images are known as B-scans. The resolution constraints will be discussed in Section 4 and are shown in Figure 1.2. An encompassing discussion on the context and structure of A-lines is given in Section 3.1.2.

Commercial applications of OCT vary widely. From art conservation and document security to medical diagnostics, OCT is applicable whenever light can penetrate the imaged media. Since OCT makes use of near-infra-red light, and light of this wavelength is known to be safe, it is well suited for medical imaging. In fact, the primary use of OCT is that of medical applications, because biological media are partially translucent and allow the light to penetrate. The drive behind consistent improvement of OCT technology is undoubtedly medicine. Although an advantage over other medical imaging technology is the relative hardware simplicity and lower cost of OCT, broad-use OCT technology remains relatively expensive. However, the use thereof is diversifying. Specific to this

research, OCT can be used to image the human fingertip [1]. The following section contextualises OCT as biometric tool.

1.2 Optical Coherence Tomography as a Biometric Tool

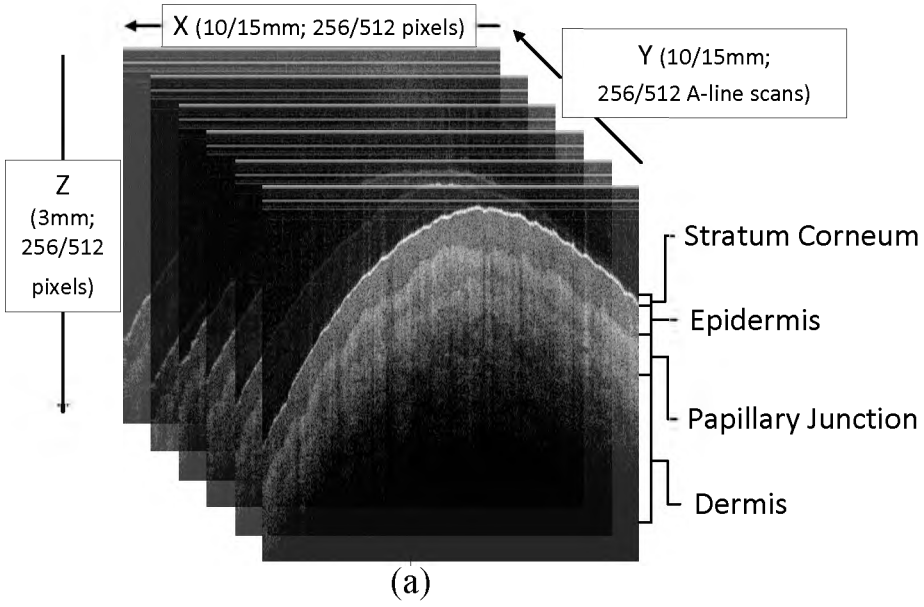

FIGURE 1.2: **An example of an OCT fingertip scan**, showing a cross-sectional representation of fingertip scan. The resolution constraints are included. **Z** shows depth into the skin. The **X-Y** plane corresponds to a 2D fingerprint. Each of these image slices are known as B-scans, and their columns are 1D signals known as A-lines.

The capability of OCT to image human skin provides a three-dimensional representation of the fingertip skin. Within this representation is contained information pertaining to the structural layout of the skin. On a coarse scale, individual skin layers are represented and visible. On a fine scale, the structural characteristics (such as ridges and valleys) are also visible. It is the presence and visibility of fingerprint ridges and valleys within the papillary junction that results in the strong potential of OCT as a biometric tool. Figure 1.2 provides an example of OCT slices and shows the visibility of skin layers and the structure of those layers.

1.3 Skin Layers and the Internal Fingerprint

The relationship between skin layers is paramount to this research. Since the primary goal of this research is to show the presence of an internal fingerprint that has a direct

structural relationship with the surface fingerprint, this correlation must be theoretically sound. Owing to the process of skin formation, the papillary junction (within which the internal fingerprint is contained) and the stratum corneum (within which the surface fingerprint is contained) have identical topographical properties.

There is no commonly accepted theory to explain the formation of fingerprints. One widely accepted theory attributes the formation of fingerprints to the difference in skin layer growth rates: the growth rate of the epidermis differs from that of the dermis, resulting in a compression stress at the papillary junction and a folding toward the dermis. Another theory argues that the layout of the nervous system in the fingertip skin is the source of fingerprints, but is not as widely accepted [2].

An alternative theory is that the papillary junction grows with ridges and valleys to increase the surface area contact between the epidermis and the dermis. However, in all cases, the ridges and valleys form in the papillary junction and propagate to the surface, resulting in what is known as the surface fingerprint [3]. Thus, the papillary junction is the source of the surface fingerprint. It is this fact that is exploited in the extraction of the internal fingerprint.

The emergence of the internal fingerprint in a subsurface layer of skin has great potential as it is protected from the effects of distortion during the scanning process (OCT is touchless), resistant to damage, and resistant to spoofing (an intentionally malicious attempt to circumvent a fingerprint acquisition device). However, the use of OCT poses challenges. The limitations of this technology will now be outlined.

1.4 Limitations and Hardware Constraints

OCT was not designed for the express purpose of internal fingerprint acquisition. Current general purpose OCT systems are cumbersome and expensive. However, the intention of this research is to provide a robust proof-of-concept internal fingerprint extraction technique as a precursor to the possible development of specialised OCT hardware.

The OCT scanner used is limited as follows:

1. The scanner is: large, immobile, and expensive.

2. The scanner requires an external system for processing and uses proprietary software.

3. The scan is performed from the top down and requires the scanned region to face upwards; which makes fingertip scanning awkward.

4. The scanned region is not easily visible during scanning. Although it is possible to use an infra-red calibration card, accurate scanning of the correct region is a challenge.

5. The scanned region is limited to $15mm \times 15mm$.

6. The scanning process takes approximately ten to fifteen seconds at a resolution of 512×512 *pixels* (the highest resolution used for this research). This is not a viable scanning time for the acquisition of a biometric. Furthermore, the scanned area must be kept as steady as possible during the scanning process – this is not always possible for humans to accomplish.

7. Speckle noise is induced through the scanning process.

8. Although the papillary junction is relatively reflective when compared to the dermis and epidermis, the contrast is still limited and low.

Overcoming most of these challenges is outside the scope of this research. Instead, dealing with the problems related to signal and image processing is pursued. Specifically, the low contrast and noisy images output from the scanner are considered to originate from a 'black box' scenario. As long as the scanner used provides an OCT scan of a fingertip, an internal fingerprint can be extracted. This means that the solution is not hardware specific and provides motivation to build an OCT system specific to the task of internal fingerprint acquisition.

Therefore, the challenges this research overcomes are:

1. Reducing noise in OCT scan images.

2. Improving contrast of the papillary junction.

3. Accurately determining the region where the internal fingerprint can be found.

4. Extracting the internal fingerprint.

The following section serves to provide context to the problems addressed in this research.

1.5 Problem Context

Biometric identification has become paramount to security, digital privacy, and access control. The authenticity and efficacy of biometrics are constant concerns that need to be addressed by inventive biometric solutions. Improving on the established and widely accepted biometric of fingerprints is a means to this end. A number of biometric identification solutions exist and are certainly comparable to fingerprints. However, fingerprints are used extensively as they are relatively non-invasive (compared to an iris scan, for example) and perform well regarding universality, distinctiveness, and false rejection and acceptance rates [4].

Although these advantages present a strong case for fingerprints as a biometric identifier, the security and reliability of surface fingerprints is known to be lacking for the following reasons [4, 5]:

1. Owing to the elasticity of the skin and varying pressure during each acquisition process, surface fingerprints are subject to distortion.
2. Any surface skin damage affects fingerprint quality and thus reduces matching capability. For example, individuals employed in heavy duty industries are often without usable fingerprints.
3. Owing to the two-dimensional (2D) representation of topographical information in a surface fingerprint scan, fingerprint spoofing is an easy task and requires only a few inexpensive household items [6, 7].

The aim of this research is to overcome the shortcomings of the surface fingerprint. This is accomplished by showing the viability of the internal fingerprint through the development of an internal fingerprint extraction algorithm.

1.6 Thesis Statement

Surface fingerprints rely on a 2D imaging of surface skin. The 2D representation gives rise to the potential for distortion, damage, and fingerprint spoofing. 3D surface fingerprint imaging with 2D unwrapping [8], and multi-spectral fingerprint imaging [9] are examples of solutions designed to compensate for these disadvantages. However, these still remain limited to the surface fingerprint. To circumvent fully surface fingerprint disadvantages, a new approach must be taken.

This research images the subsurface layers of the fingertip skin in a three-dimensional (3D) fashion. Between the epidermis and dermis is an intermediary layer of skin known as the papillary junction. This junction layer has the same structural characteristics as the skin surface (i.e., ridges and valleys). The emergence of this structure in the papillary junction results in the existence of the internal fingerprint. The imaging of subsurface skin layers is accomplished using OCT [10–15].

Lui and Chen [11] demonstrated the potential to capture the internal fingerprint using OCT. Bossen *et al.* [12] have provided a proof-of-concept extraction of the internal fingerprint from OCT scans, while da Costa *et al.* [13] strengthened this hypothesis while evaluated fingerprint deformation using OCT. Zam *et al.* [14] also showed how an internal fingerprint can be extracted and, in addition, showed that the capillary pattern yields yet another biometric and possible liveness-detector. Harms *et al.* [15] obtained greater resolution OCT scans and further exemplified the possibility of extracting an internal fingerprint.

However, the internal fingerprints obtained, in almost all cases, are low-quality and have never been shown to be a viable replacement for current surface fingerprints. This is largely because of the techniques used for extracting the internal fingerprint. Either OCT images are averaged over a pre-determined and manually chosen region, or a single slice is chosen that coincides with the internal fingerprint.

The gap this research endeavours to fill, is that of providing an approach to internal fingerprint extraction sensitive to the data most pertinent to the internal fingerprint itself. The key issue confronted, is that of accurately determining the location of the papillary junction. The upper-edge of the papillary junction is rich in fingerprint structural information as it undulates with the same topography as the surface skin. Its precise location

is an asset that has been ignored, but will be used to extract the internal fingerprint from an OCT fingertip scan.

1.6.1 Primary Research-questions and Hypotheses

In order to accomplish the task of obtaining a high-quality internal fingerprint, the following research-questions are asked:

1. Does the internal fingerprint exist?
2. Can the internal fingerprint be extracted from an OCT fingertip scan?
3. Does the internal fingerprint correspond to the surface fingerprint?
4. Is the internal fingerprint of sufficient quality?
5. Can the location of the papillary junction be determined accurately?
6. Can the signal relating to the papillary junction be enhanced?
7. Does image enhancement improve papillary junction detection accuracy?
8. Can the papillary junction location be used to extract the internal fingerprint?
9. Can the internal fingerprint be enhanced?

Hypotheses corresponding to these questions are stated as follows:

1. The internal fingerprint is described by the undulations (i.e., ridges and valleys) of the papillary junction. This will be evaluated by extracting internal fingerprints as this undulating region.
2. The internal fingerprint can be extracted from an OCT fingertip scan because the reflectivity of the papillary junction is relatively higher than the layers of skin surrounding it. This will be tested by internal fingerprint extraction.
3. The internal fingerprint corresponds with the surface fingerprint because the topography of the papillary junction propagates through the epidermis to the surface, resulting in the surface fingerprint. This will be tested by assessing the matching correspondence between the internal fingerprint and corresponding conventional counterparts.

4. The internal fingerprint is of high-quality as it is not subject to the same damage and distortion as the surface fingerprint. It can be imaged effectively, using an OCT scanner. Internal fingerprints and corresponding surface counterparts will be both quantitatively and qualitatively compared to test this hypothesis.

5. The location of the papillary junction can be determined accurately because of the inherent physical structure of skin layers and, thus, the unique brightness and thickness of the papillary junction. This will be tested by comparing an automatic detection with a ground-truth estimate of the papillary junction location.

6. The papillary junction can be enhanced using existing techniques because they are suited to problems with similar characteristics. Enhancement procedures will be applied and the resultant papillary junctions will be qualitatively assessed.

7. Image enhancement improves papillary junction detection because the papillary junction edges are made distinguishable in this manner. Edge detection will be assessed by evaluation the papillary junction location on raw OCT image slices.

8. The papillary junction location can be used to extract an internal fingerprint because this information is directly related to the ridges and valleys present in the fingerprint. If the internal fingerprint can be extracted, this will hypothesis will be accepted.

9. The internal fingerprint can be enhanced because the noise type and distribution is well known and sufficient signal information is retained during extraction. Earlier research into which noise reduction technique is best will be done and the enhanced internal fingerprints' performance will be tested.

Novel internal fingerprint zone-detection and extraction techniques are developed, in this research, to answer these questions and test these hypotheses. The internal fingerprint performance is tested using fingerprint quality assessment criteria. In addition, correlation with the surface fingerprint and internal fingerprint cross correlation is quantified. The research design will now be outlined.

1.6.2 Research Design

Similar to X-rays, ultrasound, and magnetic resonance imaging (MRI), OCT is a tomographic imaging technique: it results in a series of 2D image slices, known as B-scans. In the case of this research, each B-scan captures a cross-section of the fingertip skin and consists of a number of columns, known as A-lines (1D signals). The papillary junction is relatively reflective and results in a brighter region. This region usually manifests as intensity local maxima in the A-lines, but this is not guaranteed to be the case.

The location of the papillary junction is paramount to the process of internal fingerprint acquisition. This is because the papillary junction contains all the information, regarding the ridge and valley structure, that defines the internal fingerprint. It is the papillary junction upper-edge that describes the internal fingerprint topography. Thus, the undulations of the papillary junction upper-edge represent the internal fingerprint zone.

An approximate detection of the internal fingerprint zone is done per OCT volume using clustering. Speckle noise is inherent in OCT [16] and decreases the contrast and clarity of the papillary junction. Therefore, noise-reduction and contrast-enhancement are used to fine-tune the clustering results. This produces a set of 2D coordinates that describes the depth of the internal fingerprint zone throughout an OCT fingertip scan.

These coordinates are then used to extract the internal fingerprint. Localised *en-face* slice averaging is performed: each pixel in the internal fingerprint is the result of averaging a dynamic number of pixels per A-line. '*En-face*' means that the averaging occurs orthogonal to the fingerprint itself. The region, in each A-line, over which to average is determined using a windowed statistical evaluation of the internal fingerprint zone.

Testing this approach and the efficacy of the internal fingerprint is two-fold. First, the internal fingerprint itself is tested. The quality of the internal fingerprint is compared to that of the surface fingerprint using existing fingerprint quality assessment metrics. Furthermore, a fingerprint matching algorithm is applied to give an indication of the similarity and correlation between surface and internal fingerprints, as well as correlation between internal fingerprints from the same finger. Second, components of the techniques developed are tested using relevant quantitative assessment metrics alongside qualitative assessment.

1.7 Thesis layout

This thesis will give insight into current relevant research; provide a detailed description of the approach developed; and give the results and conclusions drawn through comprehensive testing. It is structured as follows. Related literature can be found in Chapter 2. The methodology and implementation thereof are detailed in Chapter 3 and the experimental set-up is outlined in Chapter 4. Results are discussed in Chapter 5. Conclusions drawn are given and future work is suggested, in Chapters 6 and 7, respectively.

To accomplish the task of internal fingerprint extraction from OCT fingertip scans, relevant literature was first reviewed and OCT contextualised therein. The following chapter details the associated literature.

Chapter 2

Related Work

Work related to the internal fingerprint is scarce as this is a new area of research. Thus, this chapter will serve to create a historical context for using OCT in biometrics and review literature directly associated with the task at hand. Current surface fingerprint sensor technology is outlined in Section 2.1 to highlight the need for an alternative. Following this, OCT is introduced to the reader as it was introduced to the world: through its use in diagnostics (Section 2.2). The first applications of OCT were in ophthalmology (the study concerned with diagnosis and treatment of ocular diseases). Work related to this field is reviewed in Section 2.2.1.

Owing to the low imaging penetration of OCT in most biological tissue, the next field in which OCT was used on a widespread basis is that of dermatology (the diagnosis and treatment of skin diseases and disorders). Without the advances of OCT technology by virtue of its demand and use in dermatology, imaging of the fingertip would not be possible. Relevant works in this area are outlined in Section 2.2.2.

After its history has been examined, OCT for imaging the human fingertip is reviewed. Literature associated with OCT in fingerprint biometrics is reviewed in Section 2.3. This provides direct context for the research undertaken in this thesis, and will be used to highlight the successes and shortcomings of the current work in fields relating to the internal fingerprint. Other closely related works include OCT for fingertip skin analysis, for fingertip skin deformation, and for document security. These will be reviewed in Section 2.4. Several foundational related publications from the authors will be discussed in Section 2.5. The following section is a review of current fingerprint technology.

2.1 Current Fingerprint Technology

The two main sensor technologies used to obtain a surface fingerprint are optical and capacitive sensors. Optical sensors work by applying a light source (usually an LED) to a sample placed on a glass surface. The reflection is measured using either a charge-coupled device (CCD) or a complementary metal–oxide–semiconductor (CMOS) based optical imager. Optical sensors are sensitive to external light and, furthermore, fingerprint quality is affected by surface contamination (such as scratches or dirt).

Capacitive scanners use an array of small capacitative plates upon which the sample is placed. The measured output capacitance is dependent on the distance to the skin surface. For this reason, ridges and valleys result in different measured capacitances. They are insensitive to light conditions and are not easily affected by surface contaminants. However, they are sensitive to very dry skin and fail when the skin is too wet.

Although there have been attempts to make these technologies more secure, optical and capacitative fingerprint sensors remain easy to spoof as they measure easily replicated quantities (differences in reflectance and capacitance). Moreover, the need for surface contact is unsatisfactory as it lends itself to fingerprint distortion and quality degradation from contaminants [4, 17, 18]. OCT has the advantage of being a touchless technology. Another advantage that OCT has over current fingerprint sensor technology is resolution. Modern commercial surface fingerprint scanners obtain a fingerprint of roughly 500 *pixels per inch* (*ppi*), while the internal fingerprints captured in this research have a resolution of up to 1300 *ppi*.

Other sensor technologies include thermal sensors, pressure sensors, low radio frequency sensors, and ultrasonic scanners [17]. All of these have their advantages but have never become widely used as they have significant disadvantages. For instance, even though ultrasonic sensors are able to image a subsurface fingerprint, they are slow, require surface contact, and image at much lower resolutions than OCT. However, a technology that is becoming popular and successful is multi-spectral fingerprint imaging.

Rowe *et al.* [19] first introduced multi-spectral fingerprint imaging as a solution to extract the internal fingerprint as a 2D representation. Using different wavelengths of light, different lighting conditions, and different polarizations, an array of fingerprint images were obtained. By combining multiple images they were able to enhance fingerprints

from an optical sensor [20]. When considering false rejection and acceptance rates, fingerprints obtained using multi-spectral imaging were shown to be of higher quality. An advantage of using multi-spectral imaging is the access to subsurface layers of skin. Information pertaining to subsurface layers was used for liveness-detection. By using surface penetrating light, the internal fingerprint was also imaged. A comparison of the internal and surface fingerprints was used for spoof-detection [21]. A major disadvantage of this approach to fingerprint acquisition is the 2D capture and representation: it does not make a cross-sectional analysis of subsurface skin [22]. Multi-spectral imaging is still limited regarding fingerprint quality, is complex, and is expensive [4].

OCT presents solutions to problems faced in fingerprint acquisition. It is touchless, provides relatively high resolution images, and images in 3D. Without the advent and rise of OCT in the field of medicine, the technology would not have existed and advanced to the point at which it has potential in biometrics. For this reason, the following section will serve to historically contextualise OCT.

2.2 OCT in Medicine

OCT is primarily used in biomedical applications. Huange *et al.* [1] introduced OCT as an emerging technology and highlighted its application in medicine. OCT is particularly useful in ophthalmology as ocular media is relatively opaque and allows light to penetrate more deeply. Owing to the non-invasive imaging afforded by OCT technology, it is extensively used by ophthalmologists as a tool in diagnosis and treatment.

2.2.1 Ophthalmology

Swanson *et al.* [23] demonstrated the practical use of OCT in ophthalmology. They developed an OCT scanning device capable of 14 μm resolution *in vivo* scanning that took approximately 2.4 seconds per scan. At that stage, OCT was in its infancy and this technology was a break-through for diagnosis and monitoring of retinal diseases. High resolution imaging by OCT was important because the structure of the retina is on a micrometer scale. Existing imaging techniques could not image at this resolution. By coupling expert knowledge to OCT scans of the macula (an area near the centre of

the retina), Puliafito *et al.* [24] were able to show the potential strength of OCT in this field.

Drexler *et al.* [25] presented a new ultra-high-resolution OCT technology for use in ophthalmology. Earlier resolutions were in the 10-15 μm range, while their system could image at a resolution of 2-3 μm. This improvement meant structures of finer scales could be imaged and ocular related diseases could be diagnosed and monitored more consistently and accurately. The exciting potential of OCT meant that advances were continuous. It is currently a standard tool used in ophthalmology. However, since OCT works with light, it cannot be used to diagnose diseases that interfere with the transmission of light (such as cataracts).

2.2.2 Dermatology

Another well-established field in which OCT use has become commonplace, is dermatology. The advances of OCT in this field have a direct bearing on the quality of OCT scans used for internal fingerprint acquisition. Most of dermatology is visual as the majority of skin ailments present themselves with characteristics on the surface of the skin. However, the investigation of cellular changes (such as the growth of tumours and subsurface skin alteration because of topical creams) typically required invasive biopsies. A non-invasive diagnostic was thus highly advantageous but other cross-sectional imaging technologies could not provide the required resolution [26]. OCT was able to provide a high-resolution cross-section of the skin.

During the establishment of OCT as a tool in dermatology, Welzel [26] conducted a review, highlighting OCT's efficacy for diagnosis of skin-related diseases. A contribution of this review was the construction of a commercially available OCT scanner that could scan skin at a resolution of 10 - 15 μm. Using the variables of relative layer thickness, intensity of signal, and light attenuation changes, a large number of skin properties could be deduced. The imaging of skin tumours was shown to be possible, but limited by the low penetration depth of OCT. The relative depth of the stratum corneum versus the papillary junction provided information on inflammatory diseases. Furthermore, OCT was able to provide valuable information pertaining to the effects of skin moisturisers (by measuring skin layer thickness) and the progress of skin treatments. OCT was also found to be non-invasive, safe, and without side-effects.

Pierce *et al.* [27] published findings related to advances in OCT for dermatology. They designed and built a portable OCT system capable of capturing three types of OCT images: structural, polarization-sensitive, and flow-sensitive. Polarization-sensitive OCT images measure the phase change of reflected light owing to differences in refractive index. Flow-sensitive OCT images are captured by measuring the Doppler effect of returning light – any associated flow alters the wavelength of reflected light. Both polarization- and flow-sensitive images were able to provide a useful contrast when compared to conventional structural OCT images. A significant advance over other OCT systems was the low capture-time: all three image types were captured simultaneously within one second. Furthermore, a deeper imaging depth of 1.4 mm was obtained. The usefulness of these technological advances were shown. For instance, flow-sensitivity was used to show the reduction in blood flow to cancerous cells during treatment.

A later work by Gambichler *et al.* [28] demonstrated the success of OCT in dermatology by providing a comprehensive review of current technology. They argued that the introduction of OCT in ophthalmology led to interest in its potential, eventually resulting in its widespread success as an industry standard for both ophthalmology and dermatology. Since OCT is able to provide structural and blood-flow information of the skin, it has become widely used for diagnosis and monitoring of skin diseases. Simultaneous diagnosis and monitoring of the following diseases was discussed and demonstrated: psoriasis (chronic inflammation), chronic dermatitis, lupus, various blistering, carcinomas and melanomas, lesions, and infections.

It is the need and presence of advances in technology that has resulted in the availability of OCT for broad use. OCT for fingertip scanning and internal fingerprint acquisition is historically contextualised by the advances in biomedical fields. Its subsequent use in the field of biometrics will now be discussed.

2.3 OCT in Biometrics

Matsumoto *et al.* [6] highlighted the worrying lack of security measures and liveness-detection in commercial fingerprint scanners. Their study intended to make known the simplicity of constructing a fake fingerprint that was able to fool a range of optical and capacitive fingerprint scanners. The process of making 'gummy' fingerprints from residual

fingerprints (an imprint on a glass surface, for example) was outlined. Performance was tested using eleven commercially available fingerprint scanning devices. Although the fake fingerprints had lower acceptance rates than that of the real counterparts, they still performed well enough to repeatedly fool most devices. It was proposed that if various liveness measurements were conducted, fake fingerprints could be rejected. However, although liveness-detection has come a long way since that study (with research into wavelet based liveness-detection [9], for instance), the fundamental issue remains: the 2D imaging and representation. The 3D, cross-sectional imaging capability of OCT has led to better liveness-detection propositions and solutions.

2.3.1 Liveness-Detection

Cheng and Larin [29] proposed an artificial fingerprint recognition system using OCT technology. They assume a fake fingerprint will always present purely homogeneous depth-resolved signal characteristics, whereas real fingertip skin is highly inhomogeneous but repetitive in a cross-sectional analysis. Real layers of skin differ in brightness but do so consistently over the entire fingerprint region. This difference in homogeneity was used as input for autocorrelation analysis. A-lines were analyzed for cross-correlation to identify the presence of fake fingerprints. An example of the analysis performed can be seen in Figure 2.1. A real finger exhibits a greater change in gradient in the autocorrelation analysis.

Autocorrelation yielded noticeably different results for fake and real fingerprints; but no attempt was made to recognise automatically this deviation. A disadvantage of this approach is the assumption that each skin layer will always be found at the same depth over an entire three-dimensional OCT scan. This assumption allowed for lateral averaging prior to signal analysis but certainly does not hold true for the case of touchless scanning. Although it is not directly evident, the use of lateral averaging (as well as the fingertip images presented in the work) strongly suggest the use of a surface on which the finger was placed during scanning. The result was uniformity in skin layering. However, the full capability of OCT as a touchless system was not used.

Nasiri-Avanaki *et al.* [30] used an *en-face* OCT system capable of dynamic focus to show its suitability to identifying additional layers on the skin. In their study, sellotape was applied on the fingertip skin prior to imaging. Although the presence of data useful to

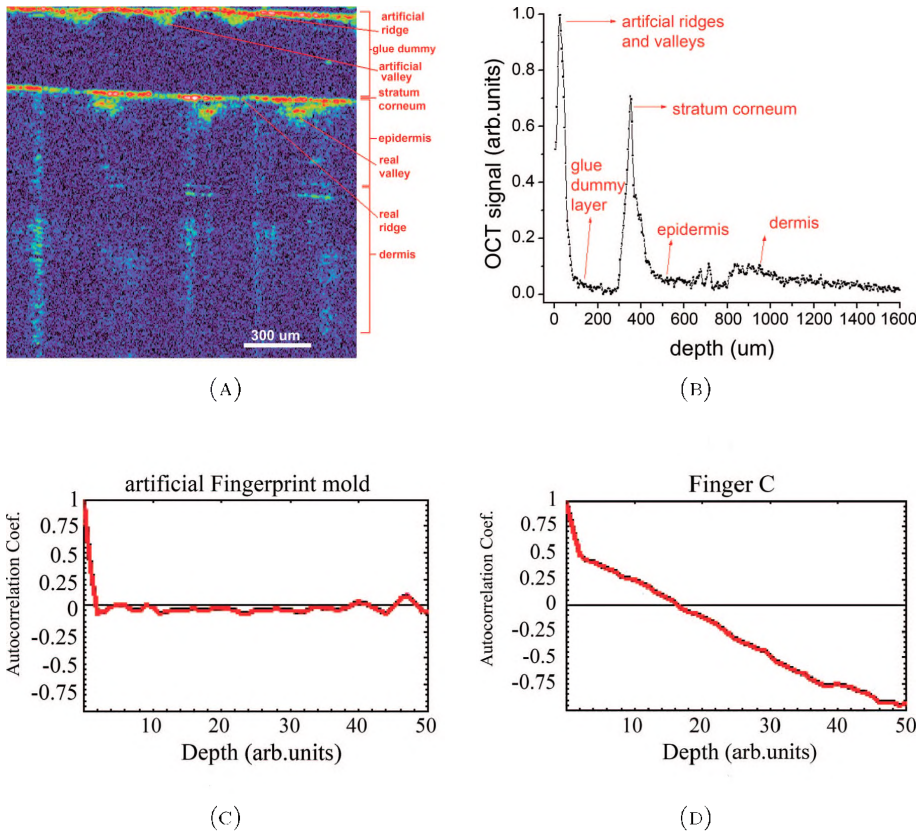

FIGURE 2.1: **Artificial fingerprint recognition using autocorrelation analysis.** (A) shows an OCT scan of a finger with an artificial fingerprint over it. (B) is the depth resolved one-dimensional signal. (C) is the result of autocorrelation analysis of the artificial fingerprint region, while (D) is the result of analysis of the real skin region. This figure was taken from Cheng and Larin [29].

liveness-detection was demonstrated, no liveness-detection scheme was developed. The potential of OCT for secure applications was made evident through earlier research such as this. However, the research presented in this thesis serves to demonstrate a robust means of extracting the internal fingerprint, the use of which may even circumvent the need for detecting fake fingerprints.

Another example of fake fingerprint detection can be seen in the work by Meissner *et al.* [31]. They argued that fake fingerprint detection on 2D surface scans is insufficient. Therefore, a manual approach to fake fingerprint detection was conducted on a large dataset of OCT fingertip scans, with a success rate of almost 100%. Fake fingerprint detection, in this manner, was two-fold: (1) qualitative identification of an additional layer and (2) identification of sweat glands. Cross-sectional OCT images revealed the presence of helix-shaped sweat glands between the stratum corneum and the papillary junction. These were not present in fake fingerprints. Automatic classification resulted

in fake-fingerprint detection of 74%. No details on the automated process were given and improvements are clearly necessary. An additional finding, relevant to internal fingerprint acquisition, was the obfuscation of the papillary junction owing to the presence of fingerprint fakes: the reflectivity of the papillary junction was made void by an extra layer of reflective material. This is relevant because under such circumstances the internal fingerprint cannot be extracted. However, if an additional layer is detected, the fingerprint need not be extracted.

OCT clearly has potential in the fields of liveness- and spoof-detection. OCT scans used for spoof-detection almost always contain information pertaining to the internal fingerprint. When compared to internal fingerprint acquisition, liveness-detection using OCT is a relatively simple task. The acquisition of a high-quality internal fingerprint is complex, but since its topography is not influenced by the presence of additional surface layers, it is a highly attractive solution to fingerprint-spoofing. For this reason, it is more relevant to focus on the internal fingerprint. Work related to internal fingerprint acquisition from OCT scans will now be detailed.

2.3.2 Extracting the Internal Fingerprint

Bossen *et al.* [12] provided one of the first examples of internal fingerprint extraction. They scanned 51 individuals' right index fingers three times each. Fingers were placed on a glass plate during scanning. Although this allowed for more control of the scanned region, it did not make use of the touchless capability of the OCT system. A manually determined region, that roughly described the papillary junction, was extracted and XY-plane (i.e., the same plane as the fingerprint) image slices were averaged, resulting in a poor-quality internal fingerprint. In fact, 36% of the scan data was used in the averaging process. Since it is the upper-edge of the papillary junction that contains rich fingerprint information, much of the contributing data was redundant and only served to reduce the internal fingerprint quality. This was recognised by the authors. However, notwithstanding this poor technique, identification against a fingerprint database showed the internal fingerprint to perform well: no false positives and only nine percent of the extracted fingerprints remained unmatched. The constructed database consisted of internal fingerprints only. Inconsistency of results was attributed to the small size of the imaged area. No testing was carried out to draw correspondence between the surface

and internal fingerprints. The successful use of the internal fingerprint for identification indicates that it can replace, or work concurrently, with current surface fingerprints. However, since no comparison was made between surface and internal fingerprints, no conclusions could be drawn regarding the integration of OCT fingerprints into existing surface fingerprint databases.

Korohoda *et al.* [32] developed a technique for obtaining internal fingerprints. Their algorithm was sensitive to the papillary junction upper-edge. They analysed the difference between a (damaged) surface fingerprint and the corresponding internal fingerprint, drawing conclusions about surface to internal fingerprint correspondence and the superiority of the internal fingerprint. The technique for detecting the stratum corneum and papillary junction upper-edge was carried out on B-scans and consisted of: (1) reducing noise using a median filter; (2) applying the Sobel [33] operator to detect edges; (3) detecting the pixels above some heuristically determined threshold; and (4) enhancing the detected stratum corneum and papillary junction depths (i.e., 2D signal) to represent the surface and internal fingerprints, respectively. Their technique was optimised for a single OCT fingertip scan. They used a glass slide during scanning to simplify internal fingerprint extraction, thus mitigating the essential touchless advantage of OCT. To detect the edge-processed pixels corresponding to the internal fingerprint, a search was commenced that started at a fixed region below the stratum corneum. This approach was not assured to be robust, although the authors did identify this fault. A disadvantage of this work is that the algorithm developed cannot be considered robust and successful as it was tested on one dataset only. Furthermore, noise-reduction was carried out on all the B-scans: an inefficient approach as this is a lengthy process.

Sousedik and Busch [34] contended with the issue of OCT scan quality regarding internal fingerprints. They developed a new algorithm for detecting skin layers. The stratum corneum and papillary junction were detected by identifying high-intensity sample points for each. Smooth surfaces were fitted to the data clusters using a back propagation neural network, trained to represent smooth surfaces as a function. Since a neural network's performance is hindered by outliers, a training technique was used where anomalous data points were removed iteratively. There was no attempt to optimise the quality of the fingerprints. Instead, the focus was layer identification for the purpose of authenticity-detection. A large dataset was used to show the success of their approach.

The following section details further advantages and technological advances that OCT affords fingerprint biometrics.

2.3.3 Extending fingerprint biometrics

Another advantage of internal fingerprints is the level of detail available. Fingerprint features are described in a hierarchical order with respect to detail: level one refers to the pattern of the fingerprint; level two refers to minutia points; and level three are finer details such as pores. Although level three features carry significant biometric information and can improve fingerprint matching significantly [35], surface fingerprint scans rarely possess level three details.

Liu and Buma [36] showed that OCT has the potential to provide level three fingerprint detail. By providing a biometric mapping of the sweat glands that exist between the papillary junction and the stratum corneum, they showed the presence of high-quality and high-contrast level three features. Furthermore, they also demonstrated the presence of the internal fingerprint in the papillary junction. Since the scans were touchless, a 'digitally straightened' version of the scanned volume was produced by normalizing the natural curvature of the skin. This was accomplished by fitting a third-degree polynomial to the stratum corneum (for each B-scan) and adjusting the images accordingly. Further details of this process were not given. Following this preparation, the region containing the internal fingerprint was manually determined and XY-plane image slices were averaged to produce the internal fingerprint. This is an inefficient technique that limits the quality of the internal fingerprint. Although it is not an aim of this thesis to make use of level three fingerprint features, their presence in, and ease of acquisition from, OCT fingertip scans further serves to warrant the use of this technology as a tool for fingerprint imaging.

OCT possesses another characteristic useful to high-security biometrics: Doppler OCT. In this manner blood flow can be imaged and recognised. Liu and Chen [11] used Doppler OCT for liveness-detection. The premise was simple: a live finger has blood flowing through the capillaries below the papillary junction, while a fake does not. Although they made no attempt at automatic liveness-detection with this information, revealing the potential of Doppler OCT for liveness-detection was pertinent. Furthermore, the correlation between the capillary structure and the papillary junction structure means

the blood flow patterns detected are unique and can be used as a further level of biometric detail in the future.

Zam *et al.* [14] demonstrated the feasibility of correlation mapping OCT (cmOCT) for fingerprint biometrics. Correlation mapping involved determining the correlation between two neighbouring OCT slices. The time delay between slices and blood flow measurements allowed for the vascular network to be mapped. Using cmOCT, they demonstrated a new means of liveness-detection by overlaying the internal fingerprint, the sweat-gland pattern, and the vascular network. Two live human thumbs were imaged at two instances, three months apart. This tested consistent correlation over time. Scans were taken with and without blood flow occlusion. Liveness-detection was accomplished by a human observer and was not entirely successful. However, the potential of cmOCT for liveness-detection is evident. They did not attempt to optimise the quality of the internal fingerprint. Detail was not given regarding the extraction process.

2.3.4 *En-face* OCT

OCT can be utilised to image the internal fingerprint in 2D directly, instead of through extraction from a 3D OCT scan. Conventional OCT scanners provide image slices orthogonal to the fingerprint, with which a 3D reconstruction can be made, and a 2D internal fingerprint can be extracted. However, advances in OCT technology [37] have resulted in *en-face* 2D OCT. This means that scanning can occur along a plane that is parallel with the fingerprint itself. The main advantage is that a single image is obtained and no extraction is necessary. Harms *et al.* [15] make use of such technology and show its potential for fast internal fingerprint acquisition. Issues with this approach are: that the fingertip skin is not uniformly straight; the internal fingerprint is not found at a fixed depth; and detail is lost when using this technique as a single slice is inefficient at capturing the internal fingerprint. The dynamic focus approach developed by Nasiri-Avanaki *et al.* [30] attempted to compensate for these problems, but they were nevertheless unable to yield high-quality and high-contrast internal fingerprints.

Current techniques for extracting an internal fingerprint are limited by the approach taken and with respect to the quality of the extracted fingerprints. This is mainly owing to a lack of definition regarding the location of information pertinent to the fingerprint. Instead of settling for a manually determined region, the research outlined in this thesis

endeavours to locate the papillary junction accurately and improve the quality of the internal fingerprint.

OCT as a technology is useful to a range of medical and research areas. Some of these uses have bearing on either the presence of the internal fingerprint, or other fingerprint biometric characteristics. These will now be discussed.

2.4 Other related uses for OCT

Shiratsuki *et al.* [38] made use of OCT to evaluate the characteristics of skin tissue under fingerprints. This was one of the first instances where OCT was used in the context of fingerprints. Their work yielded a novel fingerprint sensor. The set-up used a LED transmitting at 660 *nm* through the fingertip (from the nail side). The transmitted light revealed the fingerprint pattern as seen from under the skin and was imaged using a conventional CCD. The influence of fingerprint obscuring wrinkles was shown to decrease significantly. The system was successful in the case of touchless scanning and scanning when the finger is depressed on a glass plate. Although no attempt was made to obtain the internal fingerprint (that which exists in the papillary junction layer), this research revealed OCT as a tool for skin structure analysis.

Chang *et al.* [22] not only showed OCT's potential for spoof-detection, but also introduced the concept of an 'info chip'. An info chip is a multi-layered device constructed from some form of media OCT is able to penetrate. The OCT scanner was used to image individual layers and, in this manner, extract information from each. They demonstrated its use with a four layer sample as well as a fingerprint dummy. OCT was able to image both the dummy and the real fingerprint. Since OCT is able to image on the micrometer scale, an information carrying chip can be made small. OCT is still too costly to be a solution for document and identity security in this manner.

Da Costa *et al.* [13] evaluated fingerprint deformation using OCT. They constructed fingerprint deformation metrics based upon minutiae orientation and ridge-frequency analysis. By varying and measuring pressure with which the scanned fingers were applied to a glass plate, they were able to draw conclusions on the differences in fingerprint deformation between surface and internal fingerprints. Although the results obtained were widely inconsistent and the tested fingers were few, the study indicated that the

surface fingerprint is more subject to distortion and deformation than the internal fingerprint. Although the internal fingerprint is shielded by the epidermis layer of skin and, therefore, is less affected by surface pressure applied, it is still subject to significant deformation.

The following section serves to present earlier research by the author of this thesis. These works served as foundational components of this research.

2.5 Foundation for this thesis

A review of state-of-the-art speckle reduction techniques for optical coherence tomography fingertip scans [39] presented speckle noise as a problem specific to the domain of internal fingerprint extraction. Speckle noise is a product of OCT and arises when there are reflective elements of roughly the same size as the imaging wavelength. It is multiplicative and obscures the signal content. Six noise reduction techniques were evaluated. Three quantitative assessment criteria were used, namely the signal-to-noise ratio, the mean-squared-error, and the structural similarity. The optimized blockwise non-local means (OBNLM) algorithm was found to be the best technique for speckle noise reduction. The research presented in this thesis makes use of the OBNLM algorithm.

The above-mentioned research was followed by an assessment of fingerprint enhancement on the extracted internal fingerprint [40]. Heuristic techniques were used to locate the papillary junction in OCT image slices and various enhancement techniques were evaluated regarding their impact on the extracted internal fingerprint. The contrast improvements on the internal fingerprint, owing to the application of enhancement techniques on constituent image slices, evidenced OBNLM followed by unsharp masking as the best candidates. Unsharp masking is a contrast enhancement procedure that involves comparing an image to its blurred counterpart, and thus improving edge clarity. However, it was found that anomalies were introduced to the internal fingerprint. Thus, no enhancement procedures are applied prior to fingerprint extraction. Instead, regarding the work presented in this thesis, the enhancement techniques explored are applied to the extracted internal fingerprint itself.

A critical component of internal fingerprint extraction is the detection of the papillary junction. This is because the papillary junction contains the internal fingerprint. The concept of internal fingerprint zone detection was a topic of earlier research [41]. K-means clustering was presented as a means to detect the papillary junction and a fine-tuning technique was used to isolate the upper-edge of the papillary junction. This technique is the foundation on which Section 3.1 is built upon.

Akhoury and Darlow [42] used a similar technique for internal fingerprint zone-detection. The internal fingerprint was extracted by mapping the 3D surface describing the papillary junction upper-edge to a 2D fingerprint. This is not the approach selected for this research as the testing database was not sufficiently large and the technique was too reliant on the performance of zone-detection. A detailed description of the technique is given in Section 3.2.

The reader is referred to the above-mentioned peer-reviewed publications for an encompassing description of the techniques reviewed therein. Furthermore, the techniques selected as a result thereof are expounded upon in Chapter 3. It is not the focus of this research to review all techniques for noise reduction or enhancement. This will be a future endeavour.

This chapter served to historically contextualise OCT by demonstrating its place in ophthalmology and dermatology. The natural divergence to fingerprint-based biometrics was explained and various examples of its use were given. From simple internal fingerprint extraction to advanced level-three biometrics and liveness-detection, it is evident that OCT suits this domain. There is, however, a large gap in this field. This was somewhat addressed in the foundational works by the author, as outlined in this chapter. Fully automatic internal fingerprint zone identification and description, and fingerprint extraction have never been addressed in a single comprehensive work. The research presented here fills that gap. The following chapter explains how this is accomplished.

Chapter 3

Methodology

The questions this research intends to address are best answered through the practical application of a proof-of-concept internal fingerprint acquisition system. All the research-questions posed and hypotheses stated in Section 1.6.1 are either directly answered by the demonstrative extraction of internal fingerprints, or depend upon the success of the extraction process. The method developed for internal fingerprint extraction is thus paramount, and is described in this chapter.

A system overview flowchart is given in Figure 3.1. Internal fingerprint extraction can be abstracted into two distinct parts: (1) internal fingerprint zone-detection and (2) localised fingerprint extraction. The former of these processes answers the question: where is the internal fingerprint? Answering this question constitutes the majority of the technical innovation involved in this research. A combination of machine learning algorithms, 2D-interpolation, speckle noise-reduction, image enhancement, and edge-detection are key to internal fingerprint extraction.

This chapter is structured as follows. Internal fingerprint zone-detection is detailed in Section 3.1. Sections 3.1.1 through 3.1.4 describe the intricacies of this process. Localised internal fingerprint extraction is discussed in Section 3.2. Sections 3.2.1 and 3.2.2 explain the mapping process, and internal fingerprint enhancement, respectively.

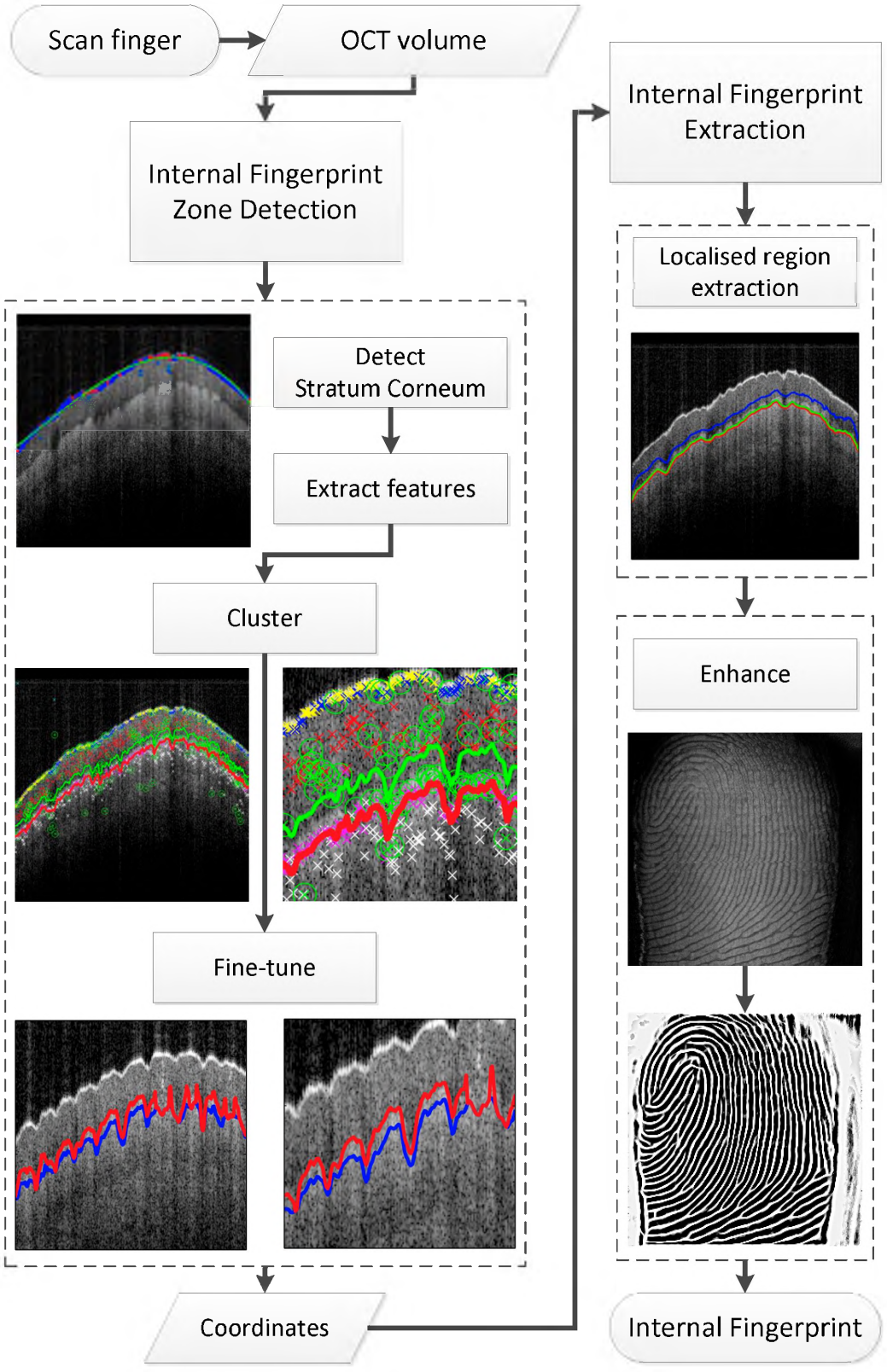

FIGURE 3.1: **System overview flowchart.** System components are expounded upon in later task-respective figures and algorithms, namely Algorithm 1 and Figure 3.3 for stratum corneum detection, the flowchart in Figure 3.2 for internal fingerprint zone-detection, and Algorithm 2 for fingerprint extraction.

3.1 Internal Fingerprint Zone-Detection

Figure 1.2 demonstrates the structure of skin layers in a single B-scan. The reflectivity of the papillary junction is higher than that of the epidermis, resulting in an edge. The undulations of this edge, referred to as the **papillary junction upper-edge** in this research, encapsulate the internal fingerprint topographical information. In addition, the internal fingerprint zone is entirely defined by this edge. Owing to the contrast present between the papillary junction and the epidermis, an estimation of this region allows for the extraction of an acceptable internal fingerprint. Earlier research usually involved a manual estimation of this region [11–15]. However, that approach is inaccurate and diminishes contrast; is not robust against noisy signal; and is not automatic.

Internal fingerprint zone-detection is arguably the most critical aspect of the research undertaken here. The approach developed by Khutlang and Nelwamondo [43] used novelty detection to locate the papillary junction upper-edge. Sousedik and Busch [34] used a neural network to fit a surface function to the papillary junction. These efforts did locate the papillary junction, but the detection of the internal fingerprint zone has never been accomplished to the degree of accuracy this research endeavours to achieve. Moreover, accurate knowledge of the location of the papillary junction upper-edge equates to accurate knowledge of the structure of the internal fingerprint. The performance of any internal fingerprint extraction depends upon this process. Certainty as to the location of the papillary junction upper-edge is directly related to the quality of knowledge regarding the internal fingerprint topography, and an accurate description of this topography is an accurate description of the internal fingerprint.

Papillary junction upper-edge detection is challenging for the following reasons:

1. The contrast of OCT scans is low.
2. OCT induces speckle noise. The origin and description of this noise is given in Section 3.1.4. Owing to the signal dependency of this noise, it is difficult to remove and has a negative effect on the clarity of the signal.
3. An OCT fingertip scan may result in some B-scans having nearly no useful data, or inconsistent skin layering. This is demonstrated in Chapter 5.

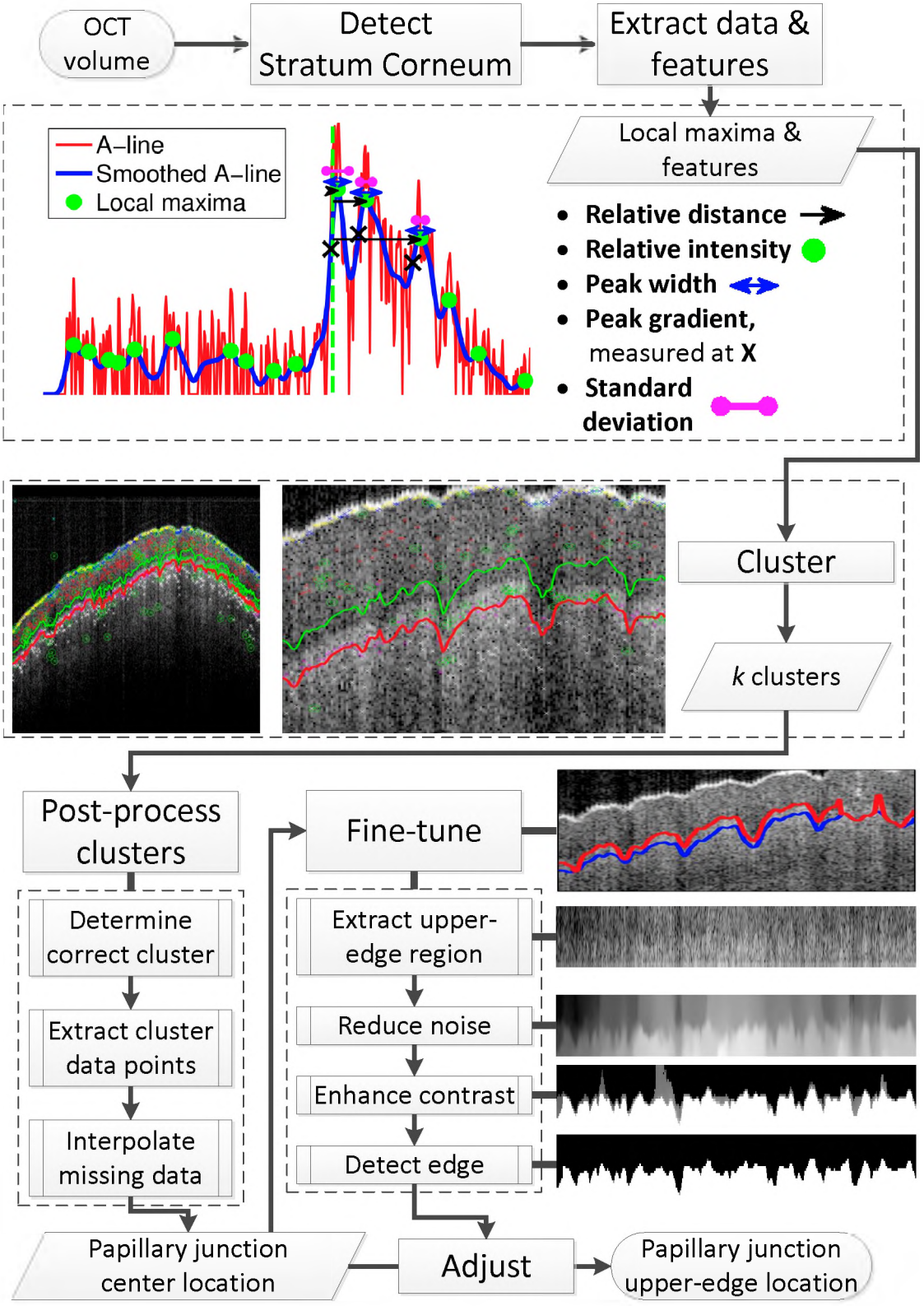

FIGURE 3.2: **Internal fingerprint zone-detection flowchart**. A detailed explanation of feature extraction can be found in Section 3.1.2; post-processing of cluster results is outlined in Section 3.1.3; and fine-tuning is discussed in Section 3.1.4. Note: local maxima heights are the origin of the relative intensity feature, hence their identical labelling.

Overcoming these challenges is accomplished through the application of clustering and image enhancement algorithms. The manner in which these are combined results in a robust, consistent, and accurate internal fingerprint zone-detection algorithm. The performance thereof is shown in Chapter 5.

A flowchart is given in Figure 3.2 to provide an overview of internal fingerprint zone-detection. The stratum corneum is first detected and used to extract features prior to clustering. The cluster determined to represent the centre of the papillary junction (the mid-point of the intensity peak exhibited in A-lines) is processed and used to extract small image regions containing the papillary junction upper-edge only. A fine-tuning approach is followed where image enhancement operations are applied to each of these image regions and the contained edge is detected. The clustering procedure and cluster output post-processing are explained in Sections 3.1.2 and 3.1.3, respectively. Fine-tuning is discussed in Section 3.1.4.

3.1.1 Stratum Corneum Detection

The presence and visibility of skin layers are assumed in an OCT fingertip volume. Earlier research has relied upon this assumption [29, 38]. This is a vital assumption to make as it is the relative reflectivity of skin layers that gives rise to the internal fingerprint. Although the structural layering of fingertip skin is useful, the automatic identification of these layers is largely an unsolved problem. In the context of this research, the location of the stratum corneum throughout an OCT fingertip volume is used for feature extraction. Feature extraction is outlined in Section 3.1.2.

Liu and Buma [36] fitted a third-degree polynomial to the stratum corneum per B-scan in order to normalise these scans for internal fingerprint extraction. Algorithm 1 extends this principle by keeping track of the previous B-scan's stratum corneum, and identifying and correcting for outliers. It works by detecting all column-wise intensity maxima in a B-scan and fitting a third degree polynomial to those (as per the shape of the fingertip). If an estimate exists from processing the previous B-scan (i.e., anything after the first B-scan), it is used in conjunction with the estimate from the fitted polynomial to find the closest column-wise (A-line) local maxima. Each A-line is smoothed (using a simple average blurring procedure) to minimise the impact of speckle noise. This smoothing is

Input: *OCT_volume*
Parameters: *poly_degree*, *smooth_window_size*, *intensity_thresh*, *distance_threshold*, *outlier_window_size*
Output: Stratum corneum coordinates
brightest_B_scan ← brightest[*OCT_volume*]
stratum_c_estimate_previous_B_scan ← zeros(length(*B_scan*))
stratum_c_coordinates ← zeros(length(*B_scan*), length(*B_scan*))
for *scan_i* ← 0 **to** *length(OCT_volume)* **do**
  B_scan ← *OCT_volume*(*scan_i*)
  intensity_thresh ← *intensity_thresh*/(*brightest_B_scan*/mean_2D(*B_scan*))
  samples_for_polyfit ← zeros(length(*B_scan*))
  for *i* ← 0 **to** *length(B_scan)* **do**
    A_line ← *B_scan*[*i*]
    if *max(A_line)* > *intensity_thresh* **then**
      samples_for_polyfit[*i*] ← indexof(max(*A_line*))
    end
  end
  stratum_c_poly ← polyfit(*samples_for_polyfit*, *poly_degree*)
  for *i* ← 0 **to** *length(B_scan)* **do**
    A_line ← *B_scan*[*i*]
    smoothed_A_line ← 1Dsmooth(*A_line*, *smooth_window_size*)
    local_maxima ← extrema(*smoothed_A_line*)
    estimate_from_poly ← *stratum_c_poly*[*i*]
    estimate_from_previous ← *stratum_c_estimate_previous_B_scan*[*i*]
    combined_estimate ← (*estimate_from_poly* + *estimate_from_previous*)/2
    distances_to_poly ← sqrt((*local_maxima* − *estimate_from_poly*)^2)
    distances_to_previous ← sqrt((*local_maxima* − *estimate_from_previous*)^2)
    distances_combined ← *distances_to_poly* + *distances_to_previous*
    closest_maxima_location ← *local_maxima*(indexof(min(*distances_combined*)))
    if *abs(closest_maxima_location* − *combined_estimate)* < *distance_threshold*
    then
      stratum_c_coordinates[*scan_i*, *i*] ← *closest_maxima_location*
    end
    else
      stratum_c_coordinates[*scan_i*, *i*] ← *estimate_from_previous*
    end
  end
  stratum_c_coordinates[*scan_i*, :] ← fix_outliers(*stratum_c_coordinates*[*scan_i*, :], *outlier_window_size*)
  stratum_c_estimate_previous_B_scan ← *stratum_c_coordinates*[*scan_i*, :]
end

Algorithm 1: Stratum corneum detection

not optimised, but that is not the focus of this work. It could, however, be explored as future research topic.

Sample points for polynomial fitting are determined by comparing intensity local maxima in A-lines to some threshold intensity. If the maximum of the considered intensity

profile is above this threshold, its depth is considered as a sample point. These sample points are used to estimate a polynomial that describes the stratum corneum contour (**PolyEstimate**).

This approach makes the assumption that the stratum corneum is the brightest peak within an A-line intensity profile. Since this is not guaranteed to hold true in all cases, it is not relied upon. To compensate for this, the stratum corneum detected for the previous B-scan is also considered (**PrevEstimate**). **PolyEstimate** and **PrevEstimate** are combined to give the stratum corneum estimate (**SCEstimate**). The Euclidean pixel-distances from each local intensity maximum in each A-line to the **SCEstimate** is calculated. This gives an indication of 'how far' each local maximum is from the **SCEstimate**. If the closest local maximum is within a pre-defined distance, it is considered to describe the stratum corneum. If not, **PrevEstimate** defines the stratum corneum location for the respective A-line.

Outliers are detected in a windowed region using the interquartile range rule [44]. They are replaced by the median of the windowed region. Although this is not a perfect solution, it is robust enough to serve for feature extraction. Figure 3.3 provides an example of stratum corneum detection.

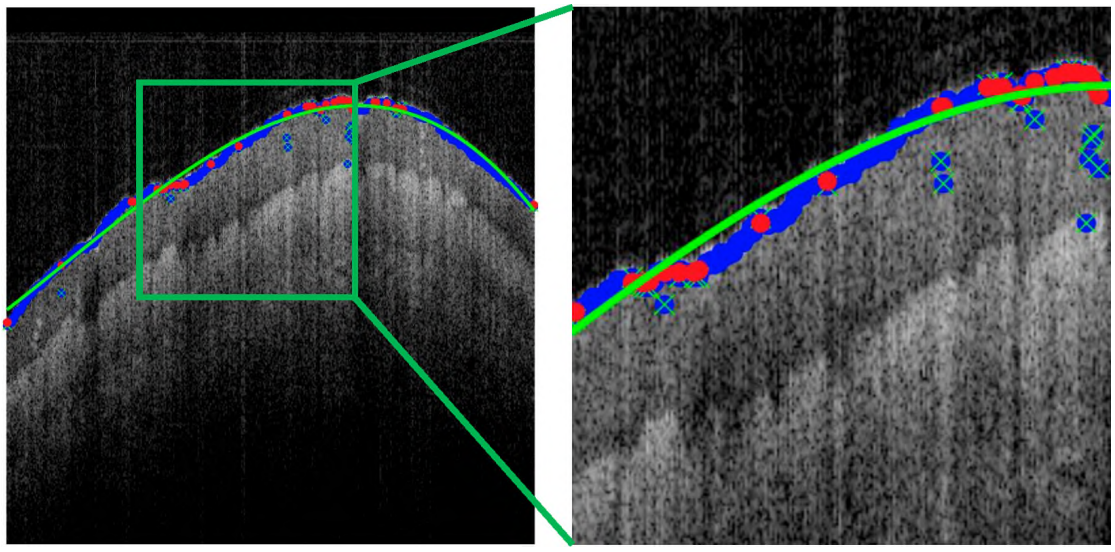

FIGURE 3.3: **Stratum corneum detection**. The blue dots are **SCEstimate**, the combination of **PrevEstimate** and **PolyEstimate** (i.e., the green curve). Green crosses are points detected as incorrect or outliers. The red dots are the corrected outliers.

The relative intensity of B-scans throughout an OCT volume is inconsistent. This is a problem inherent in OCT that can affect the performance of stratum corneum detection. It arises because the fingertip skin is contoured, and pixel intensity is depth-dependent in an OCT scan. The closer to the tip of the finger, the further the skin is from the scanner and the lower the average intensity of the corresponding B-scans. This could degrade the performance of stratum corneum detection. In order to accommodate varying pixel intensity, the threshold intensity is adjusted for every B-scan. Adjustment is performed by finding the B-scan with the brightest average intensity (of all pixels) and adjusting the threshold per B-scan according to its relative relationship with this quantity. The performance of this algorithm is evidenced in Section 5.2 in a qualitative fashion and as a contributing step to internal fingerprint zone-detection.

The detected stratum corneum location is used to define features for clustering. The clustering step is discussed in the following section.

3.1.2 Clustering

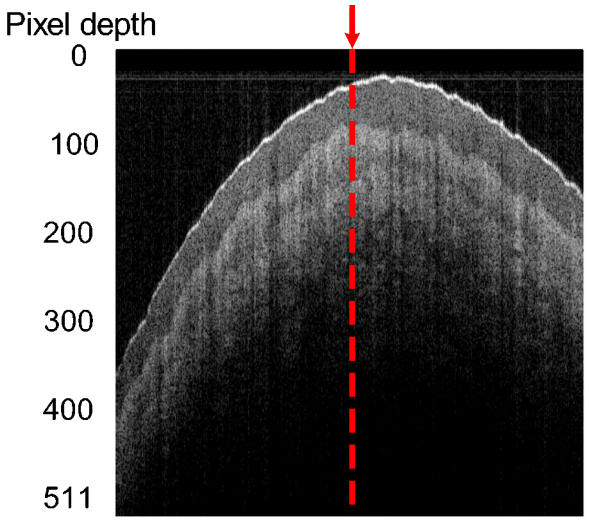

FIGURE 3.4: **A-line context**. The red line is an A-line. Figure 3.5 further exemplifies the A-line analysis undertaken. Image courtesy of Darlow *et al.*[41].

Clustering is an unsupervised machine learning technique used to segment data into a pre-defined number of clusters. Although often a seemingly intuitive process for human beings [45], cluster analysis is a complex and well researched task. There is no agreed-upon definition for the concept of a 'cluster', although it can be defined with respect to

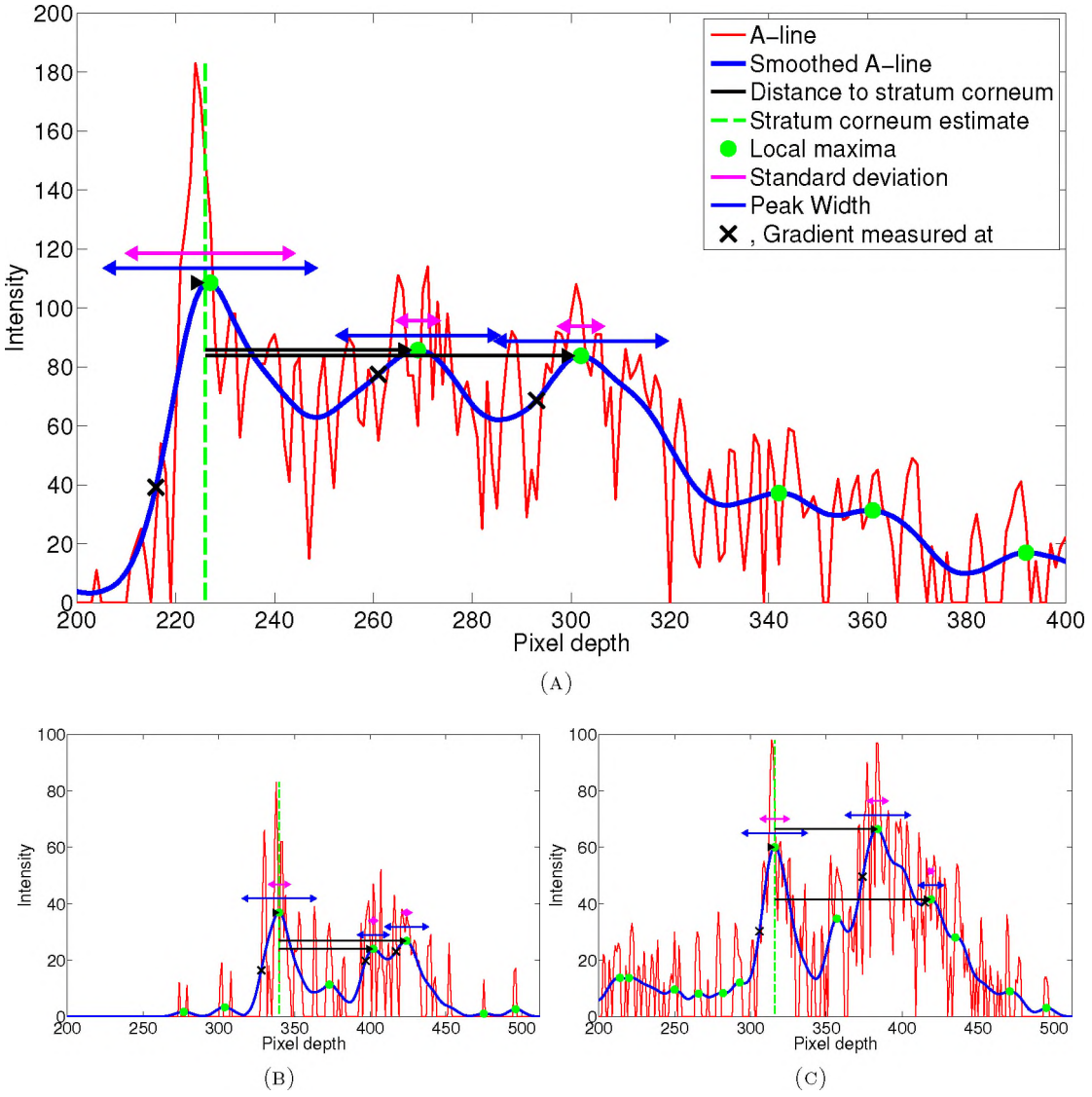

FIGURE 3.5: **A-line intensity profiles**. (A) is an an example of an expected A-line profile, where relative peak heights correlate well with skin structure theory. (B) and (C) are examples of A-line profiles that do not adhere to skin structure theory.

data homogeneity and dissimilarity; data within a cluster is more similar to data within the same cluster than it is to data outside of said cluster [46].

Since clustering is able to segment data, it has been successfully applied to image segmentation problems [47]. The segmentation ability of clustering is used in this research to identify a specific layer of skin, namely the papillary junction. Clustering algorithms require input data and related descriptive feature vectors. In the case of this research, intensity local maxima and corresponding peak-characteristics are extracted from A-lines as data and features, respectively.

Figure 3.4 exemplifies the A-lines analysed for data and feature extraction. Figure 3.5 provides three A-line intensity profiles. These are examples of inputs used for data and feature extraction from the OCT volume. The exemplified region captures the stratum corneum (as the leftmost peak) and the papillary junction (as the second left-most peak). Figure 3.5(A) exemplifies the expected A-line profile based on the relative reflectivity of skin layers: the stratum corneum is the strongest peak, followed by the papillary junction. However, this expected profile structure (regarding relative peak strengths) is not always found. Figure 3.5(B) and (C) are A-line intensity profiles that do not fit this expectation. If the intensity profiles were always structured as per the known and assumed skin reflectivity, determining the locations of the stratum corneum and the papillary junction would be trivial. Owing to the inconsistency demonstrated here, cluster analysis is applied to the problem of internal fingerprint zone-detection.

Each A-line is smoothed prior to analysis. Figure 3.5 is demonstrative of the effect this has: the peaks become well defined, although less sharp. Each of these peaks, defined by their corresponding local maxima, may become a data point for cluster analysis. Since the papillary junction usually corresponds to a strong local maximum (i.e., it is relatively bright), a limited number (n) of local maxima are extracted as data points. Therefore, the top n strongest intensity local maxima are extracted as data for clustering.

For each of the data points extracted, features to describe these data points are also extracted. Descriptive features must be context sensitive and are chosen using domain knowledge, logic, and experimentation (refer to Figure 3.5 for accompanying visual explanations of the chosen features). For each data point, the following features are extracted:

1. **Relative distance:** the normalised absolute pixel-wise distance from the stratum corneum estimate (found using Algorithm 1) to the data point. The black arrows in Figure 3.5 are indicative of this distance, while the green dots are potential data points. This distance is normalised for every B-scan. Normalisation mitigates the need for the assumption that the distance between the stratum corneum and the papillary junction remains constant throughout an entire OCT fingertip volume. However, this distance is assumed to be relatively constant in a single B-scan. A statistical estimation is thus formed regarding the average distance over a B-scan. This is done by taking the median (since it is robust against outliers) of the

distances between the two strongest local maxima in each A-line. The determined estimation is not only used to normalise this feature, but also to determine which cluster best describes the papillary junction location (as described in Section 3.1.3).

2. **Relative intensity:** the normalised intensity of the data point. The height of the green dots in Figure 3.5 exemplifies this feature. As identified in Section 3.1.1, the mean intensity of B-scans in an OCT volume cannot be assumed to be consistent. The normalisation of this feature occurs to allow for intensity inconsistency. Normalisation occurs for every B-scan through the use of an estimation of stratum corneum intensity. The median of the strongest (brightest) peaks in all A-lines in a B-scan is the stratum corneum intensity estimate for that B-scan. This estimation is used to normalise the intensities of all the data points extracted from the corresponding B-scan.

3. **Peak width:** twice the distance from the data point to the closest local minimum (considering those closer to the surface skin). The blue arrows in Figure 3.5 demonstrate this feature. No normalisation is necessary as the arrangement of local extrema is not affected by the same inconsistencies that affect the **relative distance** and the **relative intensity**. Since the peak widths of the stratum corneum and the papillary junction differ, this feature distinguishes them.

4. **Peak standard deviation:** the signal deviation as measured over the region defined by the peak width. This feature is used to differentiate between data points defined by signal strength and data points caused by the presence of speckle noise alone. Since speckle noise is signal-dependent, the standard deviation is also dependent on the level of signal present. This feature is shown as the purple arrows in Figure 3.5. The leftmost six local maxima in Figure 3.5(C) are examples of data points induced by speckle noise.

5. **Peak gradient:** the gradient as measured at the pixel depth exactly half-way between the data point and the same local minimum considered for the **peak width**. The black 'Xs' in Figure 3.5 demonstrate where the gradient is measured. This feature is an estimation of the peak strength and is used to characterise peaks originating from strong signal presence.

The depth-dependency intensity roll-off problem inherent in OCT scans of a curved surface has the potential to affect the performance of clustering. A solution to this is to make use of a glass slide during the scanning process. Doing so would render the touchless capability of OCT superfluous and induce distortion in the papillary junction [13]. The normalisation of the **relative distance** and **relative intensity** features is executed to accommodate the depth-dependency roll-off problem. The extraction of the internal fingerprint from the determined papillary junction upper-edge location must nevertheless take this roll-off into account. Section 3.2 details how this is accomplished.

The choice of clustering algorithm is complex and dependent on the problem space. Data type, cluster model, cluster overlap, and robustness with regard to outliers are factors affecting this choice [46]. Estivill-Castro [48] attempted to explain the large number of clustering algorithms by showing that a decisive idea of 'cluster' is not available.

Since the choice of clustering algorithms is not simple, initial testing was carried out on four possible choices, namely: the k-means [49], k-medoids [50], fuzzy c-means [51], and expectation maximization with Gaussian mixture models [52] clustering algorithms.

K-means clustering defines a cluster by the unweighted membership of its constituent elements. It works by partitioning data into k groups where each group's cumulative distance with respect to its centre is minimized. Optimized implementations are available that make use of heuristic procedures to improve performance. Although k-means clustering is simple and robust, it is ineffective in identifying outliers.

K-medoids clustering works in a similar fashion to k-means clustering. The difference is that the centres of clusters are defined by objects within respective clusters. For each cluster, the object defining the centre is chosen as the object with minimized dissimilarity to all other objects in the cluster. Owing to these pairwise calculations, k-medoids clustering is computationally-expensive. It is, however, more robust against outliers.

Fuzzy c-means clustering defines cluster centres in the same manner as k-means clustering. It does not assume distinct clusters. Instead, each data point is given a degree of membership to all clusters. Thresholding procedures are used to determine to which (if any) cluster the data points belong. The major advantages of fuzzy c-means clustering are that it works well with overlapping datasets and is highly robust against outliers.

The expectation maximization with Gaussian mixture models clustering algorithm is a hierarchical cluster analysis that works by decomposing the input data set. It follows a 'top down' approach: all data starts in a single cluster and is recursively split down the hierarchy. It works by calculating a number of Gaussian mixture models prior to attempting to fit the data by estimation of the maximum likelihood of Gaussian centres. Although frequently and successfully used in real-world applications, it is computationally-expensive.

The initial performance analysis of the above-mentioned four clustering algorithms is given in Section 5.1. Since it is possible for data to overlap and for outliers to be present, the fuzzy c-means clustering algorithm fits the data space well. The initial performance analysis supported this observation. Therefore, the fuzzy c-means clustering algorithm is applied to this research.

The task of thresholding fuzzy c-means clustering output is an unsolved problem and is potentially complex. In the context of this research, the membership threshold is set as a function of c (i.e., the number of clusters). Equation 3.1 is this function.

$$T(c) = min(\frac{m}{c}, threshold), \tag{3.1}$$

where $m > 1$ is the multiplication factor, c is the number of clusters, and *threshold* is the static maximum membership value. The factor of $1/c$ is used because the possiblity of membership is inversely proportional to the number of clusters. m allows for a deviation from k-means style clustering (where $m = 1$) and the static *threshold* value allows for a stricter classification of outliers, which is more suited to this task. If a data point does not have a membership of at least T in any of the c clusters, it is an outlier. Therefore, higher values of m yield more outliers.

A high threshold value (i.e., high m) is used to ensure that any membership to the cluster describing the papillary junction is strong membership. However, there is still a need for processing cluster output. This is discussed in the following section.

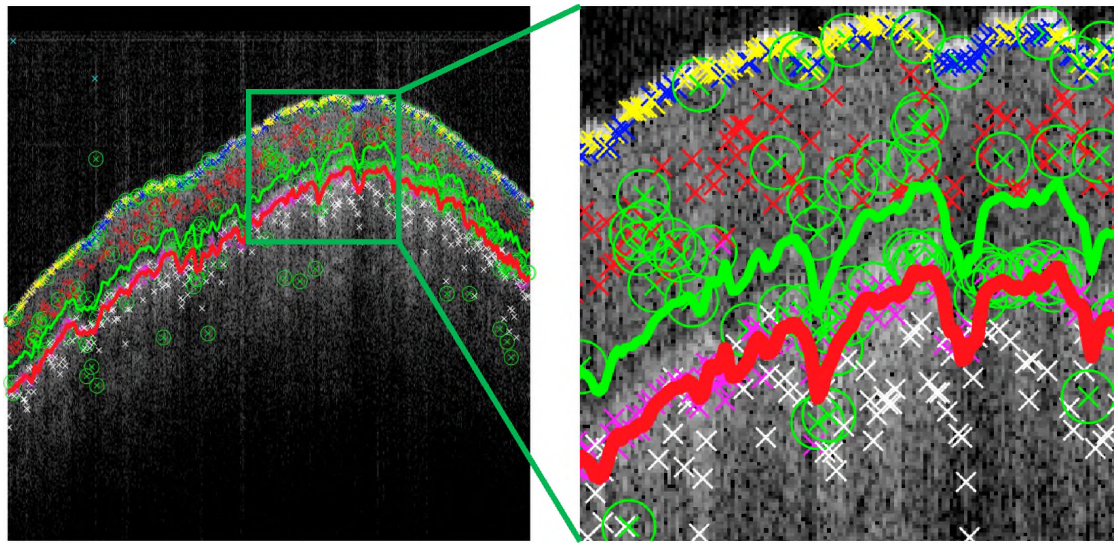

FIGURE 3.6: **Cluster analysis output**. Each marker/colour combination represents a different cluster (six, in this case). The larger green circles encircle outliers. The red line is the processed cluster output and the green line is the processed cluster output 25 pixels toward the stratum corneum. It is the region between the red and green lines that is extracted for fine-tuning. Although there is a large number of local maxima shown here, it is only to evidence the ability of clustering to nevertheless assist in papillary junction detection.

3.1.3 Processing Cluster Output

Figure 3.6 is an example of cluster analysis output. The first step in processing this output is to determine which cluster best describes the location of the papillary junction. The estimation of the average distance between the papillary junction and the stratum corneum (found when determining the **relative distance** feature) is used as a means to this end. A single B-scan's data is analysed. The correct cluster (holding data that is closest to the papillary junction location estimate) is determined as it best describes the papillary junction location. The cluster centroid is not considered for this. Instead, only the error between clustered local maxima and the above-mentioned location estimate is used. Only one B-scan needs to be analysed because there is enough data in each B-scan to make this choice.

Whilst an ideal result after clustering would be a single data point per A-line, this is not ensured to be the case. Figure 3.7 and 3.8 provide a visual explanation of cluster result post-processing.

The following inconsistencies, along with corresponding solutions, may occur:

- **Problem:** In a single A-line, several data points may be within the chosen cluster.
  Solution: If this is the case, these data points will usually be spatially close. The uppermost of these is used. If this proves to be incorrect, it will be filtered out.

- **Problem:** An A-line may contain no data points in the chosen cluster.
  Solution: Missing data is interpolated using the technique developed by Garcia [53], known as *inpaintnan*. Examples of interpolated points are the blue dots in Figure 3.7. An example of the interpolated output cluster results can be seen in Figure 3.8 (C). Owing to the curvature of the fingertip, interpolation may yield incorrect results toward the sides of the finger. This is exemplified as the yellow line in Figure 3.7(A). Figure 3.8(B) demonstrates the preparation process for interpolation. The regions where roll-off may affect the interpolation result (i.e. the leftmost and rightmost regions in Figure 3.8's *en-face* representations), the papillary junction coordinates are set to the maximum depth of the B-scan (i.e. the length of an A-line). The effect thereof can be seen as the difference between the blue (with preparation) and yellow (without preparation) lines in Figure 3.7(A).

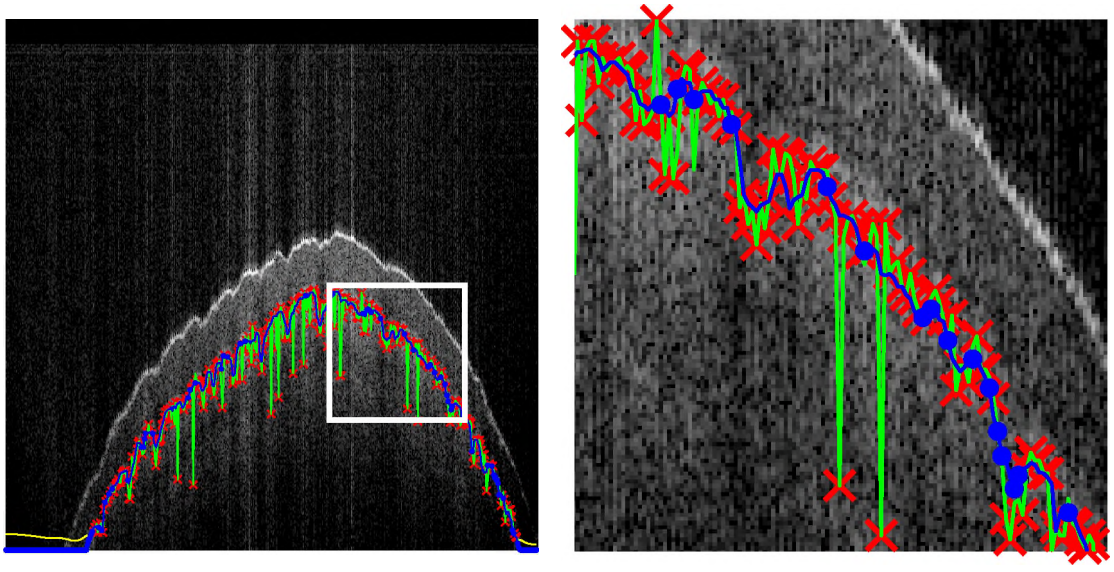

(A) (B)

FIGURE 3.7: **Cluster output post-processing: a single B-scan**. (A) and the denoted region of interest (B). The red crosses are the data points within the chosen cluster, represented as non-black pixels in Figure 3.8(A); the blue dots are interpolated points and the green line is the interpolated result, as shown in Figure 3.8(C); the blue line is the median filtered output – a single row in Figure 3.8(D); and the yellow line shows interpolation results without correct preparation: interpolation of Figure 3.8(A) instead of Figure 3.8(B).

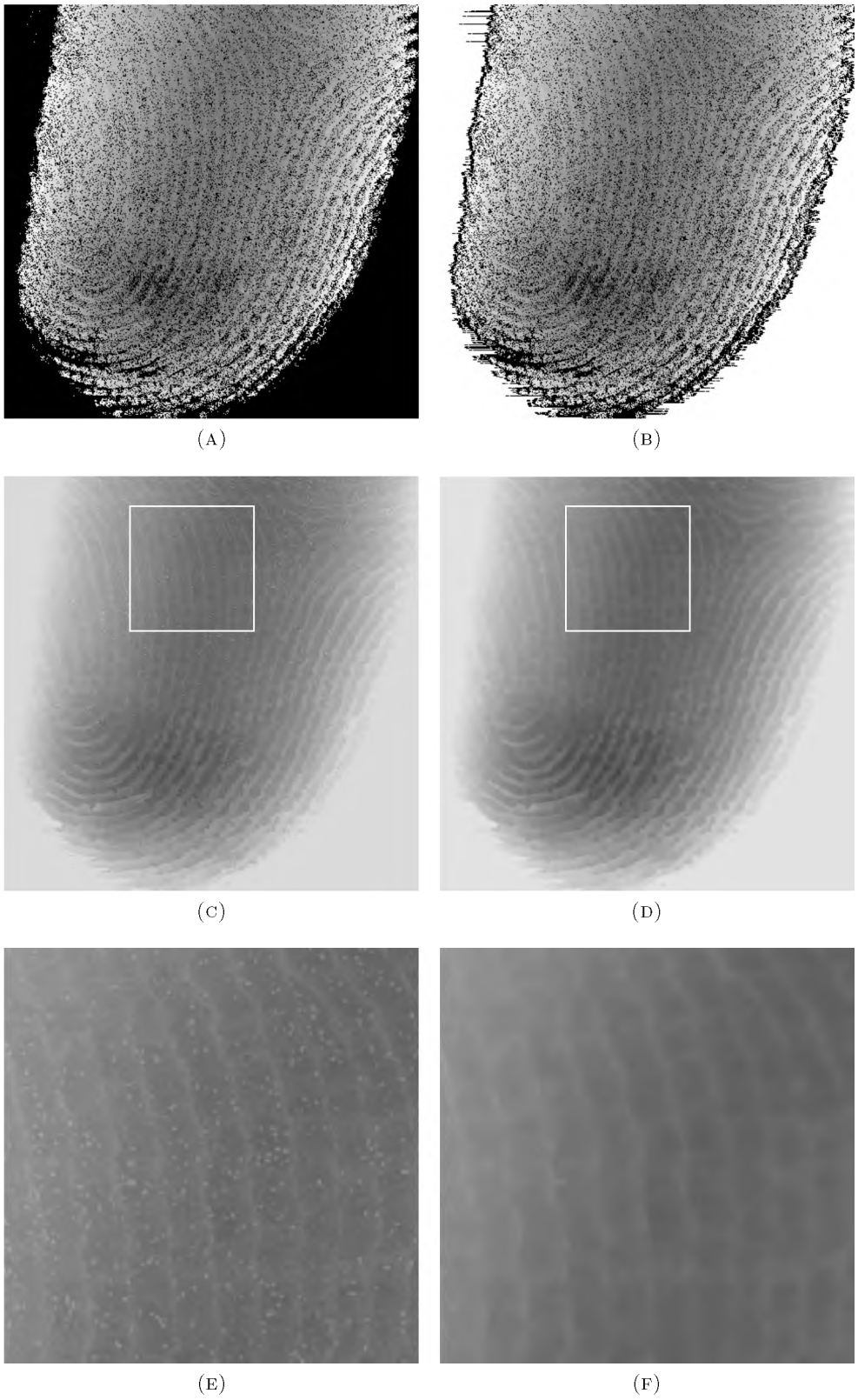

FIGURE 3.8: **Cluster output post-processing**. These images are *en-face* representations of the coordinates defining the location of the centre of the papillary junction. (A) shows all the data points within the chosen cluster, where black pixels represent A-lines containing no data points within the chosen cluster. (B) is preparation for interpolation. (C) is interpolated cluster results. (D) is the median filtered result of (C). (E) and (F) are the regions of interest in (C) and (D), respectively.

- **Problem:** Data points may be incorrectly determined to be a member of the chosen cluster. The deviations of the green line in Figure 3.7 are caused by this. Furthermore, the 'hot pixels' visible in Figure 3.8(C) and (E) are evidence of this problem.

  Solution: Filter the interpolated data. A median filter is applied as it is robust against discontinuities in data. An example of this can be seen as the blue line in Figure 3.7, and Figure 3.8(D) and (F).

The coordinates obtained in the manner detailed in this section are the location of the centre of the papillary junction in an OCT volume. They will be referred to as PC. PC describes the topography of the papillary junction to a fair degree of accuracy. It can be seen as the lower (red) line in Figure 3.6 and Figure 3.8(F). Section 4.3 details the experiments designed to test the performance of clustering for internal fingerprint zone-detection, and Section 5.2 gives both quantitative and qualitative results to demonstrate its efficacy. However, it is the upper-edge of the papillary junction that best describes the topography of the internal fingerprint. This upper-edge is defined as the region between the post-processed clustering result and 25 pixels above (i.e., toward the surface), as is shown in Figure 3.6. Fine-tuning the processed clustering results to better describe the papillary junction upper-edge is discussed in the following section.

3.1.4 Fine-tuning

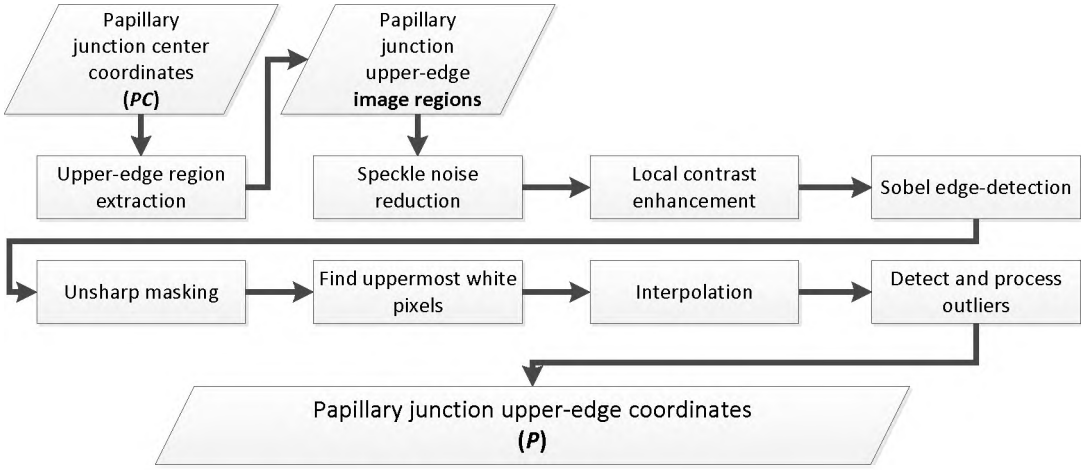

FIGURE 3.9: **Fine-tuning flowchart.**

The objective of fine-tuning PC is to determine the location of the upper-edge of the papillary junction, denoted as P. The procedures followed to find PC have been robust against speckle noise and normalised for contrast inconsistencies. However, the coordinates obtained thus far describe the centre of the papillary junction only, and do not ascertain the maximum body of knowledge in relation to internal fingerprint ridge and valley topography. Therefore, the fine-tuning process outlined in Figure 3.9 and exemplified in Figure 3.10 is applied.

PC is used to extract small image regions, containing the papillary junction upper-edge, from each B-scan. An example region can be seen in Figure 3.10(A). An ideal condition would be that PC follows the upper-edge undulations exactly, resulting in straight-line edges in the extracted image regions. Figure 3.10 shows how this is certainly not the case. The fine-tuning process serves to adjust PC, accommodating fluctuations in the papillary junction upper-edge that were not detected by clustering. It is executed in the application of edge-detection on the extracted small image regions.

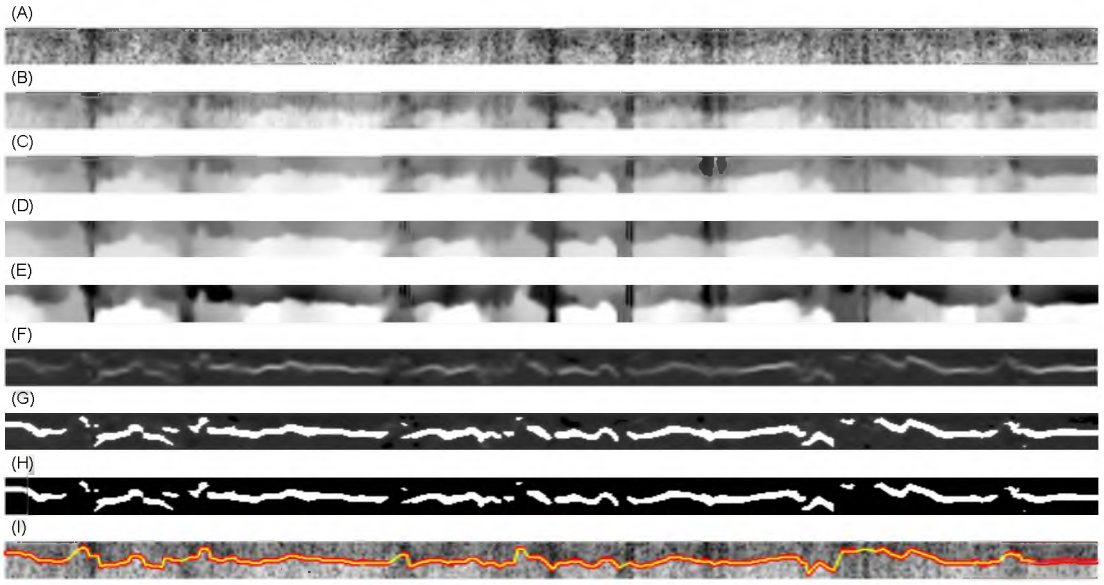

FIGURE 3.10: **Fine-tuning process**. (A) is the extracted image region, exemplified as the region between the red and green lines in Figure 3.6. (B), (C), and (D) are the results of three stage speckle noise-reduction. (E) is the result of local normalisation. (F) is after the convolution of the edge-detecting Sobel kernel. (G) is the result of unsharp masking on (F). (H) is the thresholded version of (G). (I) is (H) processed for edge-detection: the red dots are the detected white pixels in (H) and the yellow line is the interpolated and outlier insensitive processed output.

Edge-detection on extracted image regions is hampered by the presence of speckle noise and the inherent low-contrast of OCT scans. Speckle noise is signal-dependent (multiplicative). It originates when there are reflective elements that are roughly the same

size as the imaging wavelength (of the OCT scanner) [54]. The closest noise distribution describing speckle noise is the Rayleigh distribution [16, 54].

Speckle-reduction approaches have been developed [55–62]. A review of state-of-the-art speckle-reduction techniques was conducted by Darlow *et al.* [39]. The optimised blockwise non-local means (OBNLM) algorithm was found to be the best performing speckle-reduction technique when applied to OCT fingertip B-scans.

An adaptation of the non-local (NL)-means filter [63] for speckle-reduction in MRI was first proposed by Coupé *et al.* [64]. The noise model was adjusted to incorporate speckle noise. This reformulation resulted in a powerful speckle noise-reduction filter. Owing to how computationally expensive NL-means filtering is, a blockwise approach was developed as an optimisation (*viz.* OBNLM). The noise models and origins for speckle noise in MRI and OCT are similar and OBNLM can be applied in each case.

OBNLM speckle noise-reduction is applied to the edge regions in three stages because reapplying a lower level of speckle reduction retains better edges than attempting to remove all the noise at once. The effect thereof is demonstrated in Figure 3.10(B) to (D). A product of OBNLM speckle noise-reduction is improved contrast and greater homogeneity in regions with high signal presence. However, since the contrast of OCT images is inconsistent, the result of OBNLM application is also inconsistent. Local contrast-enhancement is applied to (1) improve and (2) normalise the contrast of these images. Local normalisation is an operation where pixel intensities are adjusted in a windowed fashion to increase the distinction between light and dark. A local approach is preferred as small-scale changes (such as the upper-edge of the papillary junction) are concentrated. Figure 3.10(D) and (E) are examples of OBNLM and local contrast-enhancement, respectively.

The Sobel operator [33] is applied to detect vertical gradient changes. Figure 3.10(F) is an example thereof. The Sobel operator is a well-known edge-detection tool used to emphasize edges in images. The vertical Sobel operator is convolved with the de-noised edge region images. It is defined as:

$$Sobel = \begin{array}{|c|c|c|} \hline +1 & +2 & +1 \\ \hline 0 & 0 & 0 \\ \hline -1 & -2 & -1 \\ \hline \end{array}$$

To highlight the edges detected by the Sobel operator, unsharp masking is applied. Unsharp masking compares an image with its blurred counterpart to identify and amplify high-frequency regions. Applied at the correct scale, this enhances the regions detected by the Sobel operator. The result of this is thresholded. The unsharp masking and thresholding processes are exemplified in Figure 3.10(G) and (H), respectively.

The thresholded results are processed to identify the white pixels. The detected edges are shown as the red dots in Figure 3.10(I). The missing values are interpolated using *inpaintnan* and outliers are found and replaced using the Hampel filter [65]. The choices of Sobel edge-detection, *inpaintnan*, and the Hampel filtering are owing to their widespread use and reliability. It is not the focus of this research to exhaustively search for optimised counterparts, but instead provide a robust means of extracting an internal fingerprint. An instance of this can be seen as the inner (yellow) line in Figure 3.10.

The result of fine-tuning is used to adjust PC into coordinates describing the papillary junction upper-edge (P). Figure 3.11 shows the adjustment owing to fine-tuning.

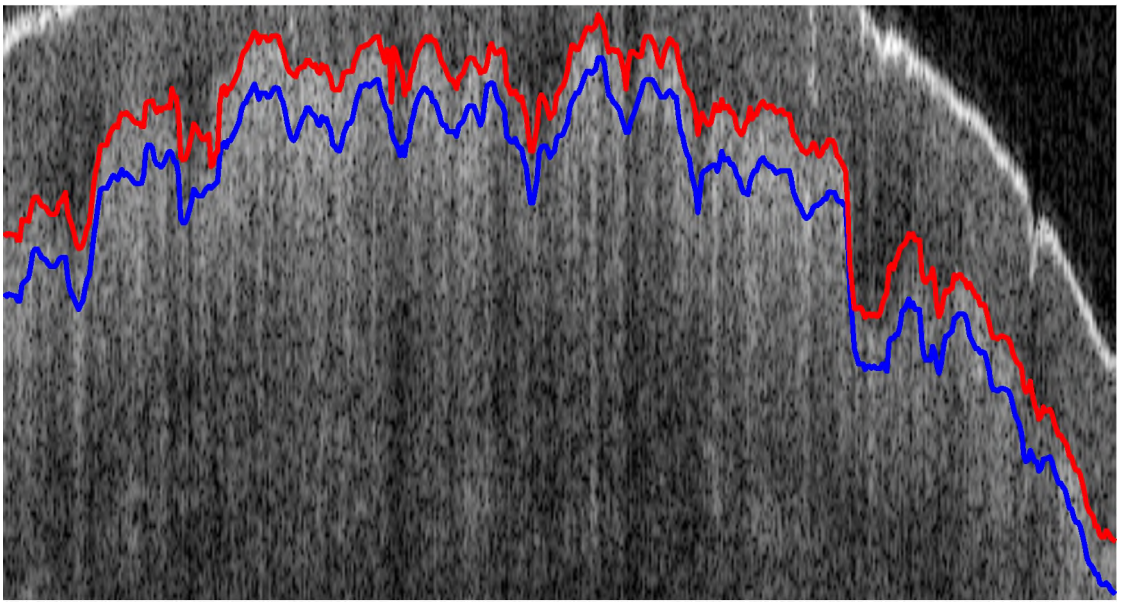

FIGURE 3.11: **Fine-tuning example**. The blue line is a single row of PC and the red line is a single row of P.

Earlier work by the authors served as initial experimentation to formulate the processes discussed in this chapter. In-depth experimentation to show the effectiveness of internal fingerprint zone-detection using k-means clustering and image enhancement is given in the work by Darlow *et al.* [41]. Akhoury and Darlow [42] demonstrated the use of internal fingerprint zone-detection in obtaining papillary junction upper-edge coordinates for 3D

to 2D papillary junction coordinate fingerprint mapping. Darlow *et al.* [40] showed the success of a heuristic approach to internal fingerprint zone-detection.

The coordinates obtained using the technique described in this section (i.e., P) are used for internal fingerprint extraction. This is discussed in the following section.

3.2 Internal Fingerprint Extraction

The authors have explored two possible approaches to internal fingerprint extraction, one of which, outlined and tested by Akhoury and Darlow [42], involved processing P directly into a 2D fingerprint representation. This was accomplished by executing the following procedures on P:

1. A smoothing filter (Gaussian low pass) was applied to P, thus correcting for outliers present.
2. A phase congruency [66] filter was used to detect ridge-valley gradients.
3. A sigmoid function was applied to saturate the detected gradients, amplifying the result of the phase congruency filter.
4. The result was filtered for anomalies by convolving it with a non-linear median filter.

The above-mentioned process is exemplified in Figure 3.12. This process is successful in detecting the ridge and valley structure present in P. It is also substantiation of the claim that the papillary junction upper-edge contains a significant level of internal fingerprint topographical information. Although the internal fingerprint can be extracted in this fashion, the approach relies on the accuracy of the detection of P. Thus, a different internal fingerprint extraction technique, that addresses the issue of robustness against anomalies in P, is developed in this research.

The fingerprint mapping technique shown in Figure 3.12 does not make use of the OCT scan data directly. Instead, it uses meta-data (i.e., the upper-edge of the papillary junction) extracted from the corresponding OCT scan. Any anomalies present in P therefore

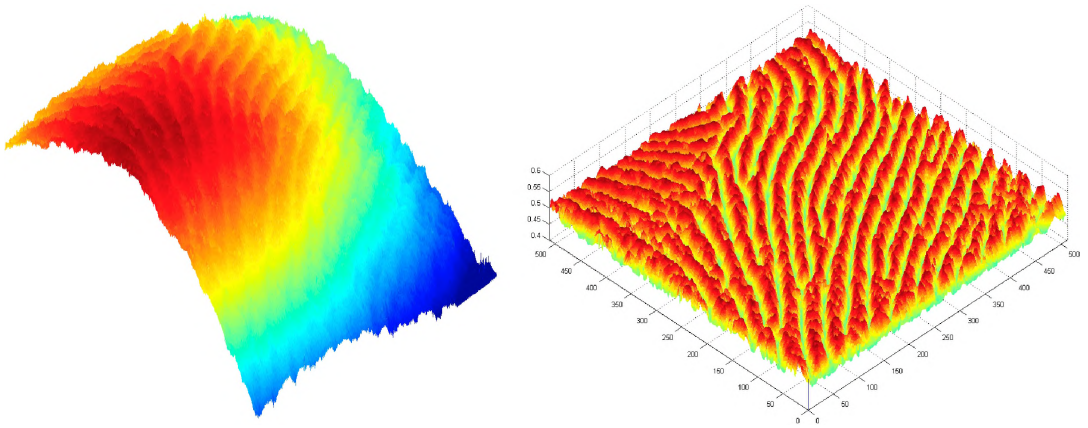

(A) (B)

FIGURE 3.12: **3D papillary junction upper-edge to 2D fingerprint representation mapping**. This image is courtesy of Akhoury and Darlow [42]. (A) is an example of 3D coordinates obtained, P. (B) is an example of processing these coordinates to a 2D fingerprint representation.

affect the result of this fingerprint mapping. The internal fingerprint extraction technique developed for this research makes use of both P and the original OCT volume for fingerprint extraction. OCT volume (3D) to internal fingerprint (2D) mapping is explained in Section 3.2.1 and the procedures followed for internal fingerprint enhancement are detailed in Section 3.2.2.

3.2.1 3D to 2D Mapping

Since P describes the undulations of the internal fingerprint, a windowed statistical evaluation of P can be assumed to describe the relative A-line-wise contributions to fingerprint topography. That is, a **2D windowed mean** and a **2D corrected windowed standard deviation**, centred on the *en-face* 2D coordinate of a considered A-line, describe the region over which to perform dynamic (i.e., per the respective A-line) *en-face* pixel averaging for the resultant 2D internal fingerprint.

The **2D windowed mean** is found by convolving P with an averaging kernel (of size equal to *window_size*). The **2D corrected windowed standard deviation**, denoted as 'corrected' because it is measured relative to the **2D windowed mean**, is simply the standard deviation as measured in a window (of the same size used for the **2D windowed mean**) surrounding the A-line being considered. Algorithm 2 details the internal fingerprint mapping process.

Input: OCT_volume, P
Parameters: $window\_size$, $start\_offset$, end_offset, $mult$
Output: $Internal\_print$
$mean\_2D \leftarrow$ convolve(P, $kernel(window\_size)$)
$std\_dev\_2D \leftarrow$ std_dev_filter($P - mean\_2D$, $kernel(window\_size)$)
foreach A_line *in* OCT_volume **do**
    $region\_start \leftarrow mean\_2D[A\_line] + start\_offset$
    $region\_end \leftarrow mean\_2D[A\_line] + std\_dev\_2D[A\_line] * mult + end\_offset$
    $Internal\_print[A\_line] \leftarrow$ average($OCT\_volume[A\_line][region\_start : region\_end]$)
end

Algorithm 2: 3D TO 2D FINGERPRINT EXTRACTION

The **2D windowed mean** and **2D corrected windowed standard deviation** allow for a definition of localised start and end points specific to each A-line, denoted as *region_start* and *region_end* in Algorithm 2, respectively. These points define the region that pixels are averaged in an A-line for a single resultant pixel in the internal fingerprint (*viz.* 3D to 2D conversion).

The $start\_offset$ adjusts the **2D windowed mean** to yield *region_start*. Furthermore, *region_end* is calculated by multiplying the **2D corrected windowed standard deviation** with the *deviation_multiplier* and adjusting it by the end_offset. $start\_offset$ and end_offset are robust parameters and were experimentally chosen to encapsulate the internal fingerprint undulations. Figure 3.13 exemplifies this localised region in two B-scans. The dependency of this region on P allows for the descriptive topographical undulations of the papillary junction upper-edge to be captured. This technique is able to follow the papillary junction upper-edge with respect to:

1. Characteristic internal fingerprint undulations. These undulations are directly related to the topography of the internal fingerprint. This is exemplified in **ROI 1** in Figure 3.13 as the light (ridges) and dark (valleys) captured between the green and blue lines.

2. Differences in the papillary junction upper-edge relative size. The difference in the strength of undulation, and thus the difference in ridge and valley definition, is variable. For instance, the topographical variations are larger in **ROI 1** than they are in **ROI 2** in Figure 3.13.

Figure 3.13 complements Algorithm 2 by showing the regions involved in fingerprint extraction. These regions are calculated as 2D quantities, slices of which are shown in

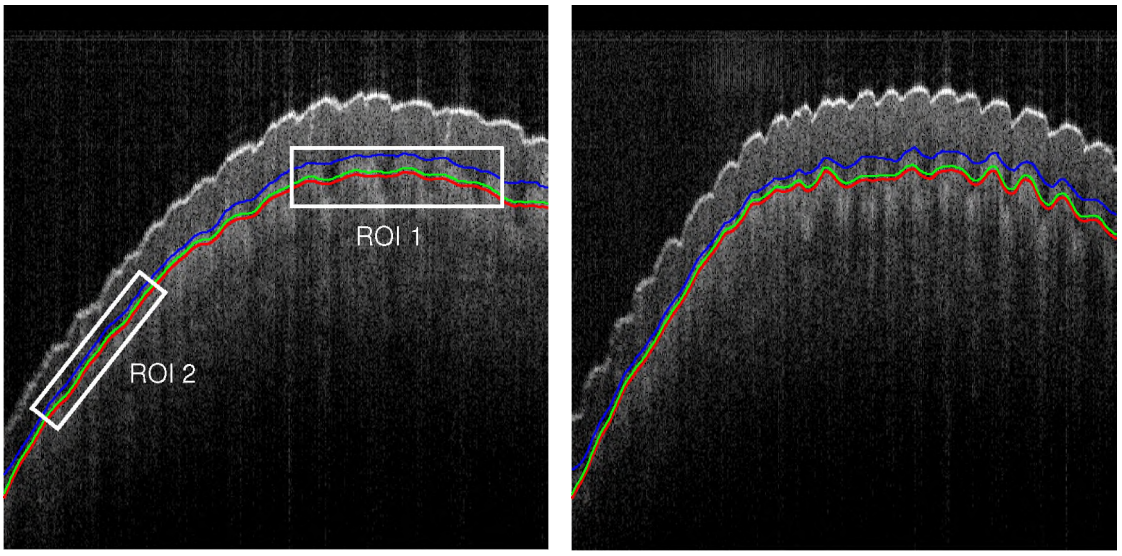

(A) (B)

FIGURE 3.13: **B-scan fingerprint mapping region examples**: (A) and (B) are B-scans showing fingerprint mapping examples. **ROI 1** and **ROI 2** denote regions that show the effectiveness of the localised statistics used for internal fingerprint mapping in correctly capturing the internal fingerprint undulations. These regions are not samples of extracted regions, but simply highlight two regions where fingerprint undulation characteristics differ. The extraction occurs between the middle (green) line and the top (blue) line. The red lines correspond to the smoothed P: the **2D windowed mean**. The green lines are the red lines offset by $start\_offset$, denoted as $region\_start$ in Algorithm 2. The blue lines are the red lines offset by the **2D corrected windowed standard deviation**, denoted as $region\_end$ in Algorithm 2.

Figure 3.13. Owing to the 2D calculation of $region\_start$ and $region\_end$, the length of the region is dynamic per A-line. It depends on the standard deviation of the internal fingerprint zone of the surrounding 2D region, and thus is longer if the fingerprint zone undulates to a greater degree.

Owing to the fact that windowed statistics of P are taken, for each A-line contributing to the internal fingerprint, this technique is robust against anomalies or deviations in P. Section 5.2 gives examples of possible errors in P. Moreover, the depth dependency intensity roll-off and fingertip curvature problems are partially dealt with by the depth independent relative regions described by P and the localised 2D signal statistics used. The contribution of these problems are further limited by internal fingerprint enhancement. This is discussed in the next section.

3.2.2 Internal Fingerprint Enhancement

The internal fingerprint extraction technique discussed in the previous section is designed to be robust against anomalies in P, and able to effectively describe the internal fingerprint undulations in a localised manner. However, the performance thereof is limited by the contrast of OCT. Additionally, owing to the fact that the internal fingerprint is dependent on the unprocessed OCT data, speckle noise is present.

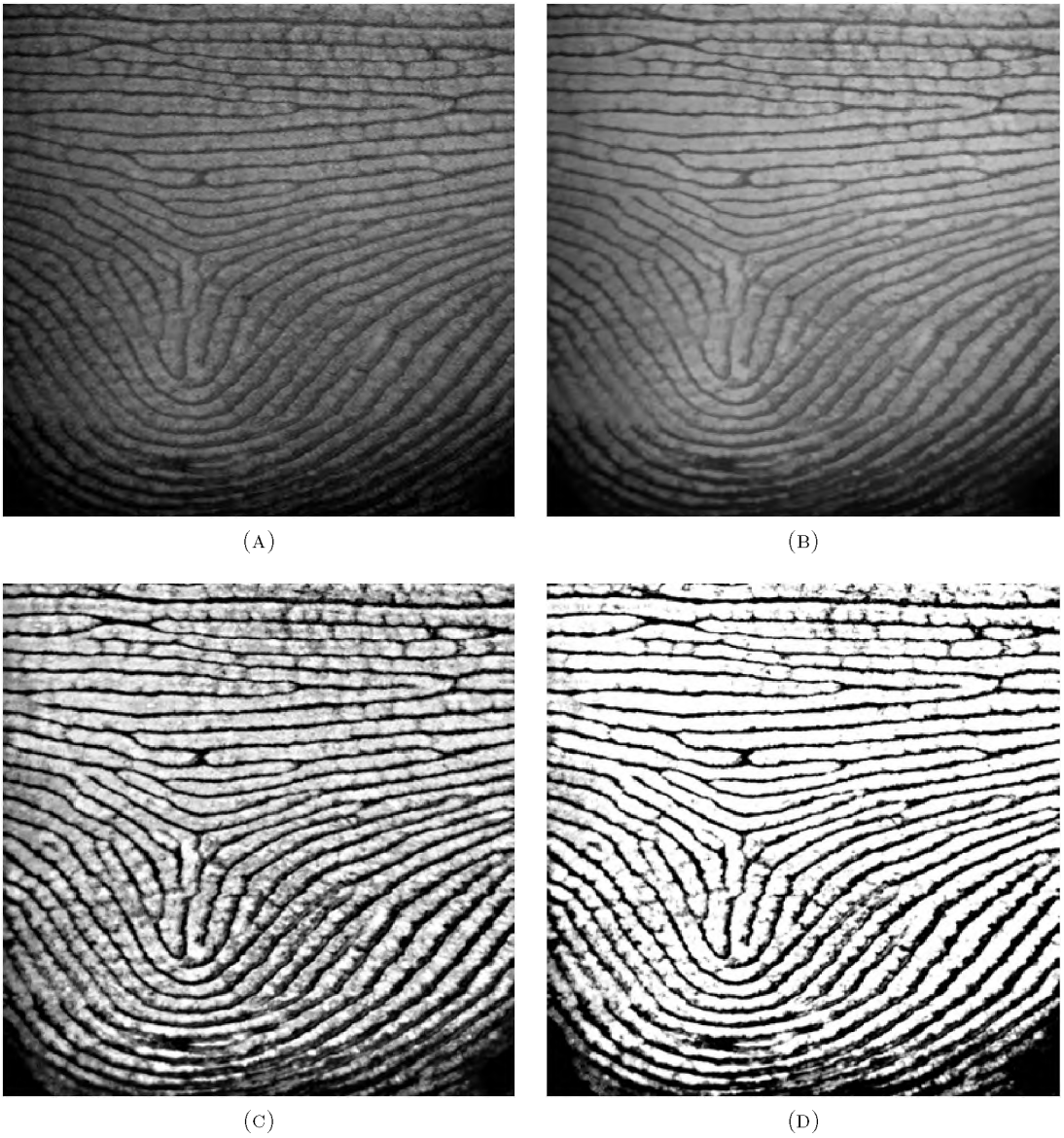

FIGURE 3.14: **Internal fingerprint enhancement**: (A) is an example internal fingerprint extracted from an OCT volume using P, as per Section 3.2.1; (B) is after OBNLM speckle noise-reduction; (C) is after local contrast normalisation; and (D) is after global intensity saturation.

In order to maximise the visibility and contrast of ridges and valleys in the extracted fingerprint, image-enhancement procedures are applied in the following order:

1. **OBNLM speckle noise-reduction**. OBNLM was shown to be the best performing speckle-reduction technique regarding error reduction, structural similarity, and signal-to-noise ratio improvements [39]. OBNLM is used to smooth homogeneous areas in the internal fingerprint.

2. **Local intensity normalisation**. The same local normalisation technique is used in fine-tuning (Section 3.1.4). It is a localised contrast-enhancement procedure that stretches a windowed region's pixel intensities to fit an appropriate range. Not only is local normalisation capable of further accentuating ridges and valleys, it neutralises the remaining effects of the intensity depth dependency roll-off and fingertip curvature problems.

3. **Global intensity saturation**. After local intensity normalisation, the fingerprint images have similar ridge-to-valley contrast throughout. To maximise this contrast, the intensity range is saturated (stretched) appropriately.

Figure 3.14 exemplifies the internal fingerprint enhancement procedure used in this research. This chapter served to detail the process developed to extract 2D internal fingerprints from 3D OCT scans. By extracting and describing 1D local maxima as data points for fuzzy c-means clustering, the internal fingerprint zone (i.e., the papillary junction upper-edge) is detected. The internal fingerprint is extracted using a statistical evaluation of this location (meta-data) to describe a dynamic region in the 3D scan (data) over which to average 1D signals. Following this, the resultant internal fingerprint is enhanced.

The internal fingerprints obtained using the techniques detailed in this chapter, and the techniques themselves, are thoroughly tested in Chapter 5. The experimental set-up is discussed in the following chapter.

Chapter 4

Experimental Set-up

This chapter outlines the processes followed to obtain fingerprint data (both internal and surface) and describes the experiments developed to assess all aspects of this research. The following section explains data acquisition.

4.1 Data Acquisition

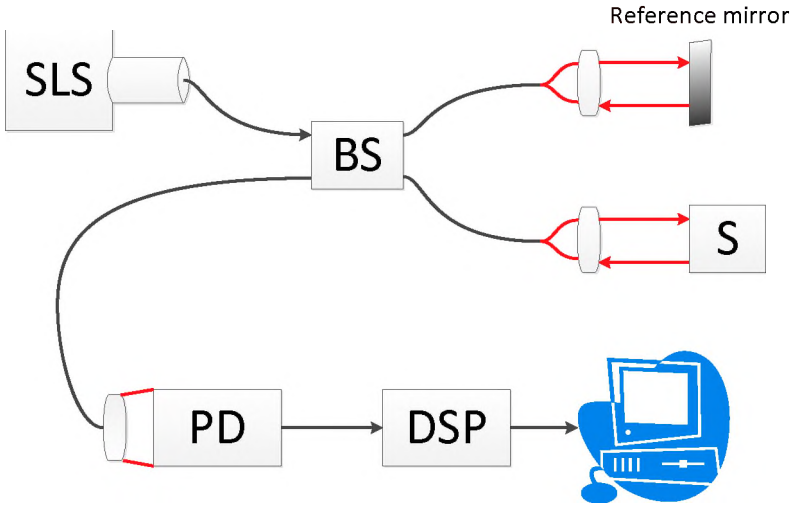

FIGURE 4.1: **OCT system: OCS1300SS, Thorlabs**. SLS: swept laser source; BS: beam splitter; S: sample; PD: photodiode detector; DSP: digital signal processor.

Fingertips were scanned using a swept source OCT system (OCS1300SS, Thorlabs). It has a central wavelength of $1325nm$, a spectral bandwidth of $100nm$, an axial scan rate of $16kHz$, and a coherence length of $6mm$. No glass slide was used for stabilisation as this negates the touchless capability of OCT. Instead, the scans were repeated until satisfactory instances were obtained. Figure 4.1 is a diagrammatic outline of the system.

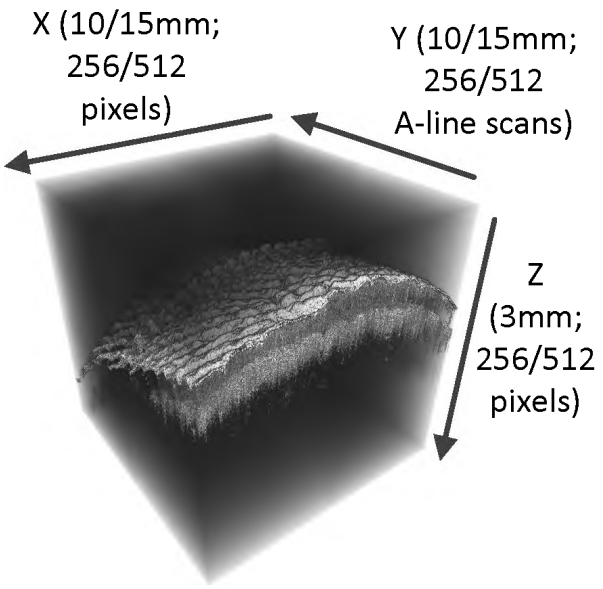

FIGURE 4.2: **Typical OCT fingertip scan**, with resolution constraints.

A typical 3D OCT fingertip scan and corresponding resolution constraints is given in Figure 4.2. The OCT system used is limited to scanning an *en-face* (X, Y) region of $15mm \times 15mm$. For this research two region sizes were used: $10mm \times 10mm$ and $15mm \times 15mm$. For each of these region sizes, scans of two *en-face* resolutions were obtained: 256×256 *pixels* and 512×512 *pixels*. The depth (Z) and corresponding resolution is constrained to $3mm$ and 512 *pixels*, respectively. The data obtained is constrained according to one of the following:

1. **Region size:** $X = Y = 15mm$; $Z = 3mm$
   Resolution: $X = Y = Z = 512$ *pixels*
   Dots per inch: 867

2. **Region size:** $X = Y = 15mm$; $Z = 3mm$
   Resolution: $X = Y = 256$ *pixels*; $Z = 512$ *pixels*
   Dots per inch: 433

3. **Region size:** $X = Y = 10mm$; $Z = 3mm$
   Resolution: $X = Y = Z = 512$ *pixels*
   Dots per inch: 1300

4. **Region size:** $X = Y = 10mm$; $Z = 3mm$
   Resolution: $X = Y = 256$ *pixels*; $Z = 512$ *pixels*
   Dots per inch: 650

The system was used to capture multiple instances of ten fingers, totalling fifty-five OCT volumes. None of the scanned fingers represented tissue types with damaged fingerprints, as that is outside the scope of this thesis and will be studied as future work. For each finger scanned, corresponding surface scans were also obtained using: the Integrated Biometrics Watson Mini (and the IBScanUltimate 1.6.10 software) and the SecuGen Hamster Plus (and the device software). Each surface fingerprint scan was repeated eight times, resulting in sixteen surface scans for each finger.

The OCT volumes were then processed to extract the internal fingerprints. The testing procedure designed to analyse the performance of the extracted internal fingerprints is detailed in Section 4.3. The approach for testing the system components is outlined in the next section.

Processing was carried out on a Windows 7 system, with an Intel i7-3770 running at 3.40 GHz and 8 GB of random access memory.

4.2 System Component Assessment

Prior to any analysis on the extracted internal fingerprints, a thorough examination of the procedures undertaken to extract said fingerprints was performed.

Papillary junction upper- and lower- edge estimations were carried out on a single OCT volume. The upper-edge estimation is denoted G, while an estimation adjusted as the centre of the papillary junction is denoted as GC. GC is compared to PC and G is compared to P for quantitative assessment. The estimations were established using unprocessed B-scans and the GNU image manipulation program [67]. These were not carried out by an expert since they are designed to give an estimation of fingerprint

zone-detection accuracy in the presence of speckle noise. Owing to the level of noise present, defining the exact upper- and lower- edges of the papillary junction is challenging. Thus, deviation in the ground-truth estimates, owing to human error, was quantified by comparing thirteen volunteers' ground-truth estimations on five B-scans. This was then used as a human-error quantification for comparison against the automatic method developed herein.

Since clustering is an integral component of the proposed algorithm, initial experimentation for cluster algorithm choice is essential. This is outlined in the following section.

4.2.1 Cluster algorithm choice initial experimentation

K-means, K-medoids, Expectation maximisation with Gaussian mixture models, and Fuzzy c-means are the clustering algorithms tested in this research.

The testing range is $n = 2 \ldots 20$ with $(c = k) = n+2$. The number of clusters is denoted as k for all the tested clustering algorithms, except for fuzzy c-means (in which case $k = c$). It is set to be higher than the number of data points per A-line (n) as some data points can be outliers. It is the presence of speckle noise that causes atypical data.

For each $n : (c = k)$ combination, PC is compared to GC and P is compared to G. The mean squared error (MSE, Equation 4.1), modified Hausdorff distance metric [68, 69] (H, Equation 4.2), structural similarity [70, 71] (SSIM, Equation 4.4), and root-mean-squared-contrast [72] (RMS-C, Equation 4.5) are used to quantify these comparisons. In addition, the time taken to perform clustering is also measured.

MSE and H are error estimation metrics. MSE is the average of the squares of the deviation between estimate and estimator. Error can occur because of real deviations between the ground-truth estimates, or because of an imperfect ground-truth estimation [73]. In this research, MSE is defined as:

$$MSE(e, a) = \frac{1}{N} \sum_{i=1}^{N} (e_i - a_i)^2 \tag{4.1}$$

where e and a are the ground-truth (GC or G) and the measured quantity (PC or P), respectively; N is the number of data points; and e_i and a_i are compared points.

H measures the degree of dissimilarity between two datasets: it is the maximum of the shortest (pixel-wise) distance between any point in one dataset (GC or G, for example) and any other point in another (PC or P, for example). It is defined as:

$$H(E, A) = \max(h(E, A), h(E, A)) \tag{4.2}$$

where

$$h(E, A) = \max_{e \in E} \min_{a \in A} \parallel e - a \parallel \tag{4.3}$$

where e and a are data points in E and A, respectively.

H and MSE are able to give a good indication of error between the ground-truth estimation and the coordinates obtained. However, they are not normalised metrics: only certain ranges of MSE and H are useful for error discernment (this is shown in Section 5.2). Another disadvantage of these error metrics is that they are not case-specific to this research. Owing to the fact that the structure and contrast of the fingerprint are important and measurable quantities, SSIM and RMS-C are also measured.

SSIM is designed to measure the structural similarity between two images, and was developed by making use of the assumptions employed by the human visual system. In this way, it attempts to detect structure and consequent similarity in a manner to which a human can relate. First developed by Wang and Bovik as a universal image quality index [70], and later refined as SSIM [71], it is a normalised (to percentage similarity) metric, and is defined as:

$$SSIM(e, a) = \frac{(2\mu_e\mu_a + St_1)(2\sigma_{ea} + St_2)}{(\mu_e^2 + \mu_a^2 + St_1)(\sigma_e^2 + \sigma_a^2 + St_2)}, \tag{4.4}$$

where SSIM is calculated locally. e and a are the measured windows. μ_e is the mean of e, and μ_a is the mean of a. The variances of e and a are σ_e^2 and σ_a^2, respectively, while σ_{ea} is the covariance of e and a. St_1 and St_2 are stabilization variables.

RMS-C is an accepted means of measuring contrast between two images. Since the measured quantities are 2D, they can be regarded as images. RMS-C is the standard deviation of pixel intensities [72], defined as:

$$RMS\text{-}C(E) = \sqrt{\frac{1}{XY}\sum_{i=0}^{X-1}\sum_{j=0}^{Y-1}(E_{ij} - \text{mean}(E))^2}, \tag{4.5}$$

where E is the measured 2D quantity; X and Y are the dimensions; E_{ij} are the $i-th$ and $j-th$ elements; and $mean(E)$ is the average of E.

The result of this testing is given in Section 5.1. Testing procedures for internal fingerprint zone-detection are given in the following section.

4.2.2 Internal fingerprint zone-detection

Testing of internal fingerprint zone-detection is conducted, in part, by using the same four quantitative metrics (MSE, H, SSIM, and RMS-C) to compare G to P.

The testing ranges for n and c are both $2 \ldots 23$. This limitation is imposed because high combinations of n and c are lengthy to process; an unsatisfactory consequence that would see high values of c and n never being used in real-world scenarios, regarding this application. Furthermore, high values of c and n may lead to overfitting and other degenerative clustering behaviour.

Time taken is also measured for: data and feature extraction, clustering, and fine-tuning. Data and feature extraction is dependent on n. Clustering is dependent on n and c. Fine-tuning is independent of both n and k.

Interpolation of the data in the chosen cluster yields PC. Percentage interpolated is measured over the entire $n : c$ testing range.

Numerous qualitative results are also given to show the efficacy, robustness, and disadvantages of internal fingerprint zone-detection. Both the quantitative and qualitative analysis is detailed in Section 5.2. The experimental set-up regarding internal fingerprint extraction (as per Section 3.2.1) is given in the next section.

4.2.3 Internal fingerprint extraction and enhancement

There is no way of estimating a ground-truth scenario for the extraction procedure. Although minutiae points detected can be evaluated for correctness, this exhibits the

performance of the minutiae extraction algorithm used, instead of the internal fingerprint itself. Therefore, testing the internal fingerprint involves testing for correspondence with surface counterparts and cross-correspondence, as per Section 4.3. This manner of testing shows both the viability of the internal fingerprint itself and performance of the internal fingerprint extraction algorithm, as these are not exclusive of each other.

The internal fingerprint extraction process is also tested in a qualitative manner. Results regarding the zone described by statistical evaluations of P and the corresponding extracted internal fingerprints are given in Section 5.3.

The testing procedures for internal to surface and internal cross-correspondence are outlined in the following section.

4.3 Internal Fingerprint Assessment

Prior to comparison with their surface counterparts, the internal fingerprints are first resized to correspond with the restriction of high-quality surface fingerprints: $500ppi$ (197×197 *pixels* and 295×295 *pixels* for the $10mm \times 10mm$ and $15mm \times 15mm$ scans, respectively).

Table 4.1 gives the parameters used in extracting the internal fingerprints for this research. The internal fingerprints extracted from the scanned OCT fingertip volumes can be subjectively divided into three categories. These are:

1. **Category 1:** Small scanned region ($10mm \times 10mm$) of a bad fingerprint area (i.e., far from the fingerprint core).
2. **Category 2:** Small scanned region ($10mm \times 10mm$) of a good fingerprint area (i.e., at or near the fingerprint core).
3. **Category 3:** Large scanned region ($15mm \times 15mm$).

This manual division of scanned fingerprints serves to ensure that the results obtained are not biased owing to scanned region size and locality to the fingerprint core. The performance of a fingerprint is dependent on these factors, and this division allows for a more independent evaluation of the internal fingerprint itself.

Component	**Parameter**	**Value**
Stratum corneum detection	Polynomial degree	3
Fuzzy c-means thresholding	m	2.2
Fuzzy c-means thresholding	$max\_threshold$	0.9
Small image region extraction	Height	28 *pixels*
Interpolation	Smoothing window size	4
Interpolation	Edge buffer	10
Fine-tuning	OBNLM 1; search size	12
Fine-tuning	OBNLM 1; patch size	2
Fine-tuning	OBNLM 1; smoothing	2
Fine-tuning	OBNLM 2,3; search size	6
Fine-tuning	OBNLM 2,3; patch size	1
Fine-tuning	OBNLM 2,3; smoothing	1
Fine-tuning	LN; amplitude	3.13
Fine-tuning	LN; radius	10
Fine-tuning	LN; neighborhood smoothness	10.09
Fine-tuning	LN; average smoothness	11.83
Fine-tuning	Unsharp masking; radius	29.9
Fine-tuning	Unsharp masking; amount	4.63
Fine-tuning	Unsharp masking; threshold	9.8%
Extraction	$window\_size$	10X10
Extraction	$start\_offset$	8 *pixels* down
Extraction	end_offset	3 *pixels* down
Extraction	$deviation\_multiplier$	5
Fingerprint enhancement	OBNLM; search size	15
Fingerprint enhancement	OBNLM; patch size	1
Fingerprint enhancement	OBNLM; smoothing	1
Fingerprint enhancement	LN; amplitude	6
Fingerprint enhancement	LN; radius	4
Fingerprint enhancement	LN; neighborhood smoothness	10.53
Fingerprint enhancement	LN; average smoothness	21.11
Fingerprint enhancement	Contrast stretch, minimum	30
Fingerprint enhancement	Contrast stretch, minimum	150

TABLE 4.1: **Algorithm parameters**. Local normalisation was carried out using GREYC's Magic for Image Computing [74]. The significant figures are as per listed therein.

Fingerprint quality metrics are used to assess the quality of the internal fingerprints. Alonso-Fernandez et al. [75] compared fingerprint image-quality estimation methods to describe the effect of image-quality on fingerprint verification. Their study divided quality metrics into several groups. Amongst these, and useful to this research, are:

- The orientation certainty level (OCL) [76] that measures the energy concentration along the dominant ridge-valley orientation. It is calculated in a local, blockwise fashion. A lower OCL score corresponds to a better quality region. A global OCL score is calculated as the average of all the respective blockwise OCL scores.
- The NFIQ number [77, 78] that predicts a fingerprint's positive or negative contribution to an overall matching system. It uses a neural network to classify fingerprints according to eleven-dimensional feature vectors, computed as image characteristics. It is a well-known and trusted image-quality estimation technique. It ranges from one (best) to five (worst), with integer divisions.

There are many quality metrics for assessing fingerprints. The reader is referred to [75] for a fuller review of these. OCL and NFIQ were chosen because they are widely accepted, the fingerprints being assessed should not contain any intentional anomalies, and they, in combination, give a broad assessment of fingerprint quality.

Although these metrics are able to give a fairly accurate estimate of fingerprint image-quality, they are unable to give a full account of fingerprint performance. The internal fingerprints obtained in this research are, therefore, tested against their surface counterparts using the NIST minutiae extraction (*mindtct*) and matching (*bozarth3*) software [79].

The match score is calculated between each internal fingerprint and all of its surface counterparts, yielding sixteen match scores per internal fingerprint. In addition, the cross-correspondence between internal fingerprints of the same fingers is measured. A match score of forty is considered to represent a 'true match', according to NIST [78].

In order to exemplify objectively the quality and performance of the internal fingerprints, a reference point must be given. This reference point is the performance of conventional surface fingerprints when matched against surface fingerprints of the same fingers. However, there are a number of factors that affect fingerprint match performance, such as:

surface fingerprint distortion upon scanning; the lack of ridge-valley clarity of some surface fingerprints; and scan area size and locality. Eliminating most of these factors is outside the scope of this research. Nevertheless, ensuring that the surface fingerprints used to define a performance reference point encompass approximately the same region (with respect to area and locality) of their corresponding internal fingerprints is necessary. In doing so, a bias that would otherwise misconstrue the performance of internal fingerprints is eliminated.

For each internal fingerprint three conventional surface counterparts were obtained. These were manually cropped to encompass regions similar to their internal counterparts. Since OCT is an emerging, yet to be established, tool for fingerprint acquisition, it cannot perform on a competitive level regarding imaged area size. A performance comparison is given in Section 5.4. Furthermore, a summary of fingerprint quality assessment; the average match scores for surface correspondence; the maximum match scores for surface correspondence; and the cross-correspondence average and maximum scores are also given in Section 5.4.

This chapter served to outline the testing procedures followed to provide quantitative evidence that the internal fingerprint is a viable replacement for the surface fingerprint. Qualitative results are also paramount in showing the effectiveness of the internal fingerprint extraction algorithm, as well as the internal fingerprint itself. The results obtained, both quantitative and qualitative, are given in the following chapter.

Chapter 5

Results and Discussion

This chapter serves to exhibit the results obtained when quantitatively and qualitatively testing the algorithms, techniques, and approaches developed in Chapter 3. Section 5.1 gives the analysis of the four clustering algorithms, and validates the use of fuzzy c-means clustering. Section 5.2 encapsulates the results of internal fingerprint zone-detection and proposes constraints on the clustering algorithms based on these results. Section 5.3 demonstrates the use of dynamic region extraction using both data (i.e., the OCT volume) and the coordinates of the papillary junction, and gives examples of extracted fingerprints. Section 5.4 serves to evaluate the performance of the internal fingerprints extracted using the techniques presented in this research.

5.1 Cluster Algorithms' Analysis

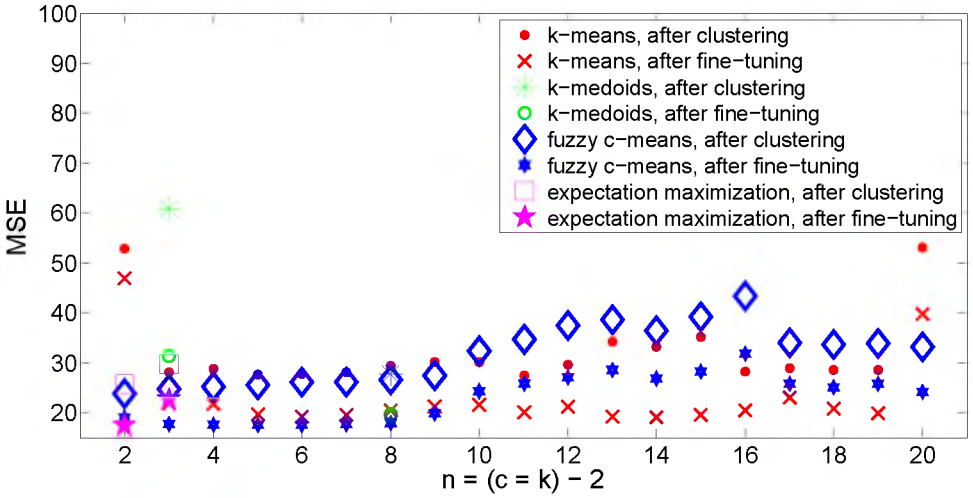

FIGURE 5.1: **Initial clustering testing**: MSE results.

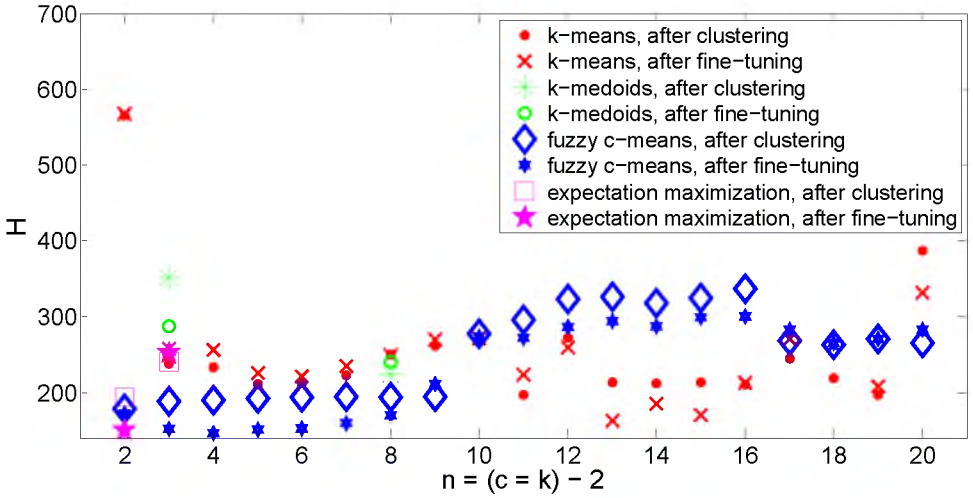

FIGURE 5.2: **Initial clustering testing**: H results.

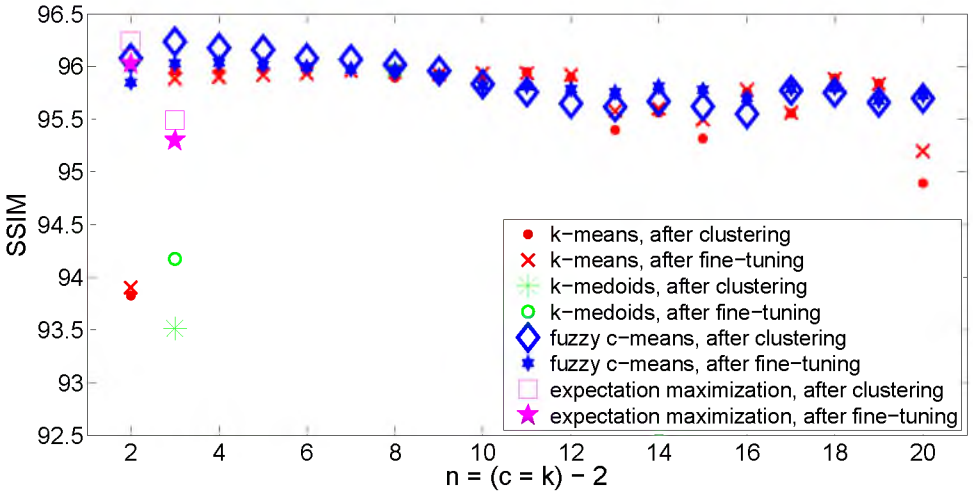

FIGURE 5.3: **Initial clustering testing**: SSIM results.

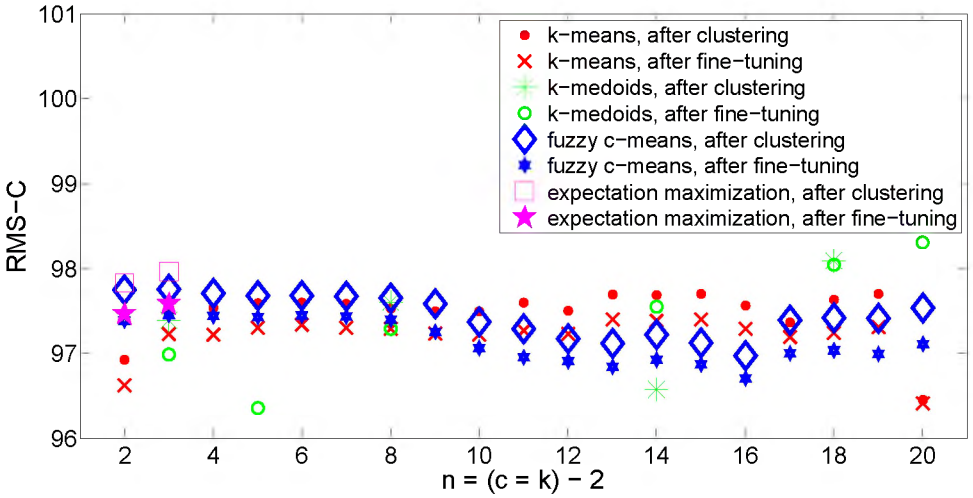

FIGURE 5.4: **Initial clustering testing**: RMS-C results.

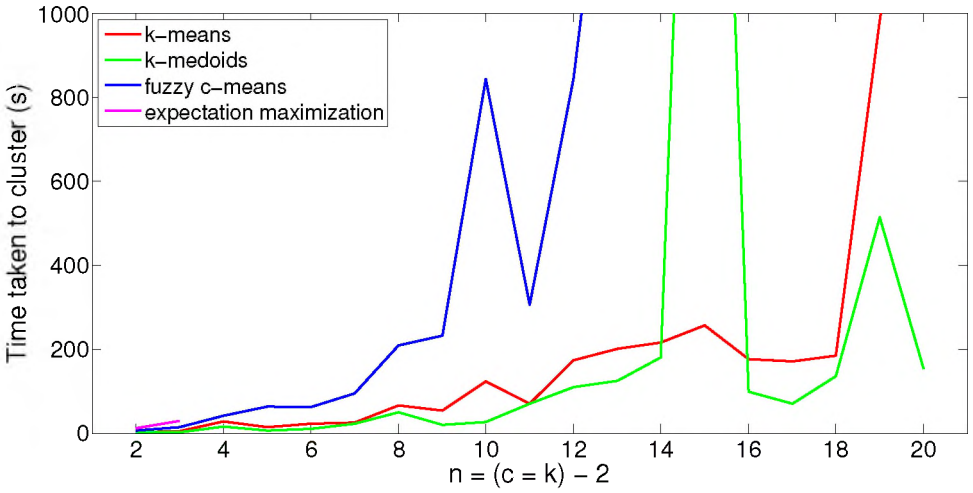

FIGURE 5.5: **Initial clustering testing**: timing results.

Figures 5.1 through 5.4 exhibit the performance results for the initial cluster algorithm experimentation. $n = (c = k) - 2$ was the constraint placed upon the ratio between the number of clusters and the number of data points per A-line. By setting the number of clusters to be higher for each $n : (c = k)$ ratio, outlying data points could be detected; each data point per A-line must fall within its own cluster, or be an outlier. This constraint is expounded upon in Section 5.2. These figures show only a region of interest because k-medoids performed very poorly, and showing all results is meaningless in assessing the performance of the better-performing clustering algorithms.

Fuzzy c-means outperformed all other clustering algorithms when $(c = n + 2) < 10$. Although k-means performed better when $(k = n + 2) \geq 10$, this region of testing is unsatisfactory with respect to time taken (see Figure 5.5). The results for k-medoids are not entirely visible in the regions of interest as it performed poorly. Expectation maximization did not converge when the number of clusters was set above five.

Fine-tuning improved all measured metrics in almost all cases. Thus, the fine-tuning procedure is able to improve the accuracy of internal fingerprint zone-detection.

Algorithm	**MSE**			**H**		
	PC	*P*	Best	*PC*	*P*	Best
k-means	32.1 ± 7.7	22.9 ± 7.4	19.1	254.4 ± 86.8	254.8 ± 85.8	162.3
fuzzy c-means	31.7 ± 5.9	23.1 ± 4.7	17.6	252.5 ± 58.2	233.2 ± 62.3	146.4

TABLE 5.1: **Initial clustering testing results**: MSE and H for k-means and fuzzy c-means.

Table 5.1 is a summary of the MSE and H results over the entire tested region for the best performing clustering algorithms: k-means and fuzzy c-means. Fuzzy c-means produced better average and lowest MSE and H values. Furthermore, fuzzy c-means is more robust and stable in this application when compared to k-means, as exhibited by the lower standard deviations in all measured quantities. The best results were shown as this initial experimentation is designed to find suitable parameters for clustering, and those corresponding to the best results obtained are used.

Owing to these initial experiments, Fuzzy c-means was used in further experimentation. It performs well at lower values of n and c – a region where time taken is low – and is suited to outlier detection.

The following section details the results of internal fingerprint zone-detection.

5.2 Internal Fingerprint Zone-Detection

This section outlines the results obtained regarding the processes developed to detect the internal fingerprint zone: a critical component of internal fingerprint extraction.

An essential step in detecting the internal fingerprint zone is the detection of the stratum corneum. Figure 5.6 shows six instances of stratum corneum detection. There was no case where stratum corneum detection failed to the degree that the internal fingerprint zone could not be located, even when the signal content was low (Figure 5.6(C) and (D), for example). Consequently, the stratum corneum is adequately detected for use in internal fingerprint zone-detection.

The main component of internal fingerprint zone-detection is fuzzy c-means clustering. Data and features are extracted from A-lines. Along with Figure 3.5, which exhibits an expected A-line profile and two anomalous A-line profiles, Figure 5.7 presents four A-line examples that do not adhere to the expected relative intensity of the skin layers.

The deviations from the expected A-line profile are attributable to the presence of speckle noise, the curvature and intensity roll-off problems, biological inconsistencies in the skin, or a combination thereof. It is the presence of these inconsistencies, that necessitate an advanced technique for internal fingerprint zone-detection and extraction.

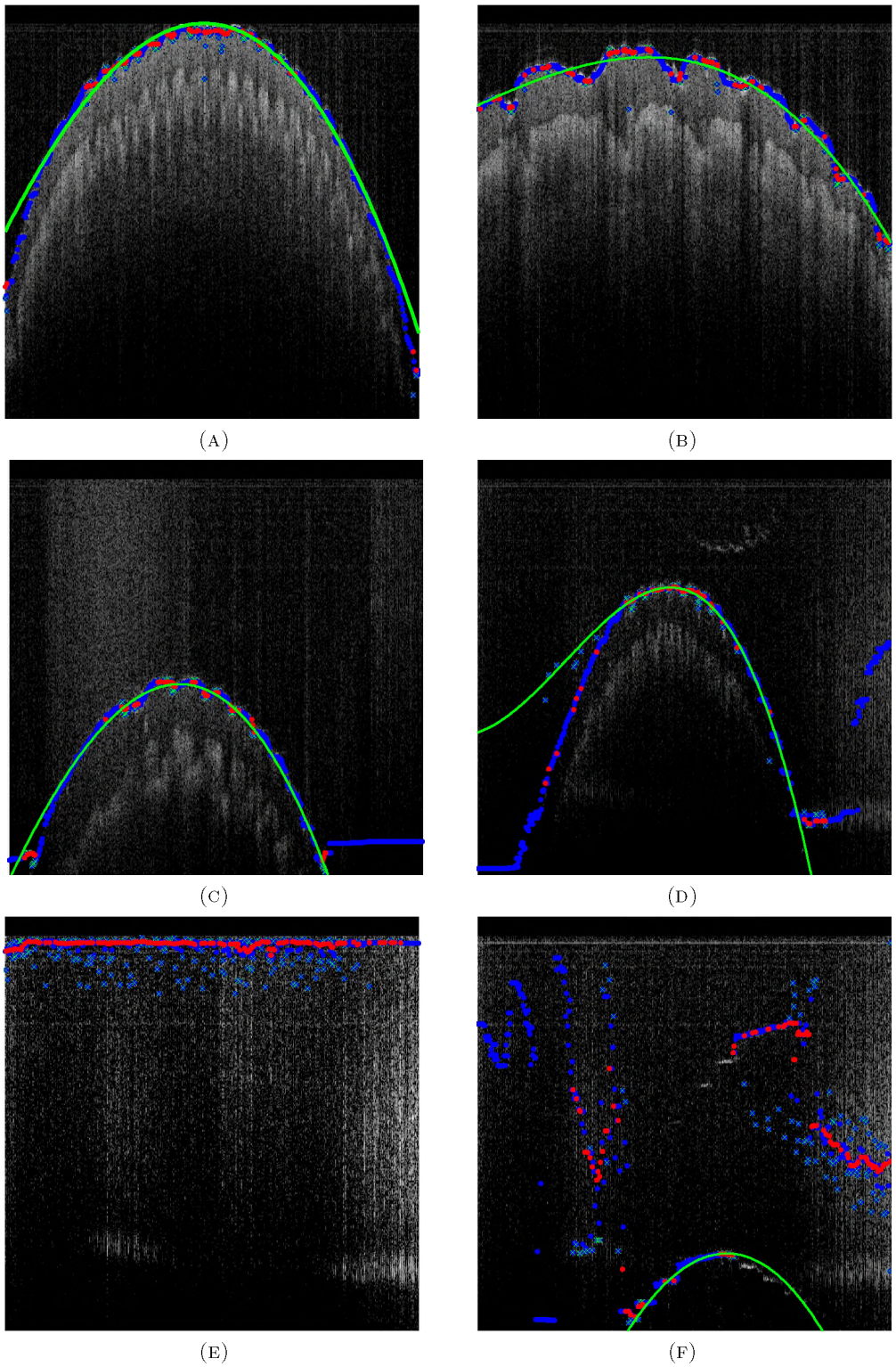

(A) (B) (C) (D) (E) (F)

FIGURE 5.6: **Stratum corneum detection examples**: (A) and (B) show good detection on B-scans with high signal content; (C) shows good detection on a B-scan with low signal content; (D) shows good detection when **PolyEstimate** deviates significantly; (E) shows detection on a B-scan that holds no useful information; and (F) shows bad detection on a B-scan with low signal content. The blue dots are the closest A-line intensity local maxima to **SCEstimate**, the green line is **PolyEstimate**, the green crosses are detected outliers, and the red dots are corrected outliers.

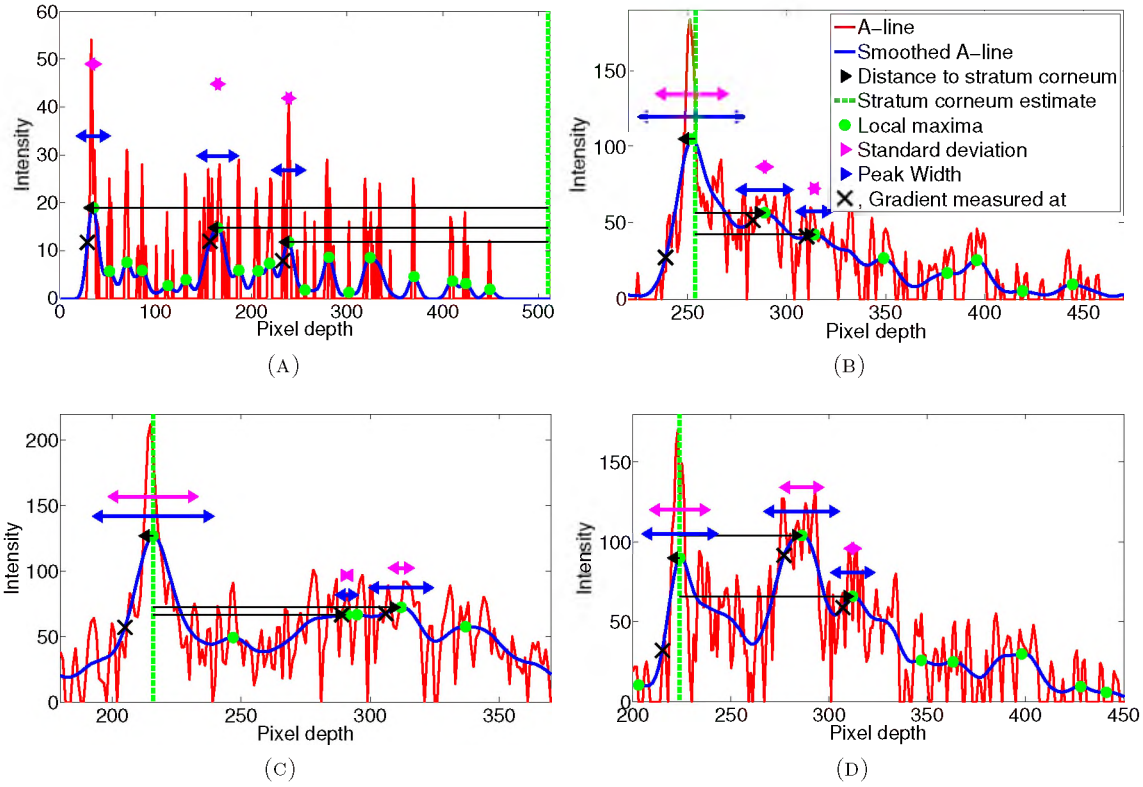

FIGURE 5.7: **A-line examples**: (A) is an A-line without a stratum corneum or papillary junction (because of curvature roll-off); (B) is an A-line where the papillary junction local maximum is weak; (C) is an A-line where the second strongest peak is not the papillary junction; and (D) is an A-line where the stratum corneum is not the strongest peak.

The algorithm developed for this research was tested by comparing automatically obtained coordinates (P) against ground-truth coordinates (G). G was estimated by a human observer. Thirteen volunteers were asked to estimate the location of the papillary junction upper-edge on five B-scans to quantify the effect of human error. A comparison of all the volunteers' estimates yielded a mean MSE of 15.6 $\pm$ 6.0, a mean H of 157.3 $\pm$ 22.0, and a mean RMS-C of 103.1 $\pm$ 0.4. SSIM was not calculated in this case as five B-scans did not suffice a meaningful SSIM result.

As was stated in Chapter 3, precursor works served to formulate the internal fingerprint zone-detection algorithm. The work by Darlow *et al.* [41] utilised k-means and a similar fine-tuning process to locate the internal fingerprint. Table 5.2 summarises the quantitative metrics obtained using the old (k-means) and new (fuzzy c-means) methods.

The ranges tested in the earlier work were larger than those tested in this work because of the time taken to perform clustering when n and c are large. The same conclusion was

Metric	***Old* k-means [41]**		***New* fuzzy c-means**		**Human**
	Candidate parameter region	**Best**	**Candidate parameter region**	**Best**	
MSE	38.4 ± 16.8	23.6	28.2 ± 11.3	21.3	15.6 ± 6.0
H	218.2 ± 53.6	142.5	234.5 ± 92.5	147.8	157.3 ± 22.0
SSIM	92.2 ± 3.3%	94.5%	95.8 ± 2.6%	96.4%	-
RMS-C	98.4 ± 0.4	143.3	97.3 ± 0.4	145.5	103.1

TABLE 5.2: **Quantitative results**. Human results are included for comparison, as are results obtained in the work by Darlow *et al.* [41].

drawn in the earlier work. It is evident that the best results obtained in this work are an improvement on results obtained earlier. Although the average H was less satisfactory, the average MSE and SSIM were improved. RMS-C was lower, yet more stable, because some combinations of n and c lead to high contrast anomalies in P. Thus, stability in RMS-C is more important than high values thereof.

Figure 5.8 exemplifies clustering output for different combinations of n and c, while Figure 5.9 encapsulates the quantitative results for all the measured metrics. A minimum MSE of 21.3, a minimum H of 147.8, a maximum SSIM of 96.4%, and a mean RMS-C (in the candidate parameter region) of 97.3 ± 0.4, show that P corresponds well with G. The performance of the internal fingerprint zone-detection algorithm is comparable to human attempts at the same task. That is, the best MSE result is within the standard deviation of the human MSE results, and the MSE results within the candidate parameter region overlap with the human MSE results, for instance.

There is a distinct, stable candidate parameter region regarding all measured metrics. This region is shown as Figure 5.9(E) and constitutes 59.9% of the measured ranges of c and n. The performance stability of internal fingerprint zone-detection is of a high standard: the region within which the results are satisfactory is largely encompassing of the tested parameter ranges, and is consistent over four different quality metrics. Furthermore, the hypothesis regarding $c > n$ procuring satisfactory results is validated herein.

Obtaining PC requires the interpolation of missing data in the chosen cluster. Figure 5.9(F) gives the percentage interpolated over the tested ranges of n and c, while Table 5.3 gives the average percentage interpolated for all the scanned fingertips (with $n = 3$

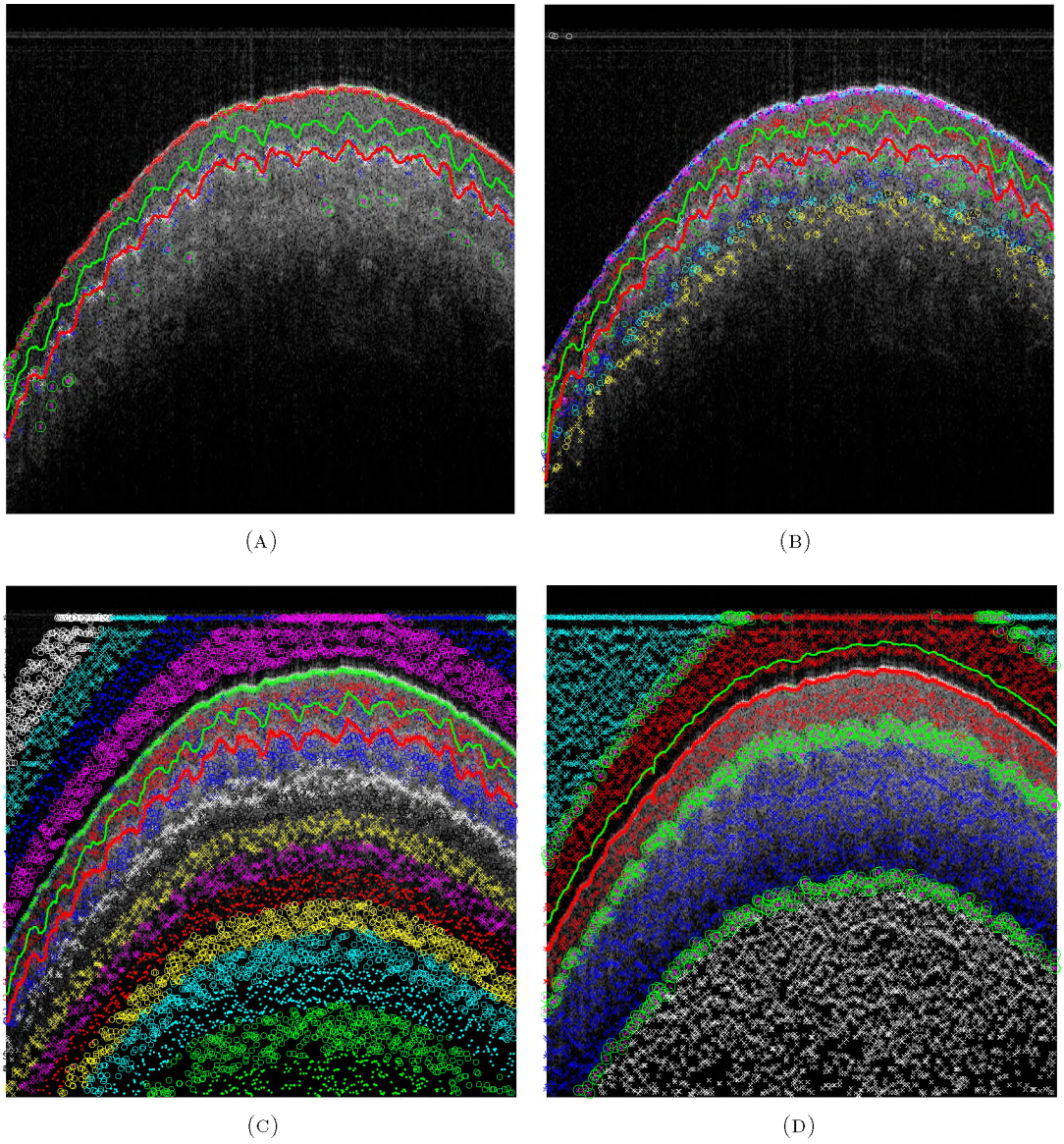

(A) (B)

(C) (D)

FIGURE 5.8: **Clustering output examples**: different colour/marker combinations represent different clusters; large green circles encircle outliers; the bottom (red) lines exhibit PC; and the region between the lines is the region extracted for fine-tuning. (A) is when n and c are low. (B) is when n is low and c is high. (C) is when n and c are high. (D) is when when n is high and c is low.

and $c = 6$). Strong cluster-membership was imposed by setting m high (see Table 4.1) in Equation 3.1. Although this results in the need for more interpolation (45.4 % on average), it must not be interpreted as poor performance. Instead, it ensures robustness in the clustering step as there is more certainty regarding cluster-membership. Figure 3.8 is an example of interpolation.

The final step in internal fingerprint zone-detection is fine-tuning. Figure 5.10 depicts two fine-tuning examples that differ in performance. As is apparent in this figure, the

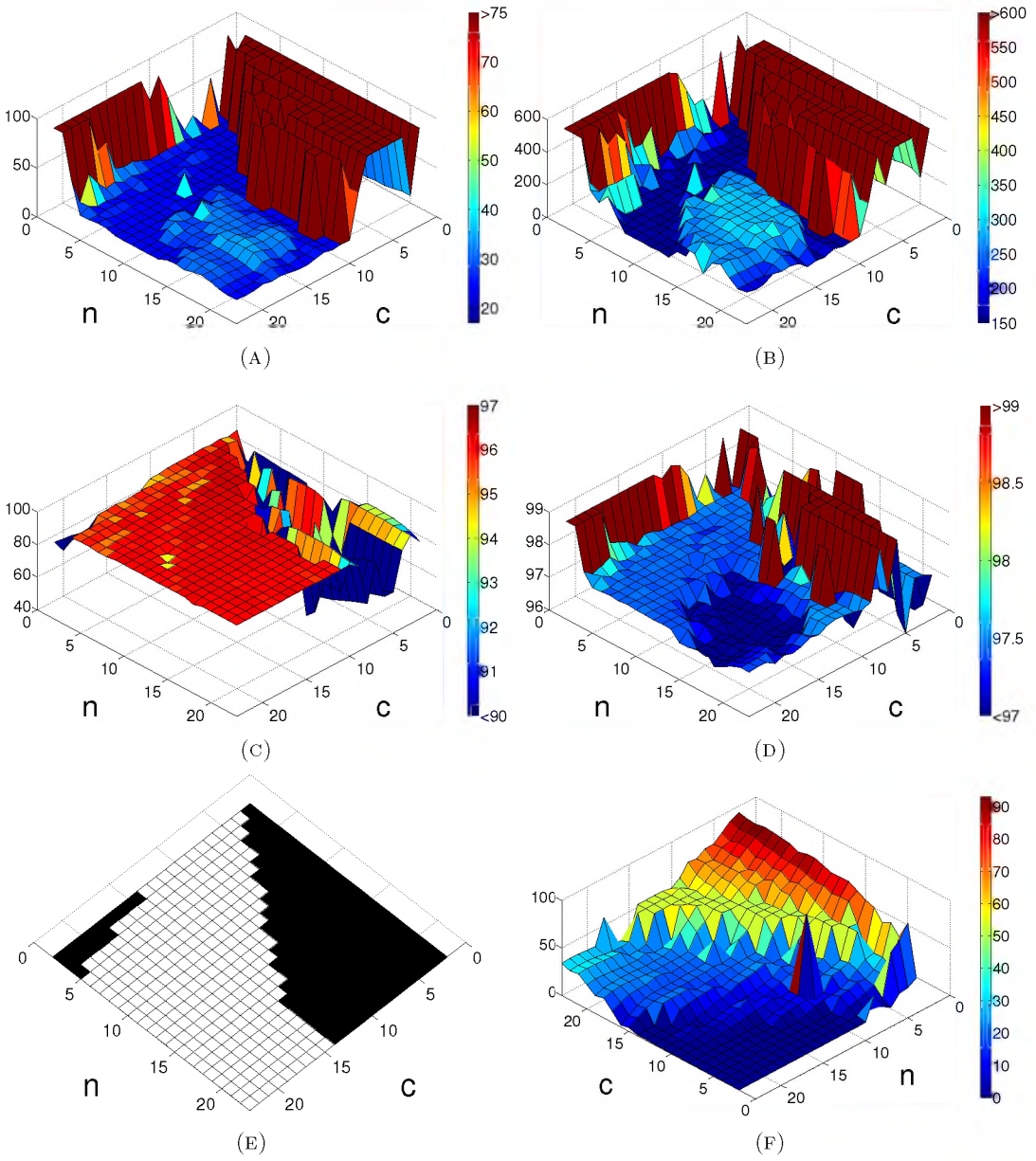

FIGURE 5.9: **Quantitative results for internal fingerprint zone-detection**. These were measured over a range of $c = n = 2 \ldots 23$. (A) are the MSE results. (B) are the H results. (C) are the SSIM results. (D) are the RMS-C results. (E) shows the determined candidate parameter region. (F) gives the percentage interpolated. The axes of (F) are swapped and reversed in order to make visible the interpolation results.

Area	**Resolution**	**% interpolated**
$10mm \times 10mm$	256×256 *pixels*	45.51 ± 12.74
$15mm \times 15mm$	256×256 *pixels*	43.40 ± 11.04
$10mm \times 10mm$	512×512 *pixels*	47.15 ± 7.44
$15mm \times 15mm$	512×512 *pixels*	46.13 ± 4.24
Overall:		45.41 ± 9.55

TABLE 5.3: **A summary of interpolation for** *PC*.

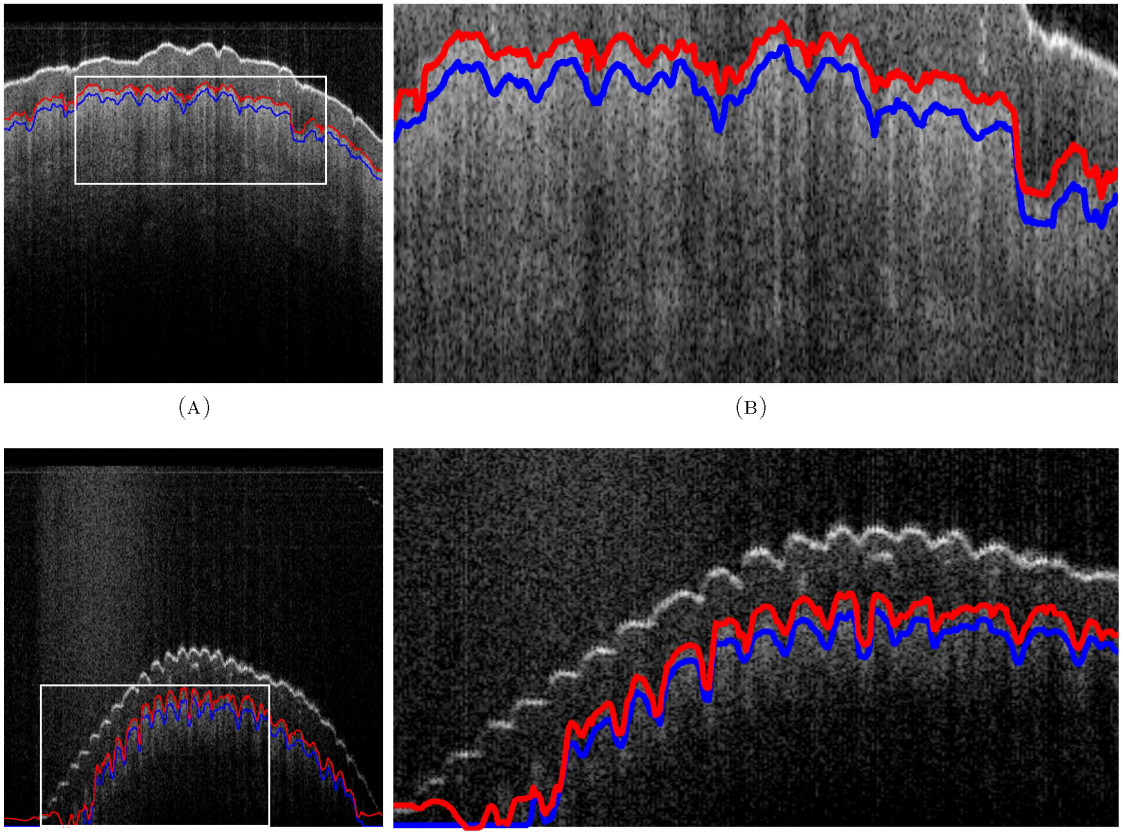

(A) (B)

(C) (D)

FIGURE 5.10: **Adjustments owing to fine-tuning**. The left column shows single B-scan images taken from different OCT fingertip volumes, and the right column exhibits the indicated regions of interest. The bottom (blue) lines are PC, while the top (red) lines are P. (A) and (B) show good detection; and (C) and (D) exhibit a case where detection fails – the lower left regions.

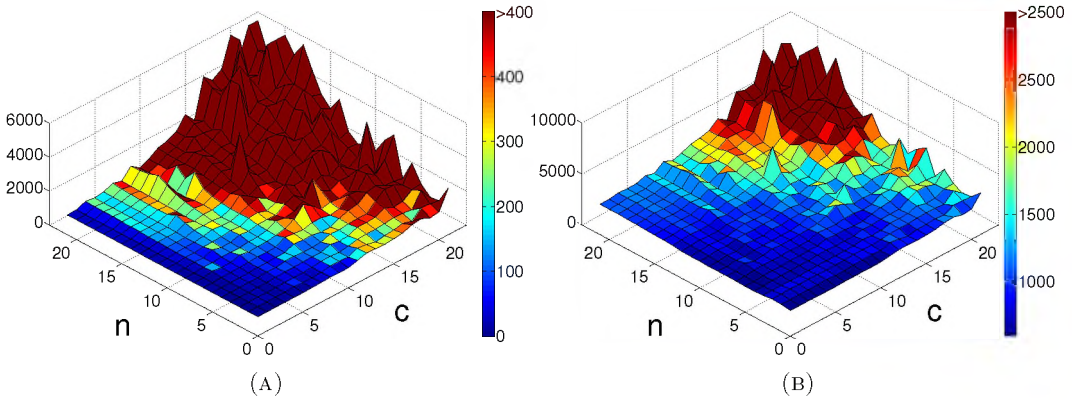

(A) (B)

FIGURE 5.11: **Timing results.** These were measured in seconds over a range of $c = n = 2 \ldots 23$. (A) shows the time taken to perform clustering, while (B) shows the time taken to perform the entire internal fingerprint zone-detection process.

performance of and contribution by fine-tuning is significant. P followed the papillary junction upper-edge consistently. Although there were some inconsistencies in P, these had a minor effect in the extraction process.

It must be noted that no aspect of the algorithms developed was optimized for running time. Therefore, the time taken to detect the internal fingerprint zone is unsatisfactory for a real-time system. The times taken for clustering and internal fingerprint zone-detection are given in Figure 5.11(A) and (B), respectively. The shortest time taken for clustering was 2.0 s and the corresponding time taken to extract features was 178.4 s. The shortest time taken to detect the internal fingerprint zone was 595.0 s. The time taken to perform fine-tuning is independent of n and c and was 327.7 s at best.

Owing to the following observations, a formulation of the optimal $n : c$ ratio can be given:

1. Performance is stable when $c > n$.
2. Higher values of c and n are unsatisfactory regarding the time taken to cluster, as per Figure 5.11(A).
3. There is a performance limited 'tapering' toward lower ratios of $n : c$, exemplified in Figure 5.9(E). This means that the variability of one parameter, with respect to the other, while still maintaining suitable performance, becomes lower toward the $(0, 0)$ point.

The restrictions on $n : c$ are that $c > n$, both n and c must be as small as possible, and the ratio of $n : c$ must be sufficiently buffered from the tapered region. Thus, $3 \leq n < c \leq 12$ is sufficient. For the extraction of internal fingerprints, as tested in Section 5.4, $n = 3$ and $c = 6$.

To answer the research-questions posed in Section 1.6: the signal relating to the papillary junction can be enhanced using OBNLM and contrast-enhancement, and the location of the papillary junction can be determined accurately.

The testing of the extraction and enhancement processes is discussed in the following section.

5.3 Internal Fingerprint Extraction

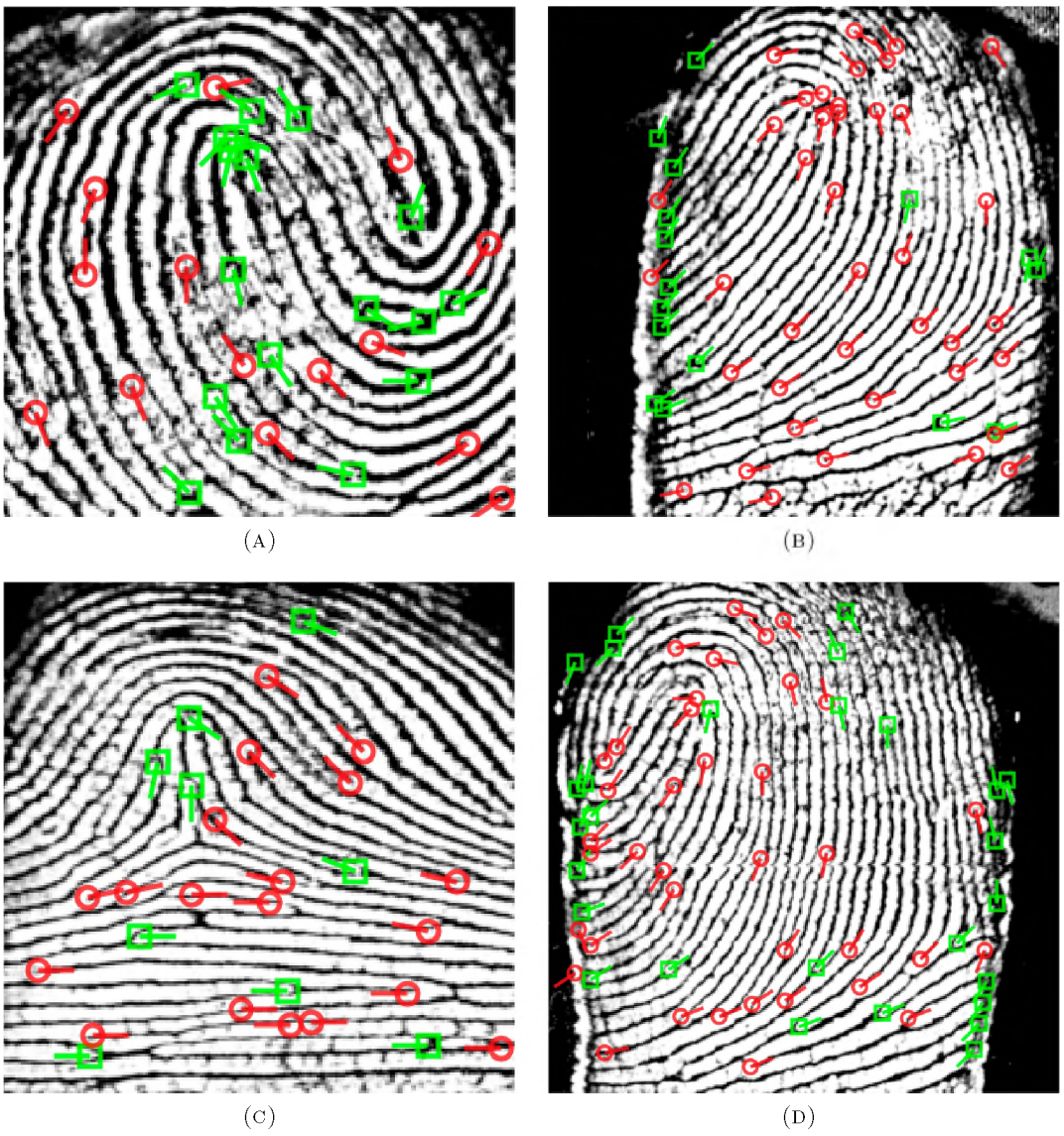

FIGURE 5.12: **Internal fingerprint examples**: (A) is from a $10mm \times 10mm$ and 256×256 *en-face* pixel scan; (B) is from a $15mm \times 15mm$ and 256×256 *en-face* pixel scan; (C) is from a $10mm \times 10mm$ and 512×512 *en-face* pixel scan; and (D) is from a $15mm \times 15mm$ and 512×512 *en-face* pixel scan. The minutiae detected are visible as red circles (ridge-endings) and green squares (bifurcations).

Figure 5.12 displays four internal fingerprints extracted from OCT scans of varying resolutions and region sizes. Minutiae were successfully detected for each combination, although the combination of 256×256 (*en-face* resolution) and $15mm \times 15mm$ exhibited some loss in contrast regarding ridge-to-valley clarity. This is visible in the upper-right corner of Figure 5.12(B) and is because the effective resolution of these scans are low (approximately $433ppi$). The curvature roll-off problem is evident in Figure 5.12(B) and

(D) as the dark regions on either side of the fingerprint. However, since these regions are consistently dark, fingerprint minutiae detection algorithms should not be hindered by them.

Figures 5.13 and 5.14 are examples of extractions from $10mm \times 10mm$ and $15mm \times 15mm$ scans, respectively. Figure 5.13(B) exhibits how the windowed statistical approach is robust against deviations, as evidenced by how the jitter of the dashed (yellow) line does not heavily affect the outcome of the extraction zone (between the two smooth blue and green lines).

Figure 5.14(B) demonstrates the efficacy of this approach even when signal content was limited. There is very little useful information in this B-scan (hence it is very dark), and even less relating to the papillary junction, yet it is detected sufficiently when present. Figure 5.13(A) and 5.14(A) exemplify the capture of the internal fingerprint undulations through the analytical description of the region that best emphasises ridges (bright) and valleys (dark).

The enhancement procedure is demonstrated in Figure 5.13(C) - (F) and Figure 5.14(C) - (F). The effect of OBNLM noise-reduction is evident in the smoothing of homogeneous zones and edge preservation. The two (local and global) contrast-enhancement procedures worked in unison to provide a clear representation of internal fingerprint ridges and valleys. The minutiae detected are shown in Figures 5.13(F) and 5.14(F), as evidence that the internal fingerprint is of sufficient quality for minutiae detection. The evaluations in this section demonstrated the high-quality of the internal fingerprint prior to comparison with surface counterparts or other internal fingerprints.

As per the research-questions posed in Section 1.6:

- The internal fingerprint exists and can be extracted from OCT fingertip scans using localised statistical evaluations of the papillary junction location.
- The extracted internal fingerprint can be successfully enhanced by applying noise-reduction and contrast-enhancement.
- The internal fingerprint is of sufficient quality and minutiae can be extracted.

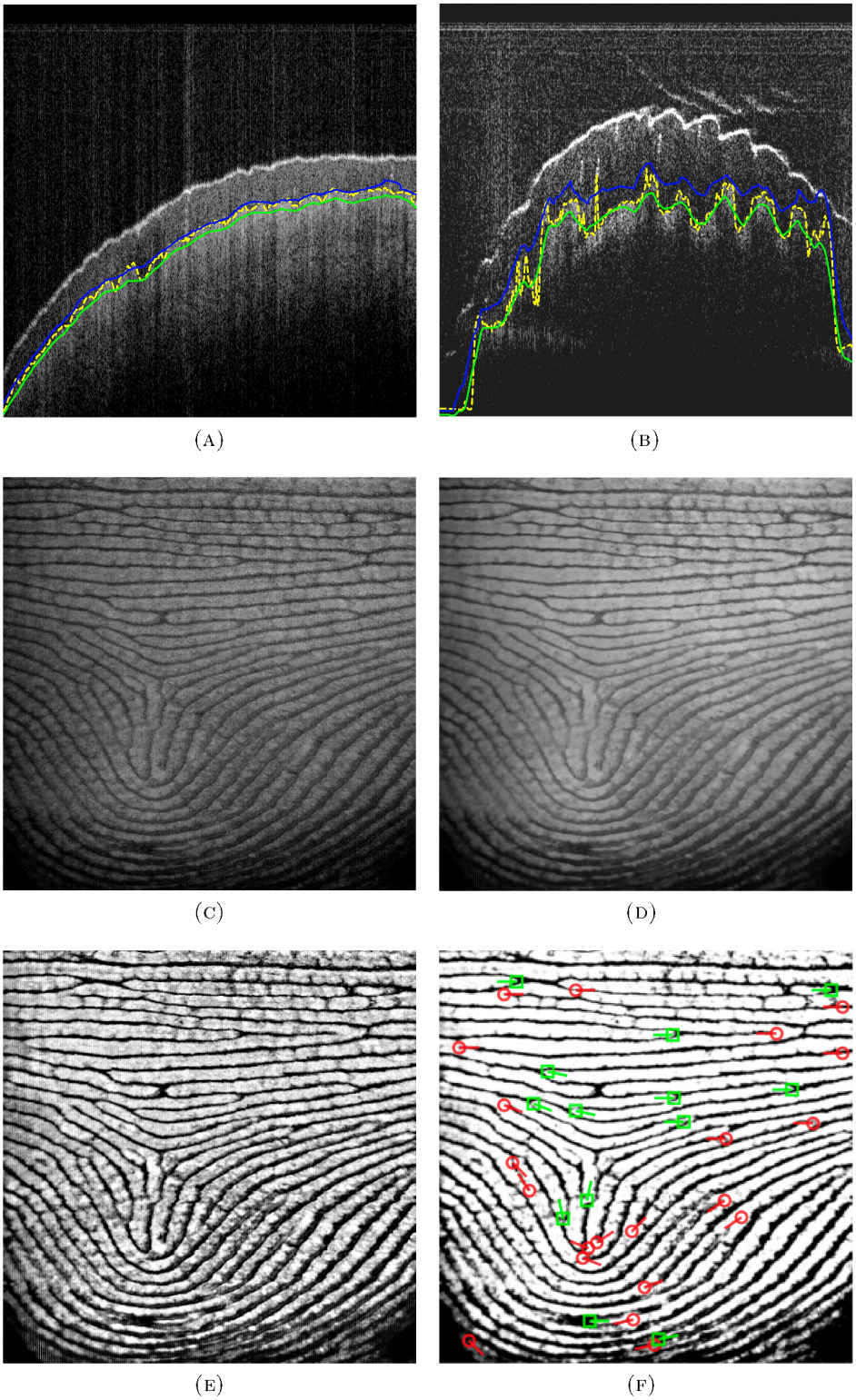

(A) (B)

(C) (D)

(E) (F)

FIGURE 5.13: **Internal fingerprint extraction**: $10mm \times 10mm$ scan. The region over which pixel intensities are averaged to produce the internal fingerprint – (C) – is between the green and blue lines, while the dashed (yellow) line is indicative of P. (A) and (B) show this for high and low signal B-scan images, respectively. (D) - (F) exhibit the enhancement procedure: (D) is after noise-reduction; and (E) and (F) are after local and global contrast-enhancement, respectively. Minutiae are also shown in (F). The brightness and contrast of (B) are adjusted for visualisation.

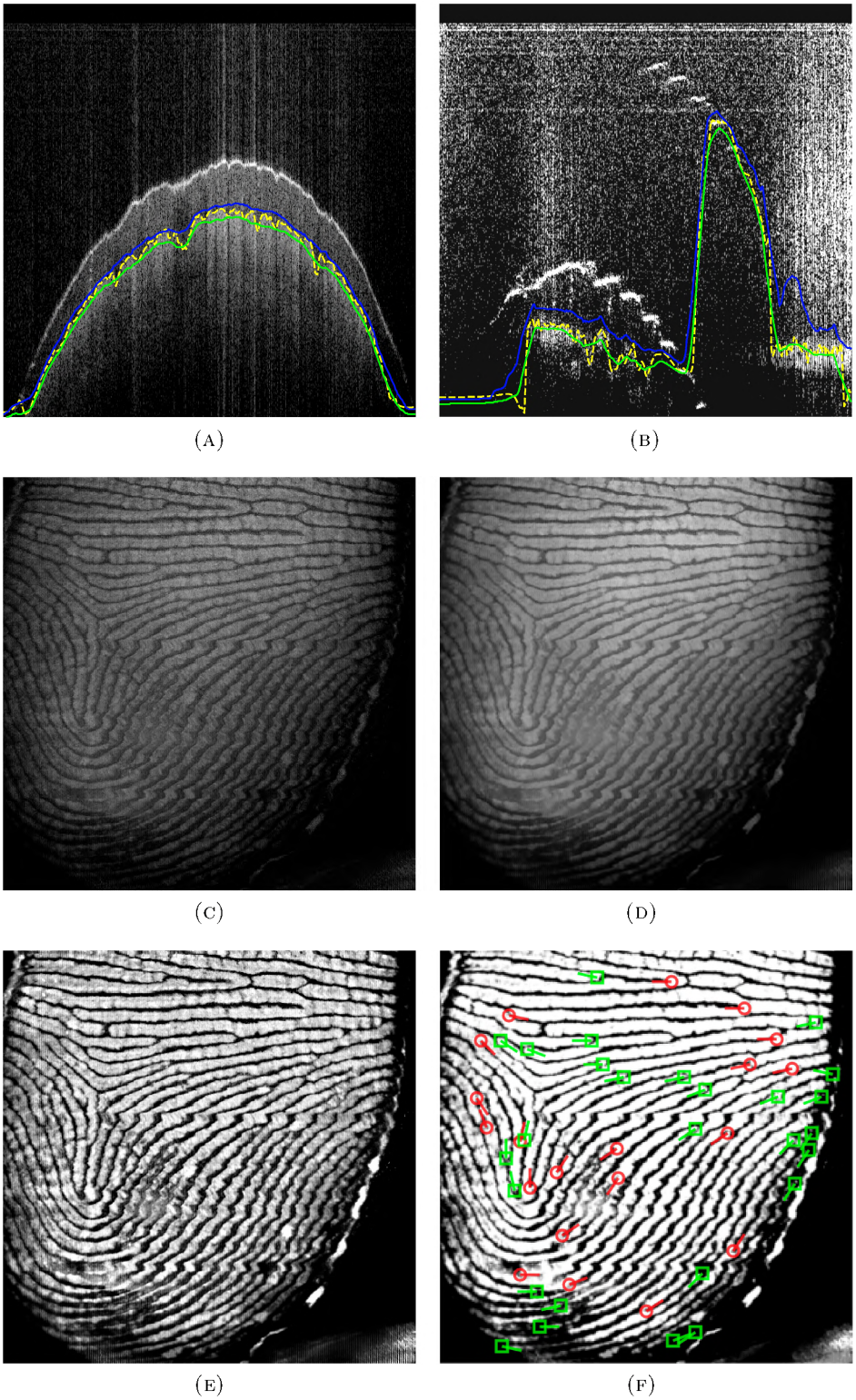

(A) (B)

(C) (D)

(E) (F)

FIGURE 5.14: **Internal fingerprint extraction**: $15mm \times 15mm$ scan. The region over which pixel intensities are averaged to produce the internal fingerprint – (C) – is between the green and blue lines, while the dashed (yellow) line is indicative of P. (A) and (B) show this for high and low signal B-scan images, respectively. (D) - (F) exhibit the enhancement procedure: (D) is after noise-reduction; and (E) and (F) are after local and global contrast-enhancement, respectively. Minutiae are also shown in (F). The brightness and contrast of (B) are adjusted for visualisation.

The following section details the performance of internal fingerprints with respect to fingerprint quality metrics, internal to surface fingerprint correspondence, and cross-correspondence.

5.4 Internal Fingerprint Evaluation

Each of the fingerprints extracted from the fifty-five OCT scans were compared to sixteen conventional surface scans. The internal fingerprint was first evaluated by measuring contrast (using RMS-C), calculating orientation certainty (using OCL), and through fingerprint categorisation (using NFIQ). Figure 5.15 displays the NFIQ scores and Table 5.4 exhibits the average RMS-C and OCL scores.

The surface fingerprints were of higher contrast than the internal fingerprints: the average RMS-C of the surface fingerprints was 11.63 ± 0.54, while the average RMS-C of the category three fingerprints (i.e., the best-case) was 10.73 ± 0.56. The parameters involved in the extraction of the internal fingerprints can be optimised in order to produce higher contrast results. However, that is not the focus of this research.

The OCL scores corresponded well with the predefined subjective internal fingerprint categorisation. In addition, both category two and category three internal fingerprints had superior average OCL scores compared to the surface fingerprints.

Owing to the dependency of NFIQ on the number of minutiae present in the fingerprint, the NFIQ scores are biased toward the surface fingerprint. Since the areas imaged with the OCT scanner were limited (particularly with regard to the category one and two internal fingerprints), the number of minutiae were limited too. However, 36% of the category three internal fingerprints had an NFIQ score of one, but only 29% of the surface fingerprints had an NFIQ score of one. The NFIQ scores calculated for the three internal fingerprint categories indicate that a larger scanned region (i.e., $15mm \times 15mm$ for category three internal fingerprints, in this research) is superior.

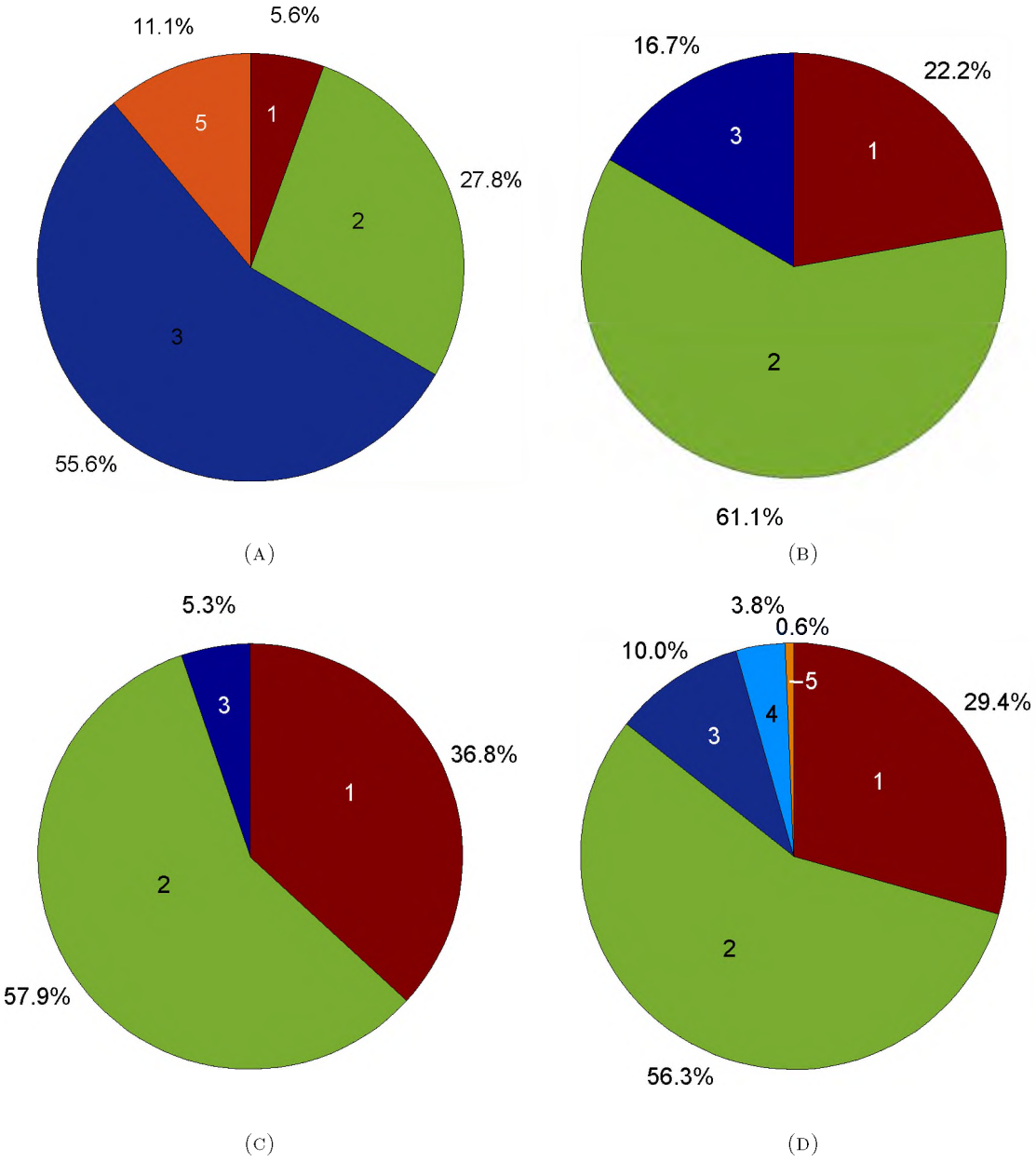

FIGURE 5.15: **NFIQ scores**. (A) are the NFIQ scores for category one internal fingerprints. (B) are the NFIQ scores for category two internal fingerprints. (C) are the NFIQ scores for category three internal fingerprints. (D) are the NFIQ scores for all the surface fingerprints. The numbers inside the pie charts denote the NFIQ score.

Category	RMS-C	OCL
1	10.04 ± 0.35	0.2395 ± 0.0747
2	10.20 ± 0.30	0.1684 ± 0.0282
3	10.73 ± 0.56	0.1328 ± 0.0196
Surface	11.63 ± 0.54	0.1824 ± 0.0561

TABLE 5.4: **Fingerprint quantitative assessment.**

Category	Surface score		Cross score	
	Mean	Max	Mean	Max
1	11.0 ± 3.3	18.0 ± 6.1	59.3 ± 35.3	112.3 ± 62.3
2	15.4 ± 4.9	24.9 ± 9.3	65.8 ± 34.8	128.6 ± 56.9
3	37.4 ± 11.5	61.6 ± 32.1	57.9 ± 48.8	152.0 ± 77.4
All	21.3 ± 17.3	34.4 ± 25.7	61.0 ± 39.3	129.3 ± 65.4

TABLE 5.5: **Average fingerprint matching results for all internal fingerprint categories.**

Table 5.5, Table 5.6, and Figure 5.16 serve to describe the surface to internal fingerprint match scores, the internal fingerprint cross match scores, and performance according to percentage true match achieved. Table 5.5 lists both the average **mean** and **maximum** match scores. Since there is no decisive manner in which to perform a one-to-one fingerprint verification, both the **mean** and the **maximum** match scores are valid. The true match criterion is indicated by the horizontal dashed lines in Figures 5.16(A) and (B). The performance according to true match percentages is given in Table 5.6.

Figure 5.16 exhibits the distribution (amongst the three predefined categories) of the fifty-five OCT scans. Figure 5.16(A) demonstrates how category one and two internal fingerprints exhibited low internal to surface fingerprint match scores and, thus, bad correspondence. Category three internal fingerprints exceeded this significantly: Table 5.6 shows how 74% had at least one true match with a corresponding surface counterpart.

Category	% True match (to surface)		% True match (cross)	
	Overall	At least one	Overall	At least one
1	0%	0%	53%	100%
2	0%	6%	43%	89%
3	39%	74%	44%	100%
All	14%	27%	47%	96%
Surface			62%	100%

TABLE 5.6: **Percentage true match results** for: all internal fingerprint categories and conventional surface fingerprints. The 'overall' percentages were calculated as the percentage of true matches when considering all comparisons. The 'at least one' columns exhibit the percentage of extracted internal fingerprints that have at least one corresponding true match with their surface counterparts.

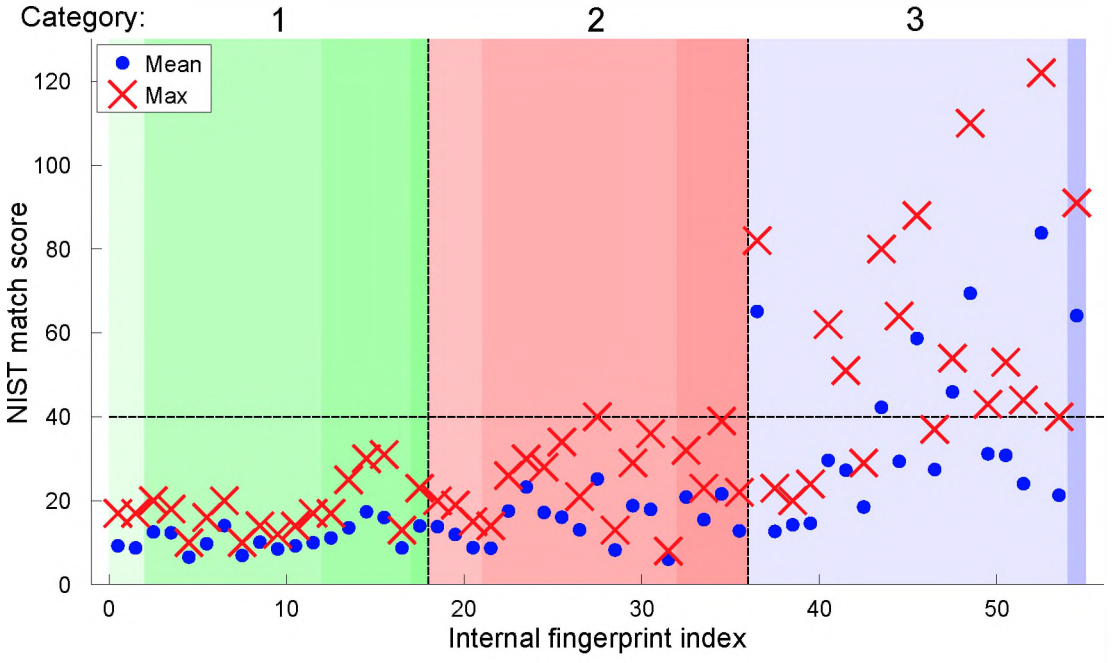

(A)

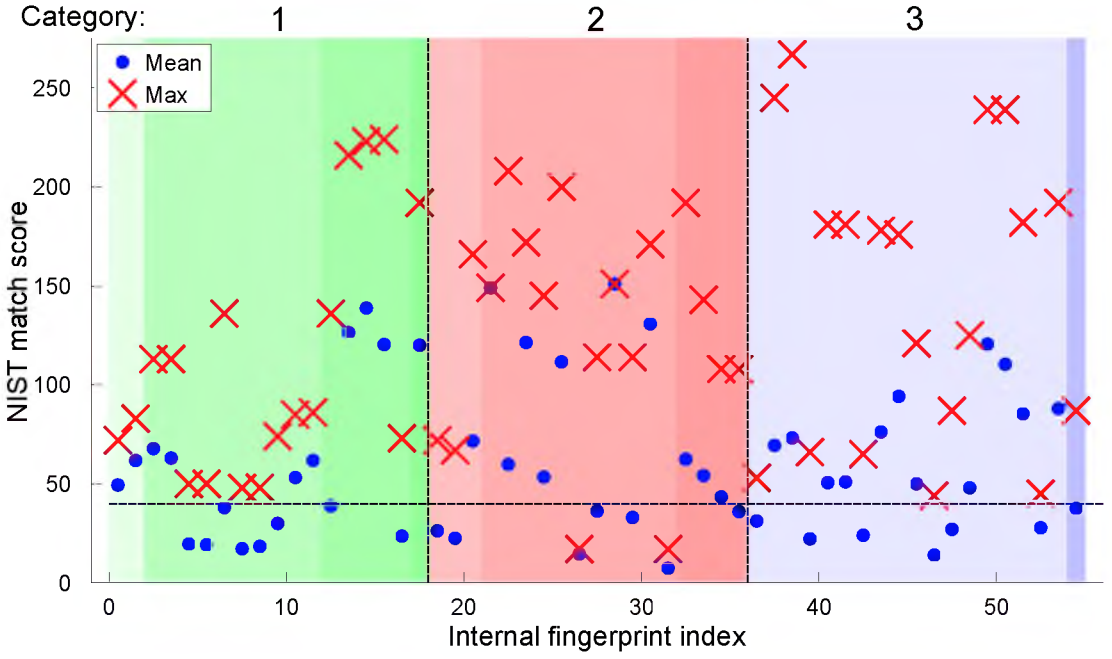

(B)

FIGURE 5.16: **Fingerprint match score results**. (A) and (B) encapsulate the NIST match scores for internal to surface fingerprint correspondence and internal fingerprint cross-correspondence, respectively. The vertical divisions denote the three internal fingerprint categories, in ascending order from left to right. The vertical light to dark colours indicate the NFIQ scores. Within each colour division, the fingerprints are arranged in ascending order according to OCL. The horizontal line denotes a true match. The x-axes shows the arrangement of the fifty-five internal fingerprints, in ascending order according to: the subjective categories, NFIQ scores, and OCL.

This indicates that the internal fingerprint performance is dependent on the size of the imaged region: a large imaged region ($15mm \times 15mm$, in this case) has more minutiae and, therefore, a better chance of matching against a surface counterpart. With this observation, OCT fingertip scans should encompass as large an area as possible. If the scanned region is sufficiently large and the internal fingerprint is extracted using the algorithms detailed here, it can be augmented with surface fingerprint databases.

The internal fingerprint cross-correspondence match scores are disclosed in Table 5.5 and Figure 5.16(B). These scores are noteworthy as they verify that internal fingerprints are consistent over various scans and can constitute a fingerprint database. Furthermore, 96% of all internal fingerprints had at least one corresponding true match (see Table 5.6). However, the conventional surface fingerprints performed better in this regard because 100% had at least one true match with another surface fingerprint.

Although Table 5.6 shows that surface fingerprints outperformed the internal fingerprints when matched against other surface fingerprints, the surface fingerprints used in this case encompassed the entire fingerprint. To exemplify the performance of the internal fingerprints, a comparison was made to the performance of surface fingerprints that were of *the same or similar region.* Figure 5.17 manifests clearly this comparison as the cropped surface fingerprints exhibit similar match scores to the internal fingerprint. The majority of the internal fingerprints either performed as well as (within the measured standard deviation), or better than, their corresponding cropped surface fingerprints.

Notwithstanding the cropping procedure, there is still evidence of factors such as surface fingerprint distortion, which is relatively consistent amongst the surface fingerprints but lacking in the internal fingerprints, affecting internal fingerprints' performance. Some of the category three internal fingerprints performed worse than their surface counterparts.

The internal fingerprints had an average match score higher than their corresponding cropped surface counterparts 64% of the time, and had better maximum match scores 53% of the time. This indicates that the internal fingerprints perform either as well as, or better than, their corresponding cropped surface counterparts, assuming the imaged area is roughly the same.

The intention of cropping surface counterparts to represent the same area as the internal fingerprints, was to eliminate some bias caused by the difference in represented

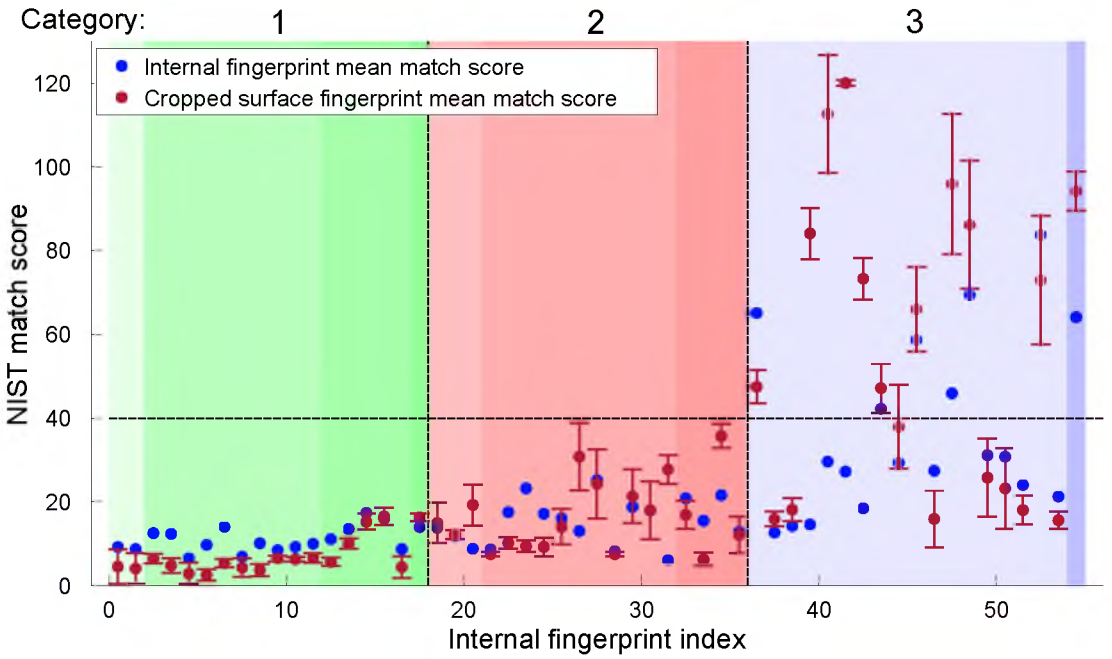

(A)

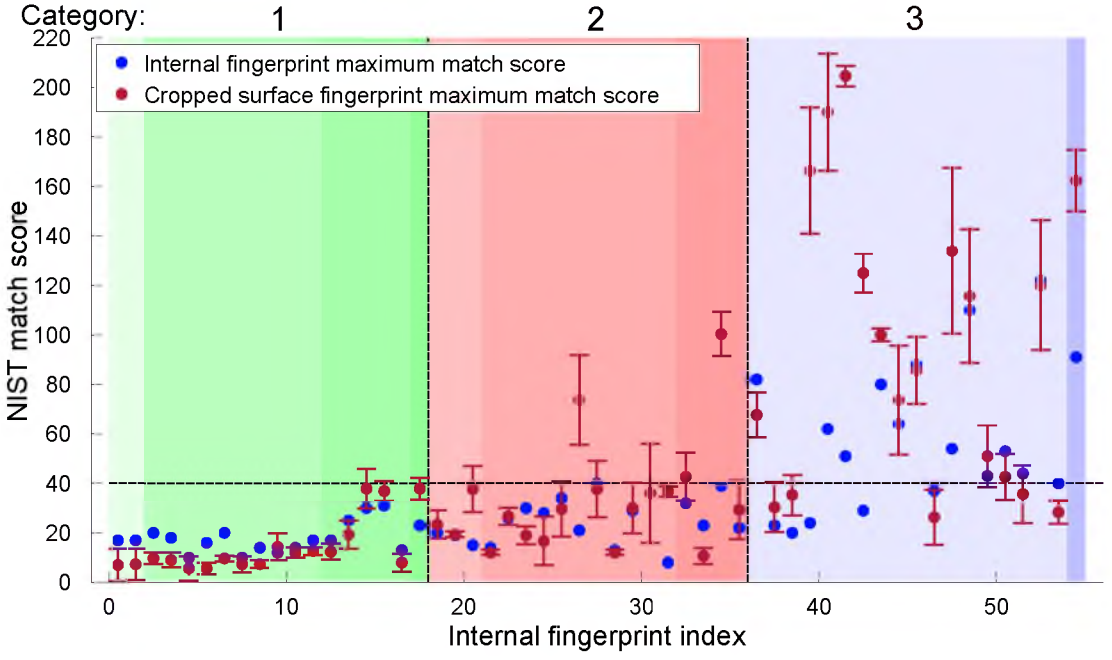

(B)

FIGURE 5.17: **Fingerprint match score results: a comparison against surface counterparts' performance**. (A) gives the internal fingerprint to conventional surface fingerprint average match scores, and the average match scores for three surface fingerprints (that were cropped to match their corresponding internal fingerprints, and compared against the same set of conventional surface counterparts). (B) gives the maximum match scores for the same fingerprints. The arrangement of fingerprints is the same as in Figure 5.16. The standard deviations of the match scores of the three cropped surface counterparts are indicated by the error boxes.

area between surface and internal fingerprints. Although a fingerprint acquisition device (whether OCT or conventional surface scanners) should image a sufficiently large area, the OCT device used in this research was not designed for fingerprint acquisition. Instead, a goal of this research is to provide a means of extracting the internal fingerprint and, in so doing, preempt and prompt the creation of an OCT specific fingerprint acquisition device.

There are, however, other less obvious sources of bias that may have influenced the comparisons between internal and surface fingerprints. Removing various forms of fingerprint distortion; accounting for the influence of inconsistent details (such as wrinkles or scars that are only visible on the surface); and improving the scan area size for OCT fingertip scanning, are examples of possible avenues for future work.

Figure 5.18 provides internal fingerprint examples, their corresponding surface counterparts, and the regions of interest. Although their characteristics are relatively similar, the internal and surface fingerprints have different ridge-to-valley thickness and contrast characteristics. An advantage of internal fingerprints is demonstrated in this figure. There were no wrinkles or scars on the internal fingerprints, even when damage was present on their surface counterparts. Figure 5.18 also serves to show qualitatively the direct correspondence between surface and internal fingerprints.

There is, however, distortion present. This is recognised as the difference in shape and minutiae to minutiae distances when comparing the internal fingerprints to their surface counterparts. It arises via three sources: (1) 'jitter' owing to movement during the OCT scanning procedure; (2) surface fingerprint distortion owing to the touch-based surface scanners; and (3) the planar perspective (i.e, flat and *en-face*) fingerprint extraction process. These may have had an effect on the matching performance between extracted internal fingerprints and their conventional surface counterparts, as exhibited in the bias toward conventional surface true match performance (see Table 5.6).

Jitter must be mitigated through hardware design. Surface distortion correction is beyond the scope of this work. Distortion induced by the *en-face* averaging approach taken can be reduced by applying a 3D to 2D unwrapping [8] procedure. Compensating for these sources of distortion is hypothesised to improve matching performance and will be undertaken as a future work.

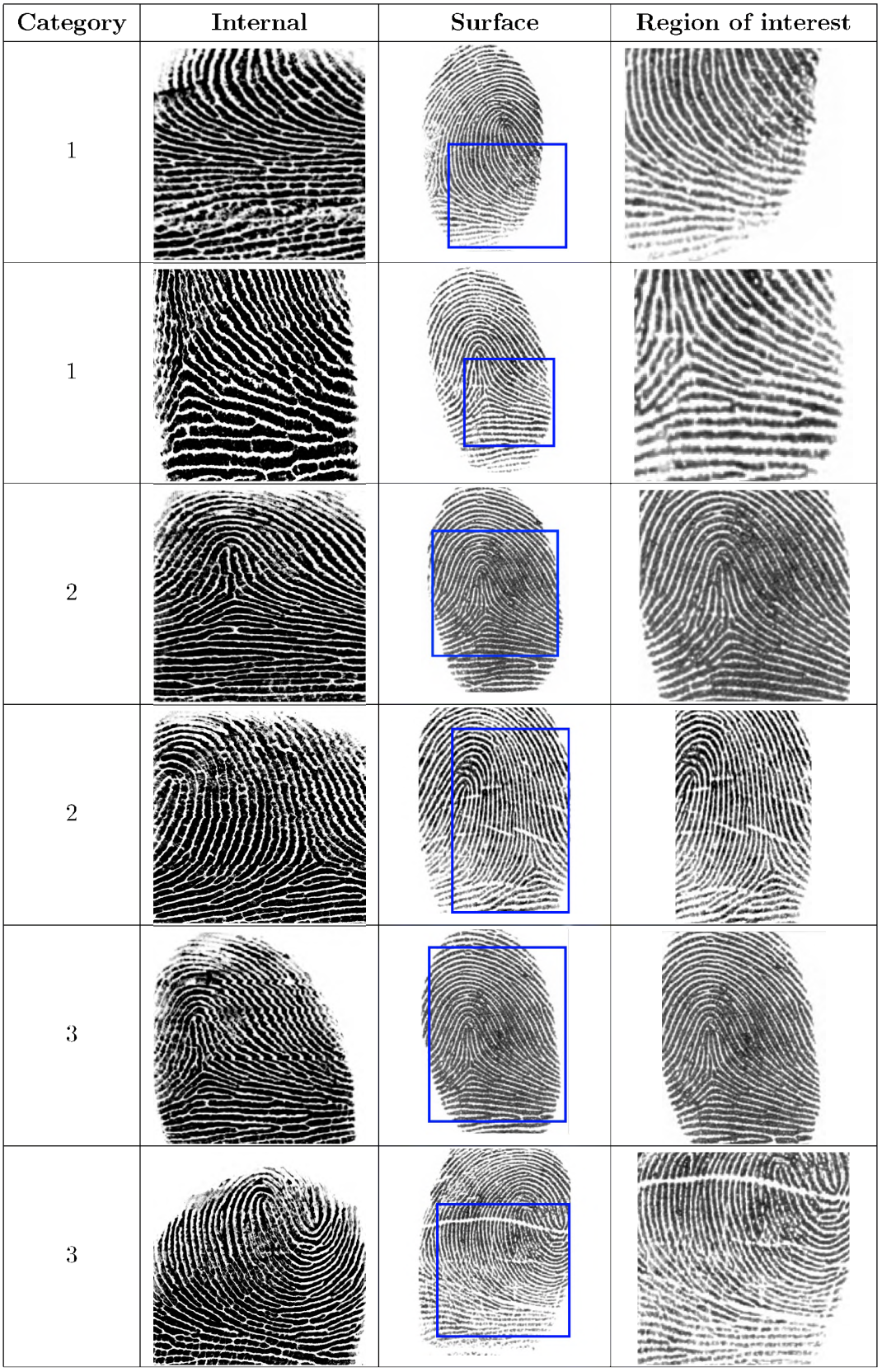

FIGURE 5.18: **Internal and surface fingerprint examples.** The internal fingerprints' intensities are inverted to correspond with the surface fingerprint convention.

Notwithstanding various sources of fingerprint distortion, the surface to internal fingerprint correspondence is acceptable when the imaged region is sufficiently large. Furthermore, cross-correspondence between internal fingerprints lends support to the claim that the internal fingerprint can be used as a stand-alone biometric solution.

As per the research-questions posed in Section 1.6: the internal fingerprint corresponds to its surface counterpart, and is of sufficient quality with respect to OCL, NFIQ, surface correspondence, and cross-correspondence.

This chapter served to exhibit experimental results evidencing the performance of the internal fingerprint. The techniques developed for internal fingerprint zone-detection, internal fingerprint extraction, and internal fingerprint enhancement were tested and results were given. The strength of these techniques was shown in their accuracy and in the quantitative correlation between the internal fingerprints extracted and their conventional surface counterparts. The following section serves to draw conclusions based on the discoveries made in this research.

Chapter 6

Conclusion

Current surface fingerprint imaging-technology is only capable of providing a 2D representation of the surface fingerprint. Furthermore, the surface fingerprint is: prone to damage and wear and tear; distorted upon touch-based scanning; and easy to spoof.

The internal fingerprint has the same advantages of the surface fingerprint – universality, distinctiveness, and high-performance – and is less vulnerable to damage, distortion, or spoofing. The research carried out and detailed in this thesis addressed the problem of extracting the internal fingerprint from an OCT fingertip scan. It was evidenced in earlier works that the internal fingerprint exists and can be extracted. However, the extraction processes demonstrated were often primitive and resulted in internal fingerprints of an insufficient quality.

It has been identified that the internal fingerprint resides in the characteristic undulations of the upper-edge of the papillary junction. Denoted as the internal fingerprint zone, the accurate and consistent identification of this surface throughout OCT fingertip scans is paramount to internal fingerprint extraction.

Fuzzy c-means clustering was recognised as possessing features that are suitable to the task of internal fingerprint zone detection. This hypothesis was confirmed by a quantitative performance comparison between four clustering algorithms. Thus, fuzzy c-means was used to detect reliably the centre of the papillary junction.

In spite of the fact that the undulations of the centre of the papillary junction do characterise the internal fingerprint to a fair degree, the most pertinent internal fingerprint information is found in the upper-edge of the papillary junction. Consequently, a fine-tuning procedure was implemented that used speckle noise-reduction, contrast-enhancement, and edge-detection to complete the detection of the internal fingerprint-zone. Quantitative and qualitative assessment showed that fine-tuning successfully adjusted the location of the papillary junction centre to its upper-edge.

A ground-truth estimation of the internal fingerprint-zone was carried out on a single OCT fingertip scan. The number of data points extracted per A-line and the number of clusters were varied to determine the parameter sensitivity and performance of the algorithm. Error, structural similarity, and contrast were measured. Performance was shown to be within the ranges of the measured human error. The internal fingerprint-zone detection approach developed in this research is able to detect the papillary junction upper-edge consistently and accurately in touchless OCT fingertip scans.

The internal fingerprint-zone was used to define localised regions for internal fingerprint extraction. Simple statistics (mean and standard deviation) were evaluated in a windowed fashion to determine which (Z) pixels to average in each A-line for individual (XY) pixels in the extracted internal fingerprint (*viz.* 3D to 2D mapping).

The extracted internal fingerprint is subject to the same signal characteristics of the OCT scans themselves: speckle noise and low contrast. Thus, speckle noise-reduction, local contrast-enhancement, and global contrast-saturation were applied to the extracted internal fingerprints.

Fifty-five OCT fingertip scans were obtained: small and large areas imaged were combined with low and high *en-face* resolutions. The result was three manually defined internal fingerprint categories: (1) small, badly positioned region; (2) small, well positioned region; and (3) large region. In addition, sixteen surface scans (using two different scanners) were obtained from each of the scanned fingers.

The contrast and orientation certainty was calculated, and a well-known fingerprint quality categorisation method was applied, for all internal fingerprints and their surface counterparts. Although the internal fingerprints had, on average, lower contrast than the surface counterparts, they yielded superior orientation certainty (regarding category

two and three internal fingerprints). 37% of the internal fingerprints extracted from a large imaged area had an NFIQ score of one, whilst only 29% of conventional surface fingerprints yielded an NFIQ score of one. The two fingerprint quality assessment metrics measured, indicated the internal fingerprints' superiority. Furthermore, a qualitative assessment evidenced the resistance of the internal fingerprint to surface damage, such as wrinkles.

The internal fingerprints were also tested for correspondence with their surface counterparts and cross-correspondence. The NIST minutiae extraction and matching algorithms were used as a means to this end. Albeit category one and two internal fingerprints performed poorly regarding surface correspondence, 75% of category three internal fingerprints had a true match with a surface counterpart. Most (96%) of the internal fingerprints had at least one true match with another internal fingerprint. The internal fingerprint can constitute a fingerprint database, although this must confirmed with further research. The conventional surface fingerprints always had at least one true match with another fingerprint from the same finger. However, the conventional surface fingerprints usually represented a larger area and, thus, had more minutiae for matching.

To circumvent the bias owing to the difference in scan area size and locality, surface fingerprints were obtained and cropped to represent similar regions as each internal fingerprint. Three cropped surface fingerprints (for each internal fingerprint) were matched against the same sets of surface fingerprints as the internal fingerprints, thus allowing for a performance comparison that is unbiased by fingerprint area size and locality. The majority of the internal fingerprints performed either as well as, or better than, their corresponding cropped surface counterparts. That said, the effects of other factors (such as fingerprint distortion and the presence of wrinkles and other anomalies) were nevertheless still present.

Deviations between the surface and internal fingerprints are present because of instability in the touchless scanning process; surface distortion owing to pressure during scanning; and the lack of a 3D to 2D unwrapping procedure.

The main system components – internal fingerprint zone-detection and localised region internal fingerprint extraction, developed to answer the research questions – can be used in numerous applications, such as skin layer detection and segmentation for medical

diagnostics, surface fingerprint extraction from OCT fingertip volumes, or analysis of damaged fingerprints. The separability and versatility of the algorithms are noteworthy.

The internal fingerprint can be extracted from touchless OCT fingertip scans, regardless of the intensity depth-dependency roll-off and curvature problems inherent in OCT scans of a curved object.

The internal fingerprint is thus a creative and high-quality biometric solution that adopts the same advantages as the well-established surface fingerprint; is not subject to the same damage as the surface fingerprint; is persistent over numerous scan instances; and has the potential to be exceptionally spoof-resistant.

This thesis successfully answered all the research questions-posed in Section 1.6.1 by confirming the correctness of the hypothesis put forward.

The following chapter suggests avenues for future work and outlines some endeavours currently being undertaken.

Chapter 7

Future Work

The algorithms developed in this research were not optimised. The performance of the following stages of the algorithm can be improved:

- **Data and feature extraction.** Smoothing can be performed in 3D, instead of individually for each A-line. A selection of A-lines can be used, instead of all A-lines.
- **Clustering.** The feature space can be diminished: the minimum set of necessary features can be extracted. Furthermore, a lower number of A-lines will improve the speed of clustering.
- **Interpolation.** An assessment of interpolation procedures must be carried out in order to select the best technique for this application.
- **Fine-tuning.** OBNLM is slow. There may be a speckle-reduction procedure that is faster and reduces noise more efficiently – this must be investigated.

The intention of this research was to provide a proof-of-concept internal fingerprint extraction algorithm, not to provide a real-time variant thereof. There are aspects of the approach that can be optimised and parallelised. Therefore, a future work will entail modifying; exploring; and perfecting the algorithms developed through the use of parallel computing.

A vital alteration to the internal fingerprint extraction algorithm would be employing a 3D to 2D unwrapping procedure. This would compensate for any distortion induced

through simple planar extraction and will be carried out in a future work. Futhermore, jitter distortion must be alleviated through hardware redesign.

An internal fingerprint database will be constructed and tested in a future work. This will serve to further exemplify OCT as a fingerprint imaging technology.

Although never explicitly tested in this work, OCT can be used for liveness-detection. Various spoofing techniques can be applied and tested. Furthermore, access to the internal fingerprint may be obscured by some of these spoofing techniques as light cannot penetrate all media. A future work will entail testing the capability of internal fingerprint extraction during a spoofing attack attempt.

The detection of the internal fingerprint zone can be utilised as an asset in other internal fingerprint extraction algorithms (aside from the two developed in this research), or as a tool for spoof-detection. These applications will be explored in a future work.

Since the algorithms developed in this research can extract successfully the internal fingerprint, fingertip specific OCT scanners can be developed. This must be undertaken as a future work.

Another useful characteristic of OCT fingertip scans is that both the internal and the surface fingerprints are present and accessible. Future work will entail extracting both of these and developing a strategy to combine them to maximise the quality of the extracted fingerprint.

An avenue for future work is that of developing new approaches to fingerprint extraction from OCT fingertip scans. This particular field of research is fairly new and unexplored. There may be approaches to fingerprint extraction that remain undiscovered. An effort currently being undertaken by the author and collaborators involves a multi-resolution technique for extracting both (internal and surface) fingerprints from an OCT fingertip scan and combining them according to local quality. This will be expounded upon in a future publication.

References

[1] D. Huang, E. A. Swanson, C. P. Lin, J. S. Schuman, W. G. Stinson, W. Chang, M. R. Hee, T. Flotte, K. Gregory, C. A. Puliafito *et al.*, "Optical coherence tomography," *Science*, vol. 254, no. 5035, pp. 1178–1181, 1991.

[2] M. Kücken and A. C. Newell, "Fingerprint formation," *Journal of Theoretical Biology*, vol. 235, no. 1, pp. 71–83, 2005.

[3] C. Champod, C. J. Lennard, P. Margot, and M. Stoilovic, *Fingerprints and Other Ridge Skin Impressions*. CRC Press, 2004.

[4] D. Maltoni, D. Maio, A. K. Jain, and S. Prabhakar, *Handbook of Fingerprint Recognition*, 2nd ed. Springer, 2009.

[5] M. Tistarelli, S. Z. Li, and R. Chellappa, *Handbook of Remote Biometrics*. Springer, 2009.

[6] T. Matsumoto, H. Matsumoto, K. Yamada, and S. Hoshino, "Impact of artificial gummy fingers on fingerprint systems," in *Proceedings of Electronic Imaging*. International Society for Optics and Photonics, 2002, pp. 275–289.

[7] S. Prabhakar, S. Pankanti, and A. K. Jain, "Biometric recognition: Security and privacy concerns," *IEEE Security & Privacy*, vol. 1, no. 2, pp. 33–42, 2003.

[8] Y. Wang, D. L. Lau, and L. G. Hassebrook, "Fit-sphere unwrapping and performance analysis of 3D fingerprints," *Applied Optics*, vol. 49, no. 4, pp. 592–600, 2010.

[9] Y. S. Moon, J. Chen, K. Chan, K. So, and K. Woo, "Wavelet based fingerprint liveness detection," *Electronics Letters*, vol. 41, no. 20, pp. 1112–1113, 2005.

[10] A. Fercher, B. Sander, T. M. Jørgensen, and P. E. Andersen, *Optical Coherence Tomography.* John Wiley & Sons, Ltd, 2006.

[11] G. Liu and Z. Chen, "Capturing the vital vascular fingerprint with optical coherence tomography," *Applied Optics*, vol. 52, no. 22, pp. 5473–5477, 2013.

[12] A. Bossen, R. Lehmann, and C. Meier, "Internal fingerprint identification with optical coherence tomography," *IEEE Photonics Technology Letters*, vol. 22, no. 7, pp. 507–509, 2010.

[13] H. S. G. da Costa, J. R. Maxey, L. Silva, and A. K. Ellerbee, "Evaluation of fingerprint deformation using optical coherence tomography," in *Proceedings of SPIE BiOS.* International Society for Optics and Photonics, 2014.

[14] A. Zam, R. Dsouza, H. M. Subhash, M.-L. O'Connell, J. Enfield, K. Larin, and M. J. Leahy, "Feasibility of correlation mapping optical coherence tomography (cmOCT) for anti-spoof sub-surface fingerprinting," *Journal of Biophotonics*, vol. 6, no. 9, pp. 663–667, 2013.

[15] F. Harms, E. Dalimier, and A. C. Boccara, "En-face full-field optical coherence tomography for fast and efficient fingerprints acquisition," in *Proceedings of SPIE Defense and Security.* International Society for Optics and Photonics, 2014.

[16] J. M. Schmitt, S. H. Xiang, and K. M. Yung, "Speckle in optical coherence tomography," *Journal of Biomedical Optics*, vol. 4, no. 1, pp. 95–105, 1999.

[17] 360biometrics. (2014) FAQ - Fingerprint Scanner. Accessed on 08/12/2014. [Online]. Available: http://360biometrics.com/faq/fingerprint_scanners.php

[18] R. Diaz. (2007) Biometrics: Security vs. Convenience. Accessed on 08/12/2014. [Online]. Available: http://www.securityworldmag.com/tech/tech_view.asp?idx=1156&part_code=030170070&page=1

[19] R. K. Rowe, K. Nixon, and S. Corcoran, "Multispectral fingerprint biometrics," in *Proceedings of the Sixth Annual IEEE SMC; Information Assurance Workshop (IAW'05).* IEEE, 2005, pp. 14–20.

[20] R. K. Rowe and K. A. Nixon, "Fingerprint enhancement using a multispectral sensor," in *Proceedings of SPIE Defense and Security.* International Society for Optics and Photonics, 2005, pp. 81–93.

[21] K. A. Nixon and R. K. Rowe, "Multispectral fingerprint imaging for spoof detection," in *Proceedings of SPIE Defense and Security*. International Society for Optics and Photonics, 2005, pp. 214–225.

[22] S. Chang, Y. Cheng, K. Larin, Y. Mao, S. Sherif, and C. Flueraru, "Optical coherence tomography used for security and fingerprint-sensing applications," *Image Processing, IET*, vol. 2, no. 1, pp. 48–58, 2008.

[23] E. A. Swanson, J. Izatt, C. Lin, J. Fujimoto, J. Schuman, M. Hee, D. Huang, and C. Puliafito, "In vivo retinal imaging by optical coherence tomography," *Optics Letters*, vol. 18, no. 21, pp. 1864–1866, 1993.

[24] C. A. Puliafito, M. R. Hee, C. P. Lin, E. Reichel, J. S. Schuman, J. S. Duker, J. A. Izatt, E. A. Swanson, and J. G. Fujimoto, "Imaging of macular diseases with optical coherence tomography," *Ophthalmology*, vol. 102, no. 2, pp. 217–229, 1995.

[25] W. Drexler, U. Morgner, R. K. Ghanta, F. X. Kärtner, J. S. Schuman, and J. G. Fujimoto, "Ultrahigh-resolution ophthalmic optical coherence tomography," *Nature Medicine*, vol. 7, no. 4, pp. 502–507, 2001.

[26] J. Welzel, "Optical coherence tomography in dermatology: a review," *Skin Research and Technology*, vol. 7, no. 1, pp. 1–9, 2001.

[27] M. C. Pierce, J. Strasswimmer, B. H. Park, B. Cense, and J. F. de Boer, "Advances in optical coherence tomography imaging for dermatology," *Journal of Investigative Dermatology*, vol. 123, no. 3, pp. 458–463, 2004.

[28] T. Gambichler, V. Jaedicke, and S. Terras, "Optical coherence tomography in dermatology: technical and clinical aspects," *Archives of Dermatological Research*, vol. 303, no. 7, pp. 457–473, 2011.

[29] Y. Cheng and K. V. Larin, "Artificial fingerprint recognition by using optical coherence tomography with autocorrelation analysis," *Applied Optics*, vol. 45, no. 36, pp. 9238–9245, 2006.

[30] M.-R. Nasiri-Avanaki, A. Meadway, A. Bradu, R. M. Khoshki, A. Hojjatoleslami, and A. G. Podoleanu, "Anti-spoof reliable biometry of fingerprints using en-face optical coherence tomography," *Optics and Photonics Journal*, vol. 1, p. 91, 2011.

[31] S. Meissner, R. Breithaupt, and E. Koch, "Defense of fake fingerprint attacks using a swept source laser optical coherence tomography setup," in *Proceedings of SPIE Lasers and Applications in Science and Engineering.* International Society for Optics and Photonics, 2013.

[32] P. Korohoda, A. Dabrowski, and P. Pawlowski, "Optical coherence tomography for fingerprint acquisition from internal layer – a case study," in *Proceedings of Signal Processing: Algorithms, Architectures, Arrangements, and Applications (SPA).* IEEE, 2014, pp. 176–180.

[33] I. Sobel and G. Feldman, "A 3x3 isotropic gradient operator for image processing," *Presentation to Stanford Artificial Intelligence Project*, 1968.

[34] C. Sousedik and C. Busch, "Quality of fingerprint scans captured using optical coherence tomography," in *Proceedings of the IEEE International Joint Conference on Biometrics (IJCB).* IEEE, 2014, pp. 1–8.

[35] A. K. Jain, Y. Chen, and M. Demirkus, "Pores and ridges: high-resolution fingerprint matching using level 3 features," *IEEE Transactions on Pattern Analysis and Machine Intelligence*, vol. 29, no. 1, pp. 15–27, 2007.

[36] M. Liu and T. Buma, "Biometric mapping of fingertip eccrine glands with optical coherence tomography," *IEEE Photonics Technology Letters*, vol. 22, no. 22, pp. 1677–1679, 2010.

[37] A. Dubois, K. Grieve, G. Moneron, R. Lecaque, L. Vabre, and C. Boccara, "Ultrahigh-resolution full-field optical coherence tomography," *Applied Optics*, vol. 43, no. 14, pp. 2874–2883, 2004.

[38] A. Shiratsuki, E. Sano, M. Shikai, T. Nakashima, T. Takashima, M. Ohmi, and M. Haruna, "Novel optical fingerprint sensor utilizing optical characteristics of skin tissue under fingerprints," in *Proceedings of Biomedical Optics.* International Society for Optics and Photonics, 2005, pp. 80–87.

[39] L. N. Darlow, S. S. Akhoury, and J. Connan, "A review of state-of-the-art speckle reduction techniques for optical coherence tomography fingertip scans," in *Proceedings of the Seventh International Conference on Machine Vision (ICMV 2014).* International Society for Optics and Photonics, 2015, pp. 944 523–944 523.

[40] ——, "Internal fingerprint acquisition from optical coherence tomography fingertip scans," in *Proceedings of the Third International Conference on Digital Information, Networking, and Wireless Communications (DINWC)*. IEEE, 2015, pp. 188–191.

[41] L. N. Darlow, J. Connan, and S. S. Akhoury, "Internal fingerprint zone detection in optical coherence tomography fingertip scans," *Journal of Electronic Imaging*, vol. 24, no. 2, pp. 023 027–023 027, 2015.

[42] S. S. Akhoury and L. N. Darlow, "Extracting subsurface fingerprints using optical coherence tomography," in *Proceedings of the Third International Conference on Digital Information, Networking, and Wireless Communications (DINWC)*. IEEE, 2015, pp. 184–187.

[43] R. Khutlang and F. V. Nelwamondo, "Novelty detection-based internal fingerprint segmentation in optical coherence tomography images," in *Proceedings of the Second International Symposium on Computing and Networking (CANDAR)*. IEEE, 2014, pp. 556–559.

[44] G. Upton and I. Cook, *Understanding statistics*. Oxford University Press, 1996.

[45] M. R. Anderberg, "Cluster analysis for applications," DTIC Document, Tech. Rep., 1973.

[46] R. Xu and D. Wunsch, "Survey of clustering algorithms," *IEEE Transactions on Neural Networks*, vol. 16, no. 3, pp. 645–678, 2005.

[47] R. M. Haralick and L. G. Shapiro, "Image segmentation techniques," in *1985 Technical Symposium East*. International Society for Optics and Photonics, 1985, pp. 2–9.

[48] V. Estivill-Castro, "Why so many clustering algorithms: a position paper," *ACM SIGKDD Explorations Newsletter*, vol. 4, no. 1, pp. 65–75, 2002.

[49] J. A. Hartigan and M. A. Wong, "Algorithm as 136: A k-means clustering algorithm," *Applied Statistics*, pp. 100–108, 1979.

[50] H.-S. Park and C.-H. Jun, "A simple and fast algorithm for k-medoids clustering," *Expert Systems with Applications*, vol. 36, no. 2, pp. 3336–3341, 2009.

[51] J. C. Bezdek, R. Ehrlich, and W. Full, "FCM: The fuzzy c-means clustering algorithm," *Computers & Geosciences*, vol. 10, no. 2, pp. 191–203, 1984.

[52] T. K. Moon, "The expectation-maximization algorithm," *IEEE Signal Processing Magazine*, vol. 13, no. 6, pp. 47–60, 1996.

[53] D. Garcia, "Robust smoothing of gridded data in one and higher dimensions with missing values," *Computational Statistics & Data Analysis*, vol. 54, no. 4, pp. 1167–1178, 2010.

[54] J. W. Goodman, "Some fundamental properties of speckle," *Journal of the Optical Society of America*, vol. 66, no. 11, pp. 1145–1150, 1976.

[55] A. Ozcan, A. Bilenca, A. E. Desjardins, B. E. Bouma, and G. J. Tearney, "Speckle reduction in optical coherence tomography images using digital filtering," *Journal of the Optical Society of America A*, vol. 24, no. 7, pp. 1901–1910, 2007.

[56] F. Forsberg, S. Leeman, and J. Jensen, "Assessment of hybrid speckle reduction algorithms," *Physics in Medicine and Biology*, vol. 36, no. 11, p. 1539, 1991.

[57] J.-S. Lee, "Digital image enhancement and noise filtering by use of local statistics," *IEEE Transactions on Pattern Analysis and Machine Intelligence*, vol. PAMI-2, no. 2, pp. 165–168, 1980.

[58] J. S. Lim and H. Nawab, "Techniques for speckle noise removal," *Optical Engineering*, vol. 20, no. 3, p. 203472, 1981. [Online]. Available: http://dx.doi.org/10.1117/12.7972744

[59] A. Pizurica, A. M. Wink, E. Vansteenkiste, W. Philips, and B. J. Roerdink, "A review of wavelet denoising in MRI and ultrasound brain imaging," *Current Medical Imaging Reviews*, vol. 2, no. 2, pp. 247–260, 2006.

[60] P. Coupé, P. Hellier, C. Kervrann, and C. Barillot, "Nonlocal means-based speckle filtering for ultrasound images," *IEEE Transactions on Image Processing*, vol. 18, no. 10, pp. 2221–2229, 2009.

[61] Y. Yu and S. T. Acton, "Speckle reducing anisotropic diffusion," *IEEE Transactions on Image Processing*, vol. 11, no. 11, pp. 1260–1270, 2002.

[62] P. Coupé, P. Yger, S. Prima, P. Hellier, C. Kervrann, and C. Barillot, "An optimized blockwise nonlocal means denoising filter for 3-D magnetic resonance images," *IEEE Transactions on Medical Imaging*, vol. 27, no. 4, pp. 425–441, 2008.

[63] A. Buades, B. Coll, and J.-M. Morel, "A review of image denoising algorithms, with a new one," *Multiscale Modeling & Simulation*, vol. 4, no. 2, pp. 490–530, 2005.

[64] P. Coupé, P. Hellier, C. Kervrann, and C. Barillot, "Bayesian non local means-based speckle filtering," in *Proceedings of the Fifth IEEE International Symposium on Biomedical Imaging: From Nano to Macro*. IEEE, 2008, pp. 1291–1294.

[65] R. K. Pearson, *Mining imperfect data: Dealing with contamination and incomplete records*. Siam, 2005.

[66] L. Hong, Y. Wan, and A. Jain, "Fingerprint image enhancement: algorithm and performance evaluation," *IEEE Transactions on Pattern Analysis and Machine Intelligence*, vol. 20, no. 8, pp. 777–789, 1998.

[67] The GIMP team. (1997 - 2016) GNU Image Manipulation Program. Accessed on 20/01/2016. [Online]. Available: http://www.gimp.org/

[68] D. P. Huttenlocher, G. A. Klanderman, and W. J. Rucklidge, "Comparing images using the Hausdorff distance," *IEEE Transactions on Pattern Analysis and Machine Intelligence*, vol. 15, no. 9, pp. 850–863, 1993.

[69] M.-P. Dubuisson and A. K. Jain, "A modified Hausdorff distance for object matching," in *Proceedings of the 12th IAPR International Conference on Pattern Recognition – Conference A: Computer Vision & Image Processing.*, vol. 1. IEEE, 1994, pp. 566–568.

[70] Z. Wang and A. C. Bovik, "A universal image quality index," *IEEE Signal Processing Letters*, vol. 9, no. 3, pp. 81–84, 2002.

[71] Z. Wang, A. C. Bovik, H. R. Sheikh, and E. P. Simoncelli, "Image quality assessment: from error visibility to structural similarity," *IEEE Transactions on Image Processing*, vol. 13, no. 4, pp. 600–612, 2004.

[72] E. Peli, "Contrast in complex images," *JOSA A*, vol. 7, no. 10, pp. 2032–2040, 1990.

[73] E. L. Lehmann and G. Casella, *Theory of Point Estimation.* Springer Science & Business Media, 1998, vol. 31.

[74] The G'MIC Team. (2016) GREYC's Magic for Image Computing. Accessed on 20/01/2016. [Online]. Available: http://gmic.eu/

[75] F. Alonso-Fernandez, J. Fierrez, J. Ortega-Garcia, J. Gonzalez-Rodriguez, H. Fronthaler, K. Kollreider, and J. Bigun, "A comparative study of fingerprint image-quality estimation methods," *IEEE Transactions on Information Forensics and Security*, vol. 2, no. 4, pp. 734–743, 2007.

[76] E. Lim, X. Jiang, and W. Yau, "Fingerprint quality and validity analysis," in *Proceedings of the International Conference on Image Processing*, vol. 1. IEEE, 2002, pp. 469–472.

[77] E. Tabassi, C. Wilson, and C. Watson, "NIST fingerprint image quality," NIST, Tech. Rep., 2004.

[78] C. I. Watson, M. D. Garris, E. Tabassi, C. L. Wilson, R. M. McCabe, and S. Janet, "Users guide to NIST fingerprint image software 2 (NFIS2)," NIST, Tech. Rep., 2004.

[79] The National Institute of Standards and Technology. (2015) NIST Biometric Image Software. U.S. Department of Commerce. Accessed on 20/01/2016. [Online]. Available: http://www.nist.gov/itl/iad/ig/nbis.cfm